VOLATILE ORGANIC COMPOUND DETECTION AND ENANTIOMER DISCRIMINATION USING A CMOS-BASED MULTI-SENSOR SYSTEM

A thesis submitted to the
SWISS FEDERAL INSTITUTE OF TECHNOLOGY ZURICH

for the degree of
DOCTOR OF TECHNICAL SCIENCE

presented by
PETRA KURZAWSKI
DIPL.-ING. UNIVERSITY OF BREMEN
BORN OCTOBER 28TH, 1973
CITIZEN OF GERMANY

accepted on the recommendation of
Prof. Dr. A. Hierlemann, examiner
Prof. Dr. J. Janata, co-examiner
Prof. Dr. H. Baltes, co-examiner

2006

Published by:

Physical Electronics Laboratory
Swiss Federal Institute of Technology (ETH), Zurich
Wolfgang-Pauli-Strasse 16
CH-8093 Zurich
Switzerland

TABLE OF CONTENTS

Seite Leer /
Blank leaf

ABSTRACT

In this thesis the discrimination of volatile organic compounds and chiral molecules by means of a single-chip, multi-transducer CMOS gas sensor microsystem is investigated. The sensor microsystem comprises three transducers: A calorimetric sensor, a mass-sensitive cantilever and an interdigitated capacitor. The sensors are monolithically integrated on a 7 by 7 mm^2 chip along with dedicated analog and digital circuitry. The single-chip chemical microsystem is fabricated in an industrial 0.8-µm double-metal, double-polysilicon CMOS process. Subsequent post-CMOS-micromachining is used to release the membranes of the calorimeter and the mass-sensitive cantilever. The three sensors rely on polymeric coatings as sensitive layers to detect airborne volatile organic compounds (VOCs) and on enantioselective coatings for the chiral discrimination. These sensitive layers are deposited onto the sensor structures by means of spray-coating.

The first part of this thesis describes the overall design, the architecture and the transduction mechanisms as well as the data interface of the gas sensor system. In this context the principles of gas detection using polymers as sensitive layers are delineated. The three different sensors respond to fundamentally different molecular properties, such as the sorption heat (calorimetric), the analyte molecular mass (mass-sensitive), and its dielectric coefficient (capacitive). The different transduction principles and the specific circuitry units are detailed. All three transducers respond simultaneously upon exposure to analytes or analyte mixtures and hence provide a set of orthogonal data. An overview over the CMOS-processing and the post-micromachining for the fabrication of the gas sensor system is given. The experimental procedures and the measurement setup, which are necessary to operate the chip, are described.

In the second part of the thesis the performance of the CMOS gas sensor microsystem for the detection of airborne volatile organic compounds is studied. For the comprehensive study several sensor chips have been coated with different partially selective polymers and have then been exposed to a large set of gaseous organic compounds. The sensitivities of the individual transducers have been determined for each polymer/analyte combination. The interactions between the chemically sensitive polymer and the analyte are based on a defined set of physisorption mechanisms. Associated with these absorption mechanisms is the enrichment of the analyte in the polymer, which is defined by a thermodynamic equilibrium constant: The partition coefficient. The transducer-specific effects have been studied by normalizing the obtained sensitivities with regard to the respective partition coefficients. It has been shown that the combination of the different transducers indeed provides complementary or "orthogonal" information on the various organic volatiles. This considerably enhances the detection and discrimination capability of the sensor system.

Finally the capability of the single-chip gas sensor microsystem for the discrimination of enantiomers is evaluated. For the general understanding an introduction on the chirality of molecules, enantioselective receptors and common methods for chiral

separation and discrimination is given. On the basis of a superposition-type absorption model the absorption mechanisms of chiral molecules in enantioselective coatings are described. Several multi-transducer chips have been coated with different enantioselective composites consisting of a cyclodextrin derivative (modified α-, β-, and γ-cyclodextrin) and PDMS at 50% (w/w), and have then been exposed to the enantiomers ((R)- and (S)-enantiomer) and the respective racemic mixture of the different compounds. The chiral discrimination abilities of the enantioselective coatings and the gas sensor chips have been studied. It has been demonstrated that reliable chiral discrimination by means of the single-chip sensor system is feasible. Particularly, the high-resolution dynamic sensor response characteristics of the capacitor offers the potential of immediate purity control of the analyte sample and has provided new information about the analyte absorption and -desorption and receptor/enantiomer interactions. Additional measurements with the capacitive sensor have been performed to determine the dielectric coefficients of the enantioselective coatings and the analytes. For comparison a similar set of measurements has been performed with gas chromatography (GC) and nuclear magnetic resonance (NMR), two conventional methods to characterize chiral discrimination and separation.

ZUSAMMENFASSUNG

Der Inhalt der vorliegenden Dissertation ist die Detektion und Diskriminierung von flüchtigen organischen Verbindungen und von chiralen Molekülen mit Hilfe eines CMOS-basierten Mikrosystems. Das monolithisch integrierten Mikrosystem besteht hauptsächlich aus drei verschiedenen Gassensoren: einem Kalorimeter, einem massensensitiven Schwingbalken und einem kapazitiven Sensor. Die Sensoren und die dazugehörige analoge und digitale Auswerteelektronik sind auf einem 7 x 7 mm^2 grossen Chip integriert. Dieses System wird in einem industriellen 0.8-µm CMOS-Prozess hergestellt. Anschliessend werden die Membranen des kalorimetrischen Sensors und der Balken des massensensitiven Sensors in mehreren mikromechanischen Prozessschritten freigeätzt. Für die Detektion der organischen Verbindungen und die Diskriminierung von Enantiomeren werden die drei verschiedenen Sensortypen mit einer dünnen Polymerschicht bzw. einer dünnen enantioselektiven Schicht versehen.

Im ersten Teil der vorliegenden Arbeit wird auf den Aufbau, die Architektur, die Signalumsetzung und die Datenübertragung des Gassensor-Chips eingegangen. Wie oben erwähnt, basiert das Mikrosystem auf drei verschiedenen, polymerbeschichteten Signalwandlern. Diese reagieren auf grundlegend verschiedene molekulare Eigenschaften der Analyten: die Sorptionswärme (Kalorimeter), die molekulare Masse (massensensitiver Schwingbalken) und die dielektrische Konstante (Kapazität). Die jeweiligen Messprinzipien und die zugehörige Schaltung der Sensoren werden beschrieben. In diesem Zusammenhang wird auch das Prinzip der Gasdetektion mittels Polymeren erläutert. Das gleichzeitige Auslesen aller Sensorsignale liefert „orthogonale" Informationen über die in der sensitiven Schicht absorbierten Analyten. Neben dem CMOS-Prozess und der anschliessenden mikromechanischen Nachprozessierung werden in diesem Abschnitt auch die experimentelle Vorgehensweise und der notwendige Messaufbau erläutert.

Im zweiten Teil der Dissertation wird auf die Wirkungsweise und Zuverlässigkeit des Gassensor-Chips bei der Detektion von flüchtigen organischen Verbindungen eingegangen. Für die umfangreiche Untersuchung wurden mehrere Chips mit unterschiedlichen, partiell selektiven Polymeren beschichtet, und anschliessend wurden Messungen mit einer Serie verschiedener organischer Substanzen durchgeführt. Für jede dieser Polymer/Analyt-Kombinationen wurden die Sensitivitäten der jeweiligen Sensoren bestimmt. Die Wechselwirkung zwischen der sensitiven Schicht und dem Analyten basiert auf einer bestimmten Anzahl von Physisorptionsmechanismen. Die Anreicherung der organischen Verbindung im Polymer ist mit diesen Absorptionsmechanismen verknüpft und wird mittels einer thermodynamischen Konstanten, dem Verteilungskoeffizienten, ausgedrückt. Durch die entsprechende Normalisierung der gemessenen Sensitivitäten können die sensorspezifischen Effekte evaluiert werden. Anhand dieser Messungen und der durchgeführten Normalisierung konnte gezeigt werden, dass die Kombination dieser drei Sensortypen tatsächlich

komplimentäre oder „orthogonale“ Informationen über die verschiedenen Analyten liefert. Daraus folgt eine erhöhte Detektions- und Diskriminierungsfähigkeit des Sensorsystems.

Abschliessend wird der mögliche Einsatz des Gassensorsystems zur Enantiomerendiskriminierung untersucht. In einem einleitenden Abschnitt werden die Chiralität von Molekülen, verschiedene enantioselektive Rezeptoren und die gängigen Methoden zur Trennung und Detektion von Enantiomeren erläutert. Anhand eines dort vorgestellten Absorptionsmodells werden die Absorptionsmechanismen chiraler Moleküle in enantioselektiven Schichten beschrieben. Für die Experimente wurden mehrere Sensorsysteme mit unterschiedlichen enantioselektiven Materialien beschichtet, die aus einem Cyclodextrin-Derivat (modifiziertes α-, β-, and γ-Cyclodextrin) und aus PDMS - zu einem Gewichtsanteil von je 50% - bestehen. Als chirale Analyten dienten sowohl die (R)- und (S)-Enantiomere als auch die Racemate zweier verschiedener Methylester-Verbindungen. Anhand der Messungen konnte gezeigt werden, dass eine zuverlässige chirale Diskriminierung mit Hilfe des Gassensor-Chips möglich ist. Speziell mittels der hochaufgelösten dynamischen Signale des kapazitiven Sensors konnten zusätzliche Informationen über die Absorptions- und Desorptionsmechanismen bei der Enantiomer/Rezeptor-Wechselwirkung gewonnen werden. Der kapazitive Sensor hat das Potential zur sofortigen „Reinheitskontrolle“ der chiralen Analytproben. Mit diesem Sensor wurden zudem Messungen zur Bestimmung der dielektrischen Konstanten der enantioselektiven Schichten und der chiralen Analyten durchgeführt. Die Richtigkeit der Sensorergebnisse wurde mittels Gaschromatografie (GC) und Kernspinresonanz-Spektroskopie (NMR) überprüft.

1 INTRODUCTION

Important gas sensor applications include, e.g., air quality control, environmental monitoring, and applications related to homeland security. Over the last years three major trends can be traced in chemical gas sensor research: (i) the search for highly selective bio and/or chemical layer materials, (ii) the use of arrays of different partially selective sensors with subsequent pattern recognition and multi-component analysis methods [1-4], and (c) efforts to miniaturize gas sensors and gas sensor systems [5-14]. Efforts in this last area of research have been fueled by the rapid development of integrated-circuit (IC) technology and have led to the fabrication of chemical sensors in planar [15], as well as three-dimensional MEMS (Micro Electro Mechanical Systems) technologies by the use of micromachining techniques [8, 9]. CMOS (Complementary Metal Oxide Semiconductor) processes have been used to, e.g., develop arrays of identical transducers, which can be coated with different, partially chemically selective layers [5-7, 10-12]. This allows for the discrimination of different analytes. Also, the effectiveness of the simultaneous use of different transduction platforms either as discrete devices [16-19] or as monolithic realizations [20] has been demonstrated in the past.

Some of the trends identified for gas sensors can also be observed in the development of chiral separation and discrimination systems. The enantioselective synthesis or the discrimination of enantiomers has become important for different biological processes, since most of the biochemical functions in living organisms involve chiral interactions [21]. The potential applications include, *inter alia*, the production of enantiomerically pure food additives, pesticides, and pharmaceuticals. The need for "enantiopure" substances and thus the need for fast and reliable discrimination or detection methods have increased with the growing number of applications. Enantiomerically pure pharmaceuticals already make up for almost 50% of all drug products worldwide with increasing tendency [22-24]. Optical isomers are difficult to differentiate with "common" physicochemical methods due to their principally identical physical and chemical properties. Different methods for liquid and gas phase applications have been developed to perform the determination and the separation of enantiomers of various classes of chemical compounds [21, 25, 26]. The developed methods are mainly based on the usage of matrices that contain enantioselective molecules or receptors [21, 25, 27-30]. Over the last years a lot of efforts have been made to miniaturize techniques for chiral separation and chiral detection, with the aim to reduce the instrument size, the reagent consumption and, consequently, the costs of operation. Moreover, the separation/detection speed and the sample throughput can be increased by the use of microsystems. The most promising approach for chiral separation is the microchip electrophoresis (MCE) relying on the same principles and techniques as the classical capillary electrophoresis (CE) on a micromachined planar device [31-34]. Other methods for on-line analysis include miniaturized immunosensors [35-38] and gas sensors [21, 35]. In most cases, the sensors rely on only one transducing principle, such as

optical [36], amperometric [39], potentiometric [40, 41] or mass-sensitive transduction [42-44]. The mass-sensitive devices, e.g., quartz crystal microbalances and surface acoustic wave sensors, have been extensively used in the past for chiral detection in the gas phase [45].

In the presented thesis the detection of VOCs and that of chiral molecules have been performed using a CMOS-based, single-chip, chemical microsensor system comprising a calorimetric, a mass-sensitive, and a capacitive sensor. The transducers rely on sensitive coatings, such as polymers for volatile organic compound detection and on enantioselective composites for chiral detection. Upon the absorption of the analyte in the sensitive layer, each transducer inherently responds to a different physical property of the detected analyte: The sorption heat is detected by the calorimeter, the molecular mass by the cantilever, and the change in the dielectric properties of the layer by the capacitor.

1.1 Structure of the Thesis

The focus of this thesis is on the applicability of a single-chip, multi-transducer CMOS gas sensor microsystem for the detection of volatile organic compounds and the discrimination of chiral molecules. The gas sensor microsystem comprises of polymer-coated calorimetric, mass-sensitive and capacitive sensors, all of which rely on different transducing principles for the detection of airborne volatile organic compounds.

In Chapter 2 the overall design and architecture of the monolithically integrated multi-transducer chip and a short description on the transducing principles of the three different sensors is given. Additionally to the general use and the requirements for polymers as chemically sensitive layers, the physisorption mechanisms upon absorption of the analyte into the polymer are described.

Chapter 3 gives an overview over the CMOS fabrication and post-micromachining of the single-chip gas sensor system. A novel approach for fabricating dense arrays of silicon membranes using standard CMOS wafers by combining deep reactive ion etching (DRIE) and electrochemical etching (ECE) techniques is presented. At the end of this chapter the experimental setup and the procedures necessary to operate the multi-transducer chip and to conduct the measurements are detailed.

The chemical detection and discrimination of volatile organic compounds in air by means of the gas sensing chips with various polymeric coatings is the focus of Chapter 4. A comprehensive study has been conducted: The coated multi-transducer chips have been exposed to a set of several different organic compounds. For the three different transducers the sensitivities upon each polymer/analyte combination have been determined. With regard to the transducer description in Chapter 2, the partition coefficient of each polymer/analyte combination caters to the sensitivity value of the sensors. A respective normalization to this enrichment factor reveals the transducer-specific effects.

In Chapter 5 the possible application of the single-chip microsystem for the detection and discrimination of enantiomers has been explored. A brief introduction on optical isomers, chiral receptors, and common methods for chiral separation and discrimination is given. An absorption model is introduced to elucidate the interactions between the enantioselective sorption layers, in particular the chiral receptors, and the different enantiomers. Within this context, the meaning of the chiral discrimination factor of the enantioselective measurements is explained. By means of the capacitive sensor preparatory investigations on the enantioselective coatings and chiral analytes, which have been used for the experiments, have been conducted. For the chiral discrimination measurements several multi-transducer chips have been coated with different enantioselective composites and then been exposed to the enantiomers and racemic mixtures of two compounds. In order to compare the results obtained by the gas sensor chips with common methods, additional gas chromatography (GC) and nuclear magnetic resonance spectrometry (NMR) measurements have been conducted.

1.2 Summary of Results

1.2.1 New Fabrication Method for Membrane-based Arrays

A novel post-processing sequence has been developed for the fabrication of narrowly spaced membrane arrays on standard CMOS wafers. The approach is based on easily accessible standard processes: It combines deep reactive ion etching (DRIE) and electrochemical etching (ECE). With its almost vertical etch profile DRIE offers the advantage of densely packed micromachined structures; the ECE allows for the fabrication of suspended structures of a defined thickness (defined, e.g., by the thickness of the n-well). For an engineering run in a CMOS foundry multi-project wafers (MPW) are used in most cases; the lateral dimensions of the different structures on the wafer that have to be etched can, therefore, diverge by one order of magnitude. Unfortunately, process effects, such as trenching, allow only for a reliable fabrication of uniform-size structures. This leads to the concept of a grid-like masking patterning, in which the lateral area of each micromechanical structure is subdivided into small subunits of unity size and shape. After the DRIE step this grid is then removed by the anisotropic wet etching. Figure 1-1 depicts the processed structures of a 2 x 2 and 3 x 3 membrane array on the same silicon substrate. Using the novel post-processing approach different membrane sizes that can be used for calorimetric or pressure sensor arrays have been fabricated on the same wafer.

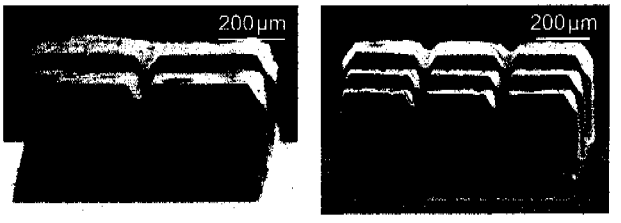

Figure 1-1. SEM micrographs of etched structures after a DRIE step and a subsequent wet etching performed on a silicon substrate. The view angle is from the backside into the etched cavity. On the left side a part of a 2 x 2 array, on the right a 3 x 3 array is shown.

1.2.2 Detection and Discrimination of Volatile Organic Compounds

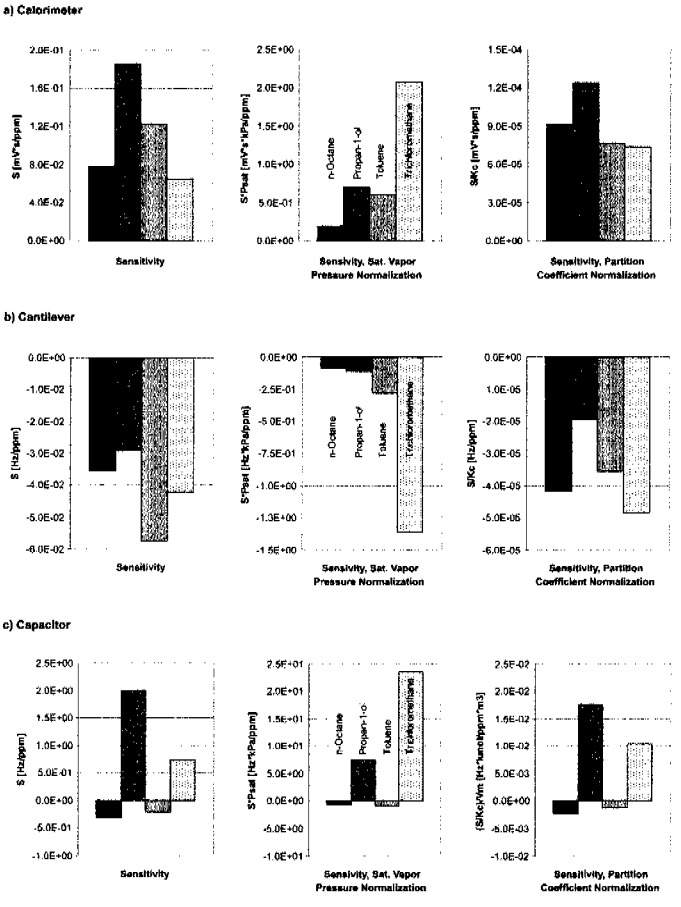

Figure 1-2. Bar graphs representing the analyte sensitivity patterns, the sensitivities as normalized with regard to the saturation vapor pressure and the sensitivities as normalized with regard to the partition coefficients for the three different transducers.

The chemical detection of volatile organic compounds in air by means of the single-chip, three-transducer CMOS gas sensor microsystem was studied. Several multi-transducer chips have been coated with five different partially selective polymers: Poly(dimethylsiloxane), (PDMS), the slightly polar polymers poly(cyanopropylmethylsiloxane), (PCPMS) and poly(etherurethane) (PEUT), and the more pronouncedly polar polymers ethyl cellulose (EC), and poly(epichlorohydrin) (PECH). The polymer-coated sensor systems were exposed to a set of 11 different organic compounds, such as n-octane and trichloromethane, and the response slope, i.e., the sensitivity values have been determined. These values were then subsequently used for data interpretation (Figure 1-2) after normalization with regard to the partition coefficients of the respective polymer/analyte combination to reveal the transducer-specific effects.

1.2.3 Detection and Discrimination of Enantiomers

Optical isomers of the same compound are difficult to distinguish with "common" sensitive layers, due to their principally identical physical and chemical properties. Therefore, materials containing enantioselective molecules or receptors are used for most chiral separation and detection methods, such as gas chromatography (GC) and capillary electrophoresis (CE). Several multi-transducers systems were coated with different enantioselective composites consisting of an modified cyclodextrin (α-, β-, and γ-cyclodextrin) and poly(dimethylsiloxane) (PDMS) at 50% (w/w) to study the applicability of the three different transducers to chiral discrimination. The multi-transducer chips were exposed to the different chiral analytes of methyl lactate and methyl-2-chloropropionate (the respective (S)-enantiomers, the (R)-enantiomers and the racemic mixtures). With the enantioselective coatings the three sensors of the gas microsystem have indeed shown chiral discrimination correlated to the respective transduction principle (Figure 1-3). It has been shown that the enantioselectivity varies with the respective coating type with the best results obtained for the modified γ-cyclodextrin/PDMS composite. More detailed information on the analyte absorption and desorption characteristics and the host/guest interaction between chiral analyte and chiral receptor structure has been obtained by evaluating the capacitive dynamic sensor signals.

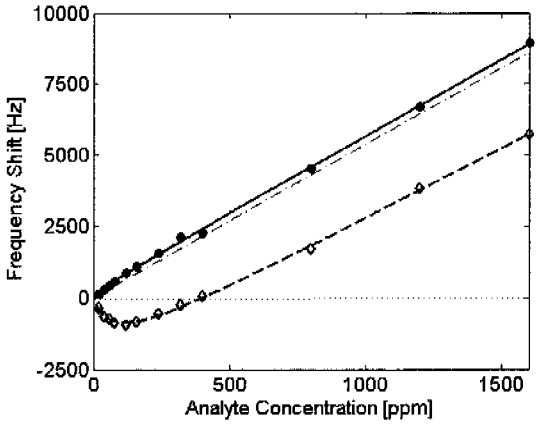

Figure 1-3. Experimental results of the capacitive sensor. Sensor response versus analyte concentration for the enantiomers of methyl-2-chloropropionate. The enantioselective coating was composed of a γ-cyclodextrin derivative and PDMS at 50% (w/w).

2 MULTI-TRANSDUCER GAS SENSOR SYSTEM

An overview over the state-of-the-art and the major research trends on chemical sensors is given in the introduction [6, 10, 18, 19, 46]. The advantages that sensor arrays offer over individual sensors are sensitivity to a wider range of analytes, improved selectivity, simultaneous multi-component analysis [1, 3, 4, 7, 11, 20], and the capability for analyte recognition rather than mere detection.

In the following a multi-transducer chip featuring three different polymer-coated transducers monolithically integrated with dedicated analog and digital circuitry will be detailed.

2.1 The Multi-transducer Chip

The single-chip chemical microsensor system is fabricated in an industrial 0.8-µm CMOS process as provided by austria*micro*systems, Unterpremstätten, Austria [47]. It includes three different transducers (mass-sensitive, capacitive, and calorimetric), all of which rely on polymeric coatings as sensitive layers to detect airborne volatile organic compounds (VOCs). Monolithic integration of microelectronic and micromechanical components allows for controlling and monitoring of the sensor functions, and enables on-chip signal amplification and conditioning, which drastically improves the sensor performance. The circuitry includes besides the sensor-specific driving circuitry, analog-to-digital (A/D) converters and a serial on-chip interface to transmit the data off chip [48].

The CMOS single-chip gas detection system comprises three polymer-coated transducers (capacitive, mass-sensitive and calorimetric) that record changes upon analyte absorption. The absorption of the analyte in the polymeric coating alters the physical properties of the polymer film, such as a) the mass and volume, which is detected by the mass-sensitive cantilever, b) the composite dielectric constant as detected by the capacitive transducer, and c) a certain amount of heat is generated during the absorption process (heat of analyte condensation and mixture), which is detected by the calorimetric transducer. All three transducer responses are simultaneously used to characterize the analyte or analyte mixture. Methanol, e.g., provides comparably low signals on mass-sensitive transducers due to its high saturation vapor pressure and low molecular mass. On the other hand, methanol has a dielectric constant of 33 and provides rather high signals on the capacitive transducer [49]. Drastic changes in the thermovoltages on the thermopiles are, e.g., measured upon exposure to chlorinated hydrocarbons, which have a low dielectric constant and thus provide only low signal intensity on the capacitor. The simultaneous probing and recording of changes of different polymer properties upon gas exposure leads to the introduction of additional dimensions into the feature space. More comprehensive and complementary information about the analyte present is collected. The combination of different transduction

principles, therefore, considerably enhances the detection and discrimination capability of the sensor system.

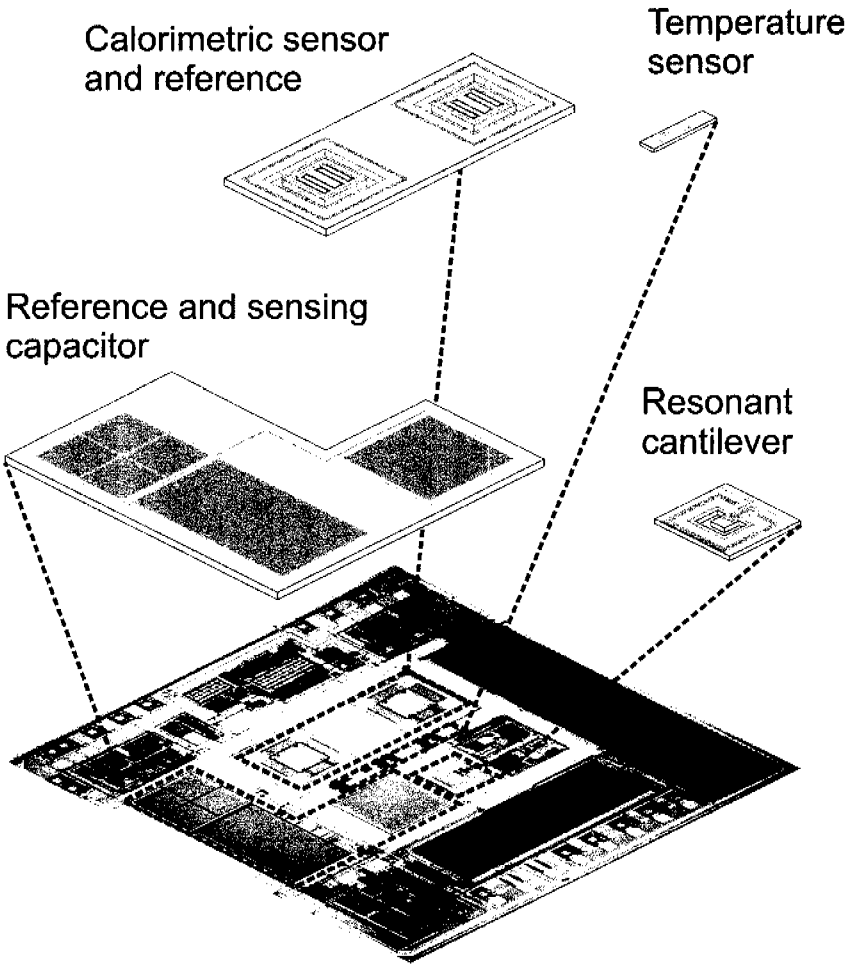

Figure 2-1. Micrograph of the single-chip CMOS gas sensor microsystem.

The overall microsensor system featuring a chip size of 7 by 7 mm^2 is shown in Figure 2-1. The sensor front end circuitry that has been integrated on the chip includes all the sensor-specific driving circuitry and signal-conditioning circuitry as will be described in Section 2.3 in the context of the different transducers. The analog/digital conversion is done on chip as well. This significantly enhances the signal-to-noise ratio since noisy connections are avoided and a robust digital signal is generated on chip and then transmitted to an off-chip data port via an I^2C digital interface. I^2C is a communication standard developed by Philips (Eindhoven, Netherlands). The I^2C bus interface offers the additional advantage of having only very few signal lines (essentially two) for bi-directional communication and also allows for operating multiple chips (up to 128) on the same bus system. An on-chip digital controller manages the sensor timing and the chip power budget. Via the I^2C digital interface the signals are transmitted to an off-chip data port (B5-X300 FPGA board, Burch, Australia). The FPGA board is then connected via a USB interface to a portable computer. A customized program allows

for the addressing of specific sensors/chips and the decoding and storage of the transmitted data.

2.2 Polymers as Sensitive Layers

Polymers are commonly used as chemically sensitive layers for the detection of volatile organic compounds (VOCs) in air. The interactions between the chemically sensitive polymer and the analyte range from weak physisorption to stronger sorption. The latter process is more selective but mostly not reversible. Therefore, a compromise between high selectivity and reversibility, which requires weak interactions, is necessary. For gas sensors relying on polymeric coatings usually polymers exhibiting only partial selectivity towards certain volatile organic compounds are used. For the chosen polymers and analytes the interaction is reversible. The interaction of organic volatiles with the polymer matrix is based on a defined number of physisorption mechanisms, which include induced dipole/induced dipole (London dispersion), dipole/induced dipole interactions, dipole/dipole interactions and hydrogen bonds (Lewis acidity/basicity-concept) [49-60].

Associated with these absorption mechanisms is the enrichment of the analyte in the polymer. The enrichment factor or partition coefficient, K_c, is a thermodynamic equilibrium constant defined as the ratio of the analyte concentration in the polymer, c_{Poly}, and the analyte concentration in the surrounding air, c_A [53].

$$K_c = \frac{c_{Poly}}{c_A}$$

Eq. 2-1

It is dependent on different parameters, such as the volatility of the vapor, the operation temperature and the interaction forces between the polymer and the analyte. The enrichment factor is constant for the chosen polymer/analyte combination at constant temperature and is independent of a transducing principle. The partition coefficient as any thermodynamic equilibrium constant is related to the Gibb's sorption energy, $\Delta G_{sorption}$:

$$\ln K_c = \frac{-\Delta G_{sorption}}{R \cdot T}$$

Eq. 2-2

Here, R denotes the molar gas constant and T the absolute temperature. Eq. 2-2 shows that the logarithm of the partition coefficient is inversely proportional to the temperature. Therefore, less analyte is absorbed into the polymer matrix at higher operation temperature, which results in a lower sensitivity of the sensor.

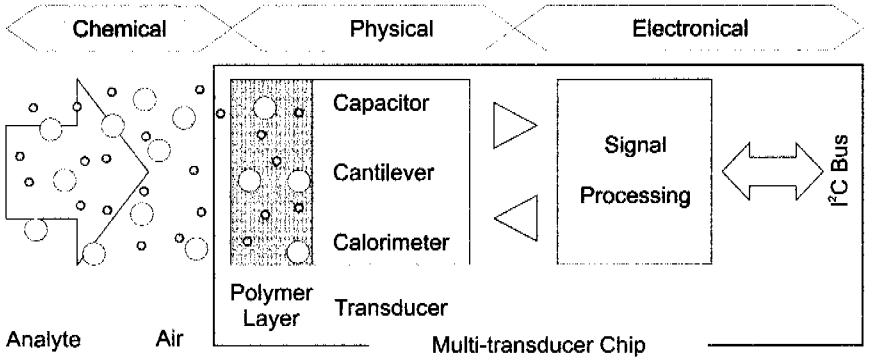

Figure 2-2. Working principle of the polymer-coated multi-transducer chip.

As has been previously mentioned, the low selectivity of the polymer coatings towards the organic compounds is acceptable in view of the reversibility of the absorption process. The desired identification of the compounds can be achieved by using an array of different partially selective sensors, and by applying numerical methods of data evaluation. Transducers probing different analyte profiles in a sensor array (multi-transducer chip) provide information on different aspects of the coating-molecule interactions. Changes in different polymer properties upon gas exposure are hence probed simultaneously, which leads to the introduction of additional dimensions into the feature space. More comprehensive and complementary information about the analytes present can be collected. Figure 2-2 shows the working principle of the single-chip gas detection system. The transducers monitor changes in three different physical properties of the sensitive layer and convert them into an electrical signal, which is then processed by the electronics.

2.3 Transduction Principles

2.3.1 Calorimetric Transducer

The thermoelectric calorimetric sensor is based on the Seebeck effect. It detects enthalpy changes evoked by the absorption (heat of condensation) or desorption (heat of vaporization) of analyte molecules in the polymer matrix. The physisorption processes lead to the release or absorption of a certain quantity of heat on the polymer-coated transducer and, hence, produce temperature variations [61, 62]. These temperature variations are measured by means of thermocouples, the hot junctions of which are located on a thermally insulated polymer-coated island (n-well) in a membrane, and the cold junctions of which are placed on the bulk silicon (Figure 2-3). The n-well acts as a heat spreader and is suspended in a membrane, which consists of the dielectric layers (silicon dioxide and silicon nitride) of the CMOS process. These dielectric materials are poor thermal conductors, the island is thermally insulated from the rest of the chip.

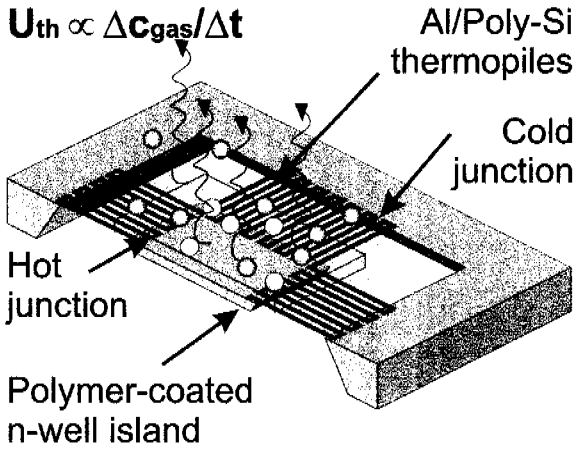

Figure 2-3. Schematic view of the calorimetric sensor.

The generated thermovoltages, which are proportional to the small temperature changes (mK range) [63], are measured by a thermopile that includes 132 thermocouples connected in series. From the materials available in a CMOS process, a polysilicon/aluminum thermocouple exhibits a Seebeck coefficient of 110 µV/K. The overall sensor system includes two 500 by 500 μm^2 membranes with 132 thermocouples each. One is coated with the chemically sensitive polymer, whereas the other membrane remains uncoated and serves as a reference [64]. The differential thermovoltage signal is then read out by connecting the outputs of the sensing and the reference thermopile to the input stage of a low-noise chopper-stabilized instrumentation amplifier on the chip. An analog-to-digital converter and decimation filter then translate the thermovoltage difference into a digital signal.

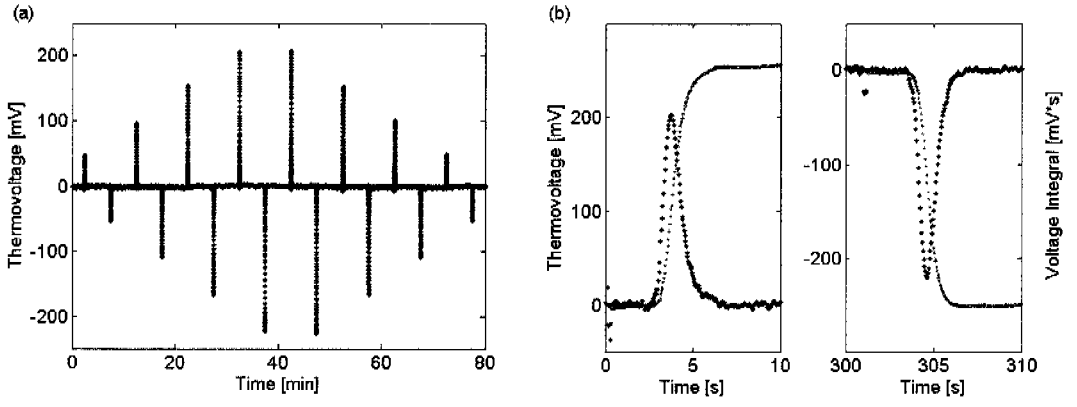

Figure 2-4. Plot of a prototype sensor signal. The transducer is coated with a approx. 2-µm-thick PDMS layer, the analyte is n-octane (concentrations of 300, 600, 900, and 1200 ppm) measured at 303 K. For better reproducibility the concentrations are ramped up and down (a). The close-up plot (b) shows the thermovoltage transients and the signal integral for the ab- and desorption of 900 ppm n-octane

In contrast to the capacitive and the gravimetric chemical sensors detailed below, which produce equilibrium-state signals, the calorimetric sensor only generates a signal as long as concentration changes occur (Figure 2-4). These are so-called transient signals, and there is zero signal at equilibrium state, since as many molecules absorb as desorb so that there is no net heat production [61, 62, 65, 66]. The absorption of analyte molecules into the polymer releases heat, mostly condensation heat (positive thermovoltage peak), whereas during desorption the heat needed for vaporization is abstracted from the environment (negative peak). Since the calorimetric sensor generates a transient signal, it is not the peak height but the integral of the thermovoltage over time or heating power, which is proportional to the analyte concentration in the gas phase, c_A. Therefore, the sensitivity, S, of the calorimetric sensor is given by:

$$S = \frac{\Delta \int U_{th} \cdot dt}{\Delta c_A} = G_{Cal} \cdot h \cdot K_c \cdot H_{sorption}$$

Eq. 2-3

where G_{Cal} includes the geometric properties of the membrane, h denotes the thickness of the polymeric layer, and K_c is the partition coefficient describing the analyte enrichment in the sensitive layer. The sensitivity is proportional to the sorption enthalpy, $H_{sorption}$. The sorption enthalpy includes the heat of condensation or vaporization and the heat released or absorbed through polymer analyte interactions, the so-called heat of mixing [49]. The condensation or vaporization heat contribution dominates in most cases [49] so that in a first-order approach, this contribution alone can be used to characterize the transducer-specific signal intensities. The calorimetric sensor has been calibrated by applying a known and well-defined heating power to the thermopile by means of polysilicon heaters that are integrated on the membranes. As an exemplary sensor signal the transient response of a poly(dimethylsiloxane)-coated calorimetric sensor upon exposure to different concentrations of n-octane (300, 600, 900, and 1200 ppm) in air at a temperature of 303 K is shown in Figure 2-4. The sensors have been alternately exposed to analyte-loaded gas and pure carrier gas (air).

The enthalpy changes can be approximated by integrating over the peak area of the sensor signals. The peak maximum and signal characteristics of the absorption and desorption signals of the same analyte concentration slightly differ. This is mainly a consequence of non-idealities in the measurement manifold (slightly different gas stream characteristics for analyte-loaded and pure carrier gas). For the data evaluation the positive and negative sensor responses (ab- and desorption process) have been taken into account, the absolute value of both integrals have been calculated and afterwards averaged for each concentration step. The calorimetric transducer is less sensitive and features less favorable signal-to-noise characteristics in comparison to the cantilever and the capacitor. Therefore, the limits of detection (LODs) of the calorimetric method are higher than those of the other transducers: The LOD is, e.g., 40-50 ppm toluene using poly(etherurethane).

2.3.2 Mass-sensitive Resonant Cantilever

The CMOS mass-sensitive chemical sensor is based on a 150 µm-long and 140 µm-wide cantilever. The cantilever consists of a stack of silicon, thermal oxide and vapor-deposited silicon oxide and silicon nitride. The cantilever is thermally actuated, i.e., the actuation relies on the different thermal expansion coefficients of the silicon and the silicon oxide or nitride (bimorph effect). The cantilever oscillation is actuated by periodically applying electric pulses to heating resistors located at the cantilever base. The beam vibration is detected by piezoresistors in a Wheatstone-bridge configuration embedded in the base of the cantilever, where the bending/stress and, thus, the achievable output signal are maximal. An on-chip low-noise, fully-differential difference amplifier with a gain of 30 dB amplifies the output signal of the Wheatstone-bridge. The cantilever acts as the frequency-determining element in a feedback oscillation circuit, which has been integrated on the chip with a counter [48, 67]. As a result, the cantilevers oscillate at their fundamental resonance frequency of approximately 380 kHz with a frequence stability better than 1 Hz.

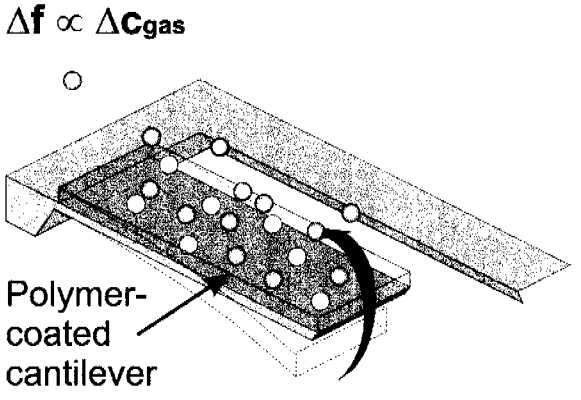

Figure 2-5. Schematic view of the mass-sensitive cantilever.

The operation principle of the resonant cantilever gas sensor is shown in Figure 2-5: Upon analyte absorption in the chemically sensitive polymer on the cantilever, the oscillating mass increases. As a consequence the resonance frequency of the system decreases. This causes a negative frequency shift, Δf. The sensitivity, S, of a polymer-coated cantilever is given by:

$$S = \frac{\Delta f}{\Delta c_A} = G_{Cant} \cdot h \cdot K_c \cdot M_A$$

Eq. 2-4

Here, Δf denotes the shift of the mechanical resonance frequency of the cantilever and c_A is the analyte concentration in the gas phase. Eq. 2-4 includes a summary term for the mechanical properties of the cantilever, G_{Cant}, see also Ref. [68]. Furthermore, the sensitivity is proportional to the polymer layer thickness, h (for $h < 5$ µm [69]) and the

partition coefficient, K_c, as well as to the molecular mass of the absorbed analyte, M_A [68].

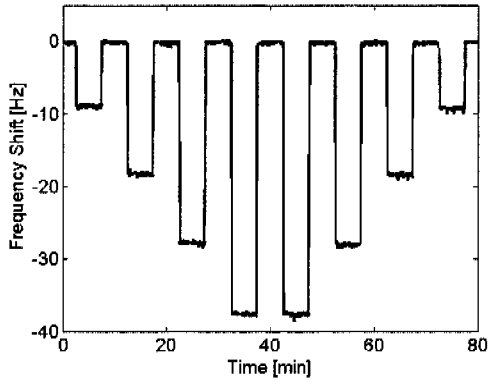

Figure 2-6. Sensor signals of the mass-sensitive cantilever. The signals represent frequency shifts of a PDMS-coated cantilever upon exposure to n-octane (300, 600, 900, and 1200 ppm) at 303 K. The thickness of the polymer layer is approx. 2 µm.

Swelling effects and analyte-induced changes in the elastic modulus of the polymer have been neglected since only very low analyte concentrations have been applied [69].

Exemplary measurements of different concentrations of n-octane detected by a poly(dimethylsiloxane) coated cantilever are shown in Figure 2-6. The concentrations are ramped up and down to test for reproducibility. The sensor drift and the offset have been subtracted from the displayed results. For the resonating cantilever the limit of detection is., e.g., 1-2 ppm for toluene using poly(etherurethane).

2.3.3 Capacitive Sensor

The capacitive sensor (Figure 2-7) is based on two sets of interdigitated electrode structures, which correspond to the two plates of a parallel plate capacitor. The sensor monitors changes in the dielectric properties of the polymer upon analyte absorption. The capacitors are fabricated using exclusively layers and materials available in a standard CMOS process. One of the electrodes is made from the first CMOS metal layer, the other is realized as a stack of the first and second metal layer. By applying this "three-dimensional" design the sensitivity of the capacitive microsensor is enhanced since the number of electric field lines and their density within the polymer volume is increased [64]. The dimensions of the capacitor are 814 by 824 μm^2 and it includes 128 finger pairs. The electrode width and spacing are 1.6 µm.

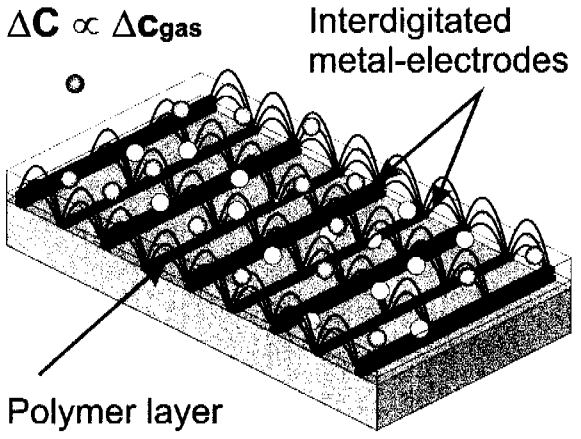

Figure 2-7. Schematic view of the capacitive sensor.

The nominal capacitance of the interdigitated capacitor is a few pF, whereas capacitance changes upon analyte absorption are in the aF range. Thus a dedicated on-chip measurement configuration and specific signal conditioning circuitry is needed. The sensor response is read out as a differential signal between a passivated reference and a polymer-coated sensing capacitor. A digital output signal is then generated by comparing the minute loading currents of both capacitors using a fully differential second-order sigma-delta-modulator circuitry [64]. The modulator provides a pulse density modulated output that can be decimated by using a frequency counter. Thus, the output signal is a frequency change, which is proportional on the capacitance change upon analyte absorption in the polymer (Eq. 2-6).

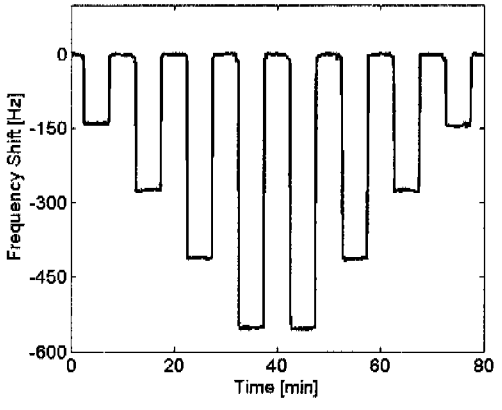

Figure 2-8. Read-out signal of the capacitive sensor. The displayed frequency shifts (sigma-delta-converter output) have been recorded using a PDMS coating to detect n-octane (300, 600, 900, and 1200 ppm) at 303 K. The thickness of the polymer is approx. 2 μm.

For thin polymer layers the swelling of the polymer upon analyte absorption always results in a capacitance increase regardless of the dielectric constant of the absorbed analyte. This is due to the swelling of the polymer, which leads to an increased

polymer/analyte volume within the field line region. The polymer/analyte composite exhibits a larger dielectric constant than the substituted air [70]. Thin polymer layers include layer thicknesses of less than half the periodicity of the electrodes. On the other hand, the capacitance change for a polymer layer thickness larger than half the periodicity of the electrodes is determined by the ratio of the dielectric constants of analyte and polymer. If the dielectric constant of the analyte is larger than that of the polymer, the capacitance will be increased, if the polymer dielectric constant is larger than that of the analyte, the capacitance will be decreased. This effect has been previously detailed and supported by simulations [71, 72]. The investigations in the present thesis have been restricted to large layer thicknesses (2 µm) so that the sensor responses are solely determined by the dielectric coefficients of analytes and polymers, and the effects of swelling are not influencing the sensor signal. The change in dielectric constant upon analyte absorption, $\Delta\varepsilon$, can be either positive or negative

$$\Delta\varepsilon \propto \varphi_A \cdot (\varepsilon_A - \varepsilon_{poly})$$

Eq. 2-5

Here, ε_A is the dielectric constant of the analyte (in liquid state), ε_{poly} is the dielectric constant of the polymer, and φ_A the amount of absorbed analyte expressed as volume fraction. The equation shows, that sensor signals are positive for analytes with a dielectric constant larger than that of the polymer and negative otherwise. For thick polymer layers the sensitivity, S, is the change in capacitance, ΔC, divided by the change in the analyte concentration, Δc_A:

$$S = \frac{\Delta C}{\Delta c_A} = G_{Cap} \cdot K_c \cdot \Delta\varepsilon$$

Eq. 2-6

where G_{Cap} includes the capacitor geometry. The sensitivity is, in contrast to the other transducers (see Eq. 2-3 & Eq. 2-4), not depending on the layer thickness since the electric field has a defined extension for a given electrode spacing. i.e., the probed polymer volume is constant and is only depending on the electrode spacing. The polymer layer was chosen to be considerably thicker than the electric field extension so that the probed volume is completely filled with polymer in any event. The partition coefficient, K_c, includes the polymer/analyte interactions, and $\Delta\varepsilon$ is the change in the dielectric properties of the polymeric matrix upon analyte absorption. More details on capacitive sensing and Eq. 2-5 can be found in Refs [48, 70, 73, 74].

Figure 2-8 displays signals of a poly(dimethylsiloxane)-coated capacitive transducer. The sensor has been exposed to n-octane at concentrations of 300, 600, 900, and 1200 ppm. The negative sensor response for this polymer/analyte combination is caused by the smaller dielectric constant of n-octane (ε_A = 1.95) with respect to that of the polymer (ε_{poly} = 2.8) [64, 74]. The capacitive sensor shows rather low noise levels

of approximately 10 Hz; the limit of detection using, e.g., a poly(etherurethane) layer is 5-8 ppm for toluene.

2.4 Architecture of the Multi-sensor Chip and System Interface

Figure 2-9 shows a block diagram of the system architecture of the multi-transducer chip. It comprises three fundamentally different sensors (capacitive, mass-sensitive and calorimetric sensor) and an additional temperature sensor.

The temperature sensor has been integrated on the system chip, since the physisorption processes of organic volatiles in polymers are strongly temperature-dependent. It enables reliable quantitative measurements. As a rule of thumb, a temperature increase of 10 °C decreases the fraction of absorbed analyte molecules by approximately 50%, which results in a drastic sensor signal change. The temperature sensor relies on the linear temperature dependence of a bipolar transistor available in the CMOS process [67]. The voltage is converted to a digital signal using a sigma-delta-converter. After calibration, the temperature sensor exhibits an accuracy of 0.1 K at operation temperatures between 223 and 383 K [75].

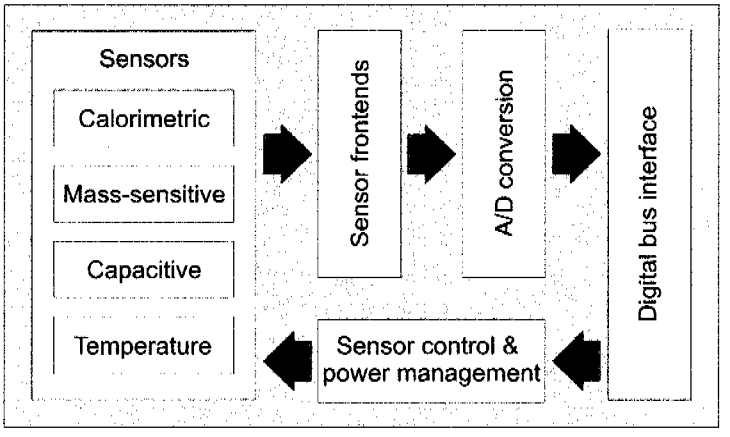

Figure 2-9. Schematic of the overall microsystem architecture. It consists of different types of sensors, driving and signal-conditioning circuitry (sensor front end), analog-to-digital converters, sensor control and power management unit, and a digital interface.

Analog sensor front ends provide the sensors with the sensor-specific driving circuitry (e.g., provision of bias voltages and currents) and signal-conditioning circuitry to detect the small sensor signals at minimal noise. The sensor signals are amplified on the spot to relax the noise requirements of subsequent stages. The analog signals are converted to robust digital signals on-chip and then transmitted to an off-chip data port via an I^2C digital interface. The I^2C-protocol clearly defines addressing, word length, master/slave communication, and the start/stop-conditions without adding extensive overhead that requires large amount of on-chip memory. For clock and data transfer

only two wires are needed. Up to 128 devices can be connected on the same bus. A simple arbitration algorithm solves the problem of data collision.

The monolithic implementation of the single chip microsystem containing three micromachined sensors requires only seven bondpads: Three for supply voltages, one for a clock signal, one for reset and two for the serial interface. The additional four pads are needed to define the address of each individual chip.

Via the I^2C-interface the individual addresses and the settings of the different programmable parameters, such as amplification factors, can be defined for the three sensors. An on-chip digital controller receives and interprets the commands from an external signal processing unit. This controller also manages the sensor timing, the chip power budget and the access of the single sensors to the serial interface, when the measurements of the three sensors are transmitted simultaneously [67, 75].

The multi-sensor chip is fixed on a standard 24-pin ceramic dual-in-line-package (CERDIP) and electrically connected by wire-bonding. A dedicated custom-built printed-circuit-board (PCB) provides the operational system with stable supply voltages and currents. The PCB also allows for addressing different sensor chips, if several systems are working simultaneously. Via the two signal lines of the systems' I^2C bus the coded sensor signals are then transmitted to an off-chip data port (B5-X300 FPGA board, Burch, Australia). The FPGA board is connected via the USB interface to a computer. A customized program allows for addressing specific sensors/chips and for decoding and storage of the sent data.

3 CHIP FABRICATION AND EXPERIMENTAL SETUP

CMOS technology is the most common technology for the fabrication of integrated circuits. It also allows for the integration of different transducers or an array of identical transducers with signal conditioning and –processing circuitry on the same chip. The multi-transducer gas sensing system used throughout this work is based on this technology. A well-established industrial CMOS-process has been used for the fabrication of the transducers and the circuitry. Afterwards, the micromechanical features such as calorimetric membranes and the resonating cantilever beam are released using post-process micromachining.

In this chapter the fabrication of the multi-transducer chip, a new post-processing procedure for membrane-based sensor arrays [76] and the experimental setup are presented.

3.1 CMOS Fabrication and Post-micromachining

The circuitry and the basic sensor elements have been fabricated in a modified industrial CMOS process in combination with post-CMOS micromachining [77, 78]. The used CMOS process is a 0.8-µm double-metal, double-polysilicon CMOS process provided by austria*micro*systems, Unterpremstätten, Austria [47]. The fully processed wafers have been thinned down to a thickness of 380 µm and a silicon nitride layer, which serves as a passivation layer and, later on, as a mask for the post-processing, has been deposited on the wafer back side. The use of a monolithic CMOS MEMS approach limits the temperature for further post-processing steps to 400 °C, since higher temperatures would destroy the aluminum metallization and affect the transistor parameters.

After completion of the industrial CMOS process sequence, several post-processing steps, conducted on wafer level, are necessary to release the membranes of the calorimeter and the mass-sensitive cantilever beam. The silicon nitride on the wafer back side that has been deposited after the CMOS-fabrication is opened with a reactive ion etching (RIE) step. Next, membranes are formed by etching the bulk silicon from the wafer back side. Here, it has been taken into account that the sidewalls of the etch pit exhibit an angle of 54.74° with the wafer surface as a result of the anisotropic silicon etching with potassium hydroxide (KOH). Thus, the thickness of the bulk wafer has to be included into the mask design. To assure a defined membrane thickness, the anisotropic wet etching is performed in combination with an electrochemical etch stop technique (ECE) [78, 79].

ECE is, in principle, based on the anodic oxidation of silicon [80, 81]. This oxidation can be achieved using a highly n-doped area (n-well), which is connected in a reverse-biased diode configuration to the slightly p-doped bulk silicon. The implantation of the n-well is part of the standard CMOS process sequence. The implantation shape and depth determine the thickness of the composite sensor membranes (silicon oxide,

silicon nitride and silicon) and suspended sensor structures to be fabricated. The implantation depth in the n-doped areas is approximately 3.5 µm. During the metallization steps of the CMOS process all n-well structures are electrically contacted by a network of conducting lines and linked to a small circuitry unit that provides a bias potential. The bulk substrate that is adjacent to the membrane structures constitutes the counter electrode for the ECE.

After the anisotropic wet etching the cantilever is released by reactive ion etching from the wafer front side. The remaining passivation layers on the front side and the n-well membrane around the designated cantilever are removed by using CHF_3/CF_4 and SF_6, respectively.

Before dicing the wafers precautionary measures have to be taken to avoid fissures of the fragile membrane structures or particle contamination. A back side stabilization of the mechanical structures constitutes of a thick layer of photoresist, which has been spun onto the wafer before the cantilever release by RIE. Thereafter, the front side is coated by another layer of photoresist. Alternatively a special adhesive foil can be used on the wafer front side. This foil (Adwill P-5780, Lintec Corp., Japan) can be safely removed after exposure to UV-light and a subsequent heating step.

3.2 New Fabrication Method for Membrane-based Arrays

The fabrication of narrowly spaced membrane arrays is of interest in many MEMS applications, particularly for integrated sensors and actuators fabricated in CMOS-MEMS technology [82]. The co-integration of electronics with sensor structures allows for a first-order signal processing already on the chip. Moreover, larger numbers of active devices or transducer structures such as cantilevers or thermopiles can be addressed and controlled, while keeping the number of needed interconnections reasonably low [75].

For the fabrication of suspended, deformable micromechanical structures two methods are commonly used: (i) anisotropic wet etching with KOH (potassium hydroxide) or TMAH (tetramethyl ammonium hydroxide) or (ii) deep reactive ion etching (DRIE) [8, 83, 84]. These bulk-micromachining techniques are usually applied from the wafer back side since the release of membranes from the front side of the device requires a subsequent and cumbersome resealing step (for the protection of the metal structures), if a sealing is feasible at all.

Wet anisotropic etching entails the use of a simple setup at low cost [83]. To fabricate a silicon membrane, the timed etch stop is the simplest solution. However, parameters such as the etchant concentration and temperature, the solution agitation, the wafer thickness uniformity, as well as impurities in the wafer have a strong effect on the etching rate. Consequently, the timed etch stop is not very precise and reproducible so that the resulting membrane thickness may vary. For CMOS-based sensor systems a well-defined thicknesses of silicon membranes and suspended structures can be achieved by using an "electrochemical etch stop" (ECE) technique. However, due to

the characteristically inclined sidewalls of the etch pits that represent the (111) crystal planes (54.74°) the area required for a micromachined structure on the wafer back side is significantly larger than the micromachined structure itself [85]. This precludes the fabrication of narrowly spaced micromachined structures using only anisotropic wet etching techniques.

Time-multiplexed deep etching (TMDE) [86], commonly known as DRIE, on the other hand, leads to almost straight sidewalls and, therefore, enables high-aspect-ratio structures to be etched in close proximity to each other into a silicon substrate. It thus allows for a close packing of micromachined sensor structures in arrays. The fabrication of silicon-based membranes with DRIE requires silicon-on-insulator (SOI) wafers, where a silicon oxide layer is sandwiched between two silicon layers and serves as reliable etch stop [83]. Furthermore, this technique also has some problems and limitations with regard to flexibility and applicability. Additionally, there are issues concerning the non-uniformity of the etching depth over the wafer and the formation of silicon-grass or black-silicon at the bottom of the etch pit [87-91]. Owing to these difficulties the fabrication of membranes of different size as required, e.g., on multi-project wafers (MPW), or the fabrication of suspended silicon structures is not feasible using DRIE techniques.

In the course of this thesis, a novel approach has been developed that combines DRIE and ECE. The process sequence enables the fabrication of silicon-based membranes, as well as sensor arrays featuring different membrane sizes. The described method has been used to process bare silicon substrates for test purposes, as well as wafers from an industrial CMOS process as provided by austria*micro*systems, Unterpremstaetten, Austria [47]. The CMOS wafers feature n-well-based microstructures, such as cantilevers and microhotplates that have been monolithically integrated with the associated circuitry [11, 92].

3.2.1 Motivation

As already described in the previous section wet anisotropic etching in combination with an electrochemical etch stop allows for the fabrication of suspended structures of a defined thickness (given, e.g., by the thickness of the n-well). Nevertheless, the angled sidewalls obviate the arrangement of structures in close proximity. With its almost vertical etch profile DRIE offers the advantage of densely packed micromachined structures, but process effects, such as trenching, allow for fabricating only uniform-size structures on a wafer.

All these considerations lead to the idea of developing a process sequence that combines the favorable characteristics of wet and dry etching techniques of silicon. In recent years, several groups have pursued such a process sequence for various purposes [46, 93, 94]. However, with respect to DRIE etch openings the published work encompasses designs of equal opening dimensions, the uniformity of the final etching depth is less important, or a thermal oxidation step is performed after the DRIE trench etching.

For an engineering run at a CMOS foundry multi-project wafers (MPW) are used in most cases; the lateral dimensions of the different structures to be etched can, therefore, diverge by one order of magnitude. A higher density of the structures also decreases the costs of a single device for production runs. The RIE lag causes problems in using dry etching techniques for such wafers as the etching rate varies strongly in dependence of the etch opening size as shown in Figure 3-1. The RIE lag can be compensated for by sophisticated process tuning as proposed in Ref. [95], but this necessitates a rather expensive setup of processing equipment.

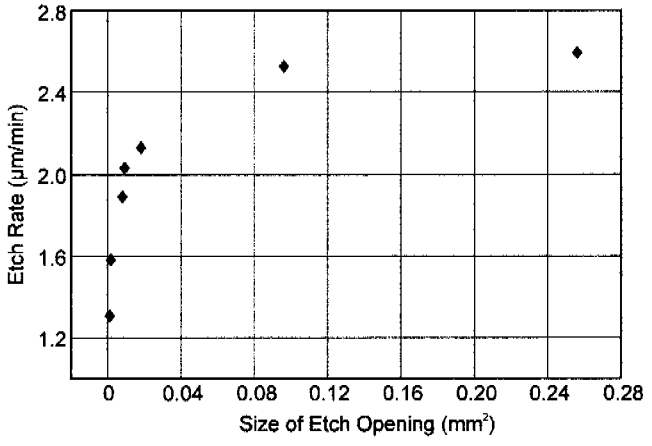

Figure 3-1. Etching rate versus size of the etch opening for the DRIE process. The graph shows the variation of the etching rate over a wafer featuring different opening sizes. Membranes of different size cannot be released in a single DRIE step.

The goal of the process development done in this work is to devise a concept that is suitable for post-processing in a fabless, foundry-based approach. This concept is based on easily accessible standard processes. After thorough characterization the employed techniques are usable as long as the foundry and post-CMOS processes remain the same.

3.2.2 Experimental

3.2.2.1 Approach

To combine the possibility of tightly packing micromachined structures using DRIE with the precise etch stop that is attainable using ECE on a standard MPW CMOS wafer, the concept of a grid-like masking pattern has been introduced. This way, the lateral area of each micromechanical structure is subdivided into small subunits of unity size and shape.

After the standard CMOS process sequence, the back sides of the 380-µm-thick wafers from the foundry have been polished. A low-temperature silicon nitride of 1 µm thickness has been deposited for passivation and as an etch mask for the wet anisotropic etching. The processing temperature of the nitride is 300 °C and is below the critical temperature for the metallization layers of the CMOS process (approximately 400 °C). Apart from the back side silicon nitride layer no additional dielectric layers have been deposited.

The process flow of the developed fabrication sequence is described in Figure 3-2. After the CMOS process, the wafer accommodates a variety of micromechanical structures to be released, e.g., silicon and dielectric membranes (Figure 3-2 (a)). To start the post-processing sequence, a photoresist is applied on the wafer back side (opposite side to the CMOS layers) as an etch mask for the dry etching. Then, the resist is exposed and developed. The mask pattern is afterwards transferred to the passivating silicon nitride layer with an RIE step - (b) and (c). The subsequent DRIE etching step extends the grid pattern deep into the wafer, just 20 µm short of the wafer top surface (d). The residual photoresist is then removed, and the patterned silicon nitride passivation layer serves as an etch mask during the short wet etching of the remaining silicon using the ECE network (e).

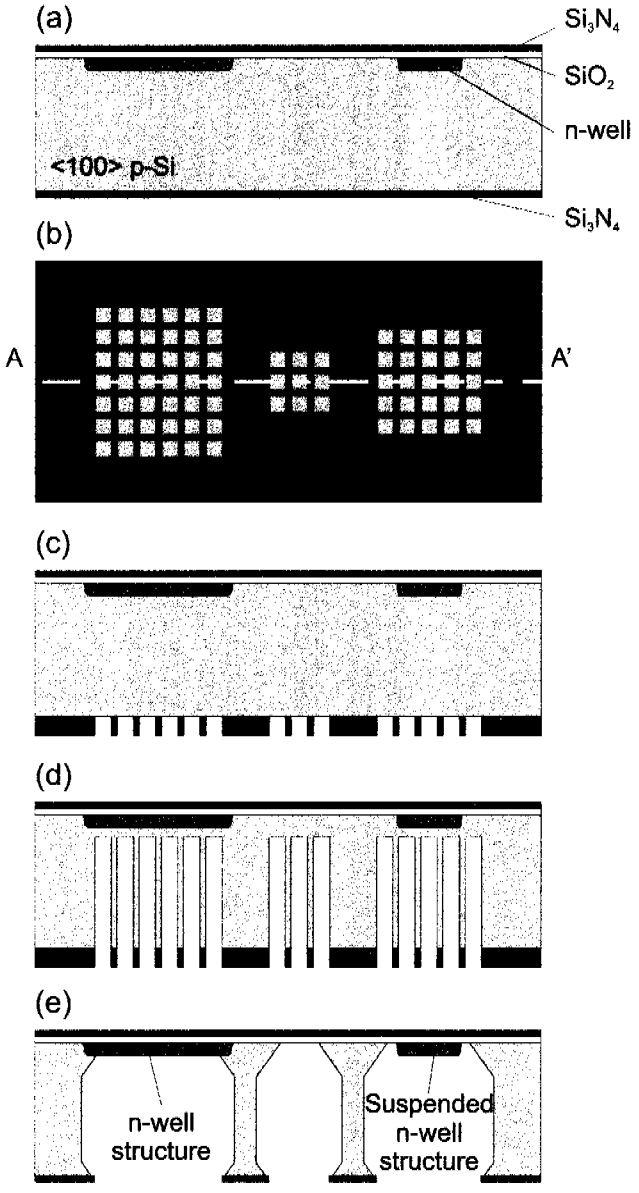

Figure 3-2. Process flow for a membrane release combining DRIE with KOH and ECE steps: (a) Substrate after the CMOS process. (b) Top view through the photoresist and the opened silicon nitride. (c) Cross section AA' after resist development and silicon nitride etching. (d) AA' after a DRIE etching of a defined time. (e) Cross section AA' after the subsequent ECE etching step.

3.2.2.2 Deep Reactive Ion Etching

For the removal of the passivating PECVD silicon nitride on the wafer back side and the following DRIE (Figure 3-2 (c) and (d)) a conventional photoresist can be used as etch mask. The photoresist has to be chosen thick enough to withstand both process steps. A 6-µm-thick resist has been used (AZ4562 by Hoechst, Frankfurt, Germany)

that features an etching selectivity of silicon to resist of approximately 120:1. With this photoresist a minimal resolution of 2 µm has been achieved.

In Figure 3-3 the grid-like photoresist patterning to fabricate different membranes and membrane arrays is depicted for two different wafers. A Multiplex ICP System (Surface Technology Systems (STS), Abercarn, UK) has been utilized for the DRIE in this work. The process temperature was 15 °C.

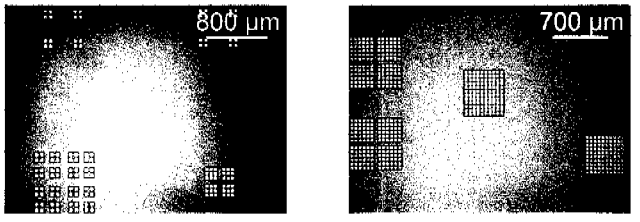

Figure 3-3. Micrograph of the mask pattern for membrane arrays and structures of different size.

3.2.2.3 Electrochemical Etch Stop

After the reactive ion etching steps the remaining photoresist is removed from the wafer back side. The silicon nitride as patterned during the RIE process provides the etch mask for the following wet chemical etching. ECE in principle is based on the anodic oxidation of silicon [46, 78, 79, 93-96]. This oxidation can be achieved using a highly n-doped area (n-well), which is connected in a reverse-biased diode configuration to the slightly p-doped bulk silicon. The implantation of the n-well is part of the CMOS process. The implantation shape and thickness determine that of the silicon sensor membranes and suspended sensor structures to be fabricated. The implantation depth of the n-doped areas is approximately 3.5 µm. As described earlier all the n-well structures are electrically contacted by a network of conducting lines and linked to a small circuitry unit that provides a bias potential. The bulk substrate that is adjacent to the membrane structures constitutes the counter electrode for the ECE. Moreover, a dedicated contact reticle is included on the wafer that hosts macroscopic aluminum contact pads on the wafer front side close to the wafer edge. These aluminum pads provide electrical contact to the bulk substrate and the n-well based membrane structures.

During the wet anisotropic etching it is mandatory that the wafer front side with all its aluminum pads and the circuitry is protected against KOH exposure, so that a dedicated wafer holder (AMMT, Germany [97]) has to be used. The wafer front side is sealed in a chamber filled with air; a glass cover allows for visual control, if there is any leakage. On the protected front side of the wafer, spring contacts provide electrical connection to the ECE pads on the wafer. The electrode contacts are routed via wires through the wafer holder to contacts outside the etching solution. The wafer back side is exposed to the etchant with the patterned silicon nitride serving as an etch mask.

Additionally, an adhesion promoter (AR 300-80, Allresist GmbH, Germany) and a protective poly(methylmethacrylate) (PMMA) (XAR-PC5000, Allresist GmbH, Germany) layer have been applied to the wafer front side by means of spin-coating. During the coating process the ECE pads have been covered with tape so that they can afterwards be electrically connected using the spring contacts of the wafer holder. The polymeric front-side coating is only a precaution measure in case a membrane should break owing to, e.g., intrinsic stress, during the last step of the wet etching. The polymer precludes that the etching fluid leaks into the sealed chamber and damages the CMOS structures on the wafer front side. The PMMA layer only withstands several minutes of exposure to the etching solution.

During the ECE process the n-type silicon is kept at a potential, at which anodic oxidation occurs by a reverse biasing of the pn-junction between the n-well and the bulk substrate. The p-type silicon is maintained at the open-circuit potential (OCP). In practice, there is often a small leakage current through the pn-junction. A minute current already suffices to passivate the silicon so that the p-substrate may not be etched. To overcome this problem, a setup denoted "four-electrode setup" (4EC) [80, 93] has been used. A potentiostat controls the solution potential in a currentless manner through a reference electrode and regulates the counter electrode potential accordingly. The p-type silicon is biased by the potentiostat and kept close to the OCP, i.e., between -1.5 to –5 V with respect to the reference electrode. An additional voltage supply maintains the n-silicon potential at 0 V.

In this work, the KOH etching has been performed using a 6-molar (27 wt %) KOH at 80 °C with an etching rate of approximately 1.5 µm/min. The relatively low etching temperature allows for a better control of the etching process. The thickness of the n-well membrane is approximately 5.5 µm after the ECE due to the additional depletion area of the reverse-biased pn-junction. The original n-well thickness is 3.5 µm.

3.2.3 Results

Using the described process, various micromachined silicon-based membranes and structures have been realized. The MPWs have been fabricated in a standard 0.8-µm-CMOS process on p-type (100) 4-inch-wafers with a substrate thickness of approximately 380 µm.

3.2.3.1 Mask Design and Lithography

The smallest common area unit has been calculated with regard to the different structure and membrane sizes on the MPW design. It has to allow for enough space for sufficient lateral etch pit separation. To adapt the grid pattern to the dimensions of the different structures the width of the grid separation can vary: Its minimum width is determined by the maximum resolution of the photolithography step, while the maximum should be correlated to the intended etching time/depth of the ECE process step, i.e., the walls should still be completely removed during the final wet etching step.

The smallest common subunit is a square-shape etch opening of 49 by 49 μm^2, and the separation of the etch openings ranges from 3 to 23 µm for the different structures and membrane sizes. It was found that for larger membranes or structure sizes the separation wall of the etch pits should be wider than the thickness of the resist, since there are considerable refraction effects during exposure: The thickness of the photoresist decreases after the development for membrane dimensions larger than 200 µm. If the separation walls are chosen too narrow, the remaining resist grid might not withstand the following RIE and DRIE process steps. If the pit separation wall is selected too wide, residues of the grid pattern may not be completely removed during the final ECE process (Figure 3-4).

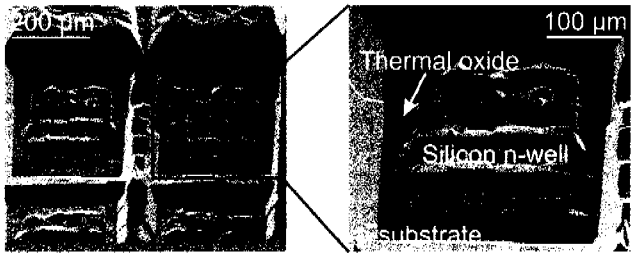

Figure 3-4. SEM micrographs of the back side of a silicon n-well membrane structure after the ECE process. The grid walls were too large (15 µm), so that the grid pattern is still visible on the n-well after the etch stop was reached.

The overall grid pattern area exceeds the target membrane size by 11 µm on each side. For 20 µm remaining to be etched during the ECE process the margin in the lateral dimensions should be around 14 µm. Selecting a smaller margin allows for additional over-etching time in the KOH-solution, which ensures the complete removal of the pit separation walls. Some examples of transducers and suspended structures, as well as the feature and subunit sizes are given in Table 3-1.

	Membrane size [μm^2]	Window size for etching [μm^2]	Number of subunits	Spacing between subunits [µm]
Calorimetric sensor array	300x300	319x319	6x6	5
	200x200	211x211	4x4	5
Tactile pressure sensor array	104x104	121x121	2x2	23
	140x140	166x166	3x3	9.5
Hotplate	500x500	517x517	9x9	9.5
AFM array	1900x700	1919x721	35x13	6
Cantilever array	600x2000	622x2025	12x39	3.1

Table 3-1. Examples of different sensor structures relying on suspended silicon structures on a multi-project wafer. The size of the subunits is 49 by 49 μm^2.

In cases, in which the sensor structures are very sensitive to over-etching, the margins can be chosen even smaller than 11 µm. In Figure 3-5 a micrograph of a 2 x 2 calorimetric sensor array is shown. The new combined etching process allowed to place the individual membranes in close proximity to each other, in this case 51 µm, whereas the distance would have been 580 µm using a standard ECE etching process.

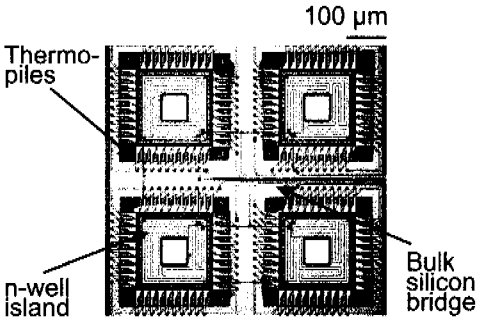

Figure 3-5. Micrograph of a calorimetric sensor array. The center of the membrane is an n-well island suspended in a dielectric membrane.

3.2.3.2 DRIE

In several test runs, the etching rate using the 49 by 49 μm^2 etch opening (mask) to a depth of approximately 360 µm was determined to be 2.3 µm/min under the etching conditions specified in the previous experimental section. The etching rate is also influenced by the loading, i.e., the overall area of silicon exposed to the etchant. The etching time has to be adjusted in view of the varying thickness of the CMOS wafer. The target thickness of the silicon to remain unetched is 20 µm. The major source for etching depth variations in the DRIE step is the wafer thickness variation. It can be as much as ±2 µm. To determine the important parameters such as etching rate, minimal resolution, etc., dummy wafers with a low-temperature silicon nitride layer of 1 µm thickness have been used for the test runs.

Scanning electron (SEM) micrographs of several array structures on bare Si-substrate after the DRIE step and the subsequent ECE are shown in Figure 3-6. On the left side of Figure 3-6 the results of the DRIE process are shown. The uniform etching depth within the grid area is remarkable, especially in Figure 3-6 (b). The remaining silicon walls between the etch pits have been damaged during the dicing of the samples. This can be seen particularly well in Figure 3-6 (a).

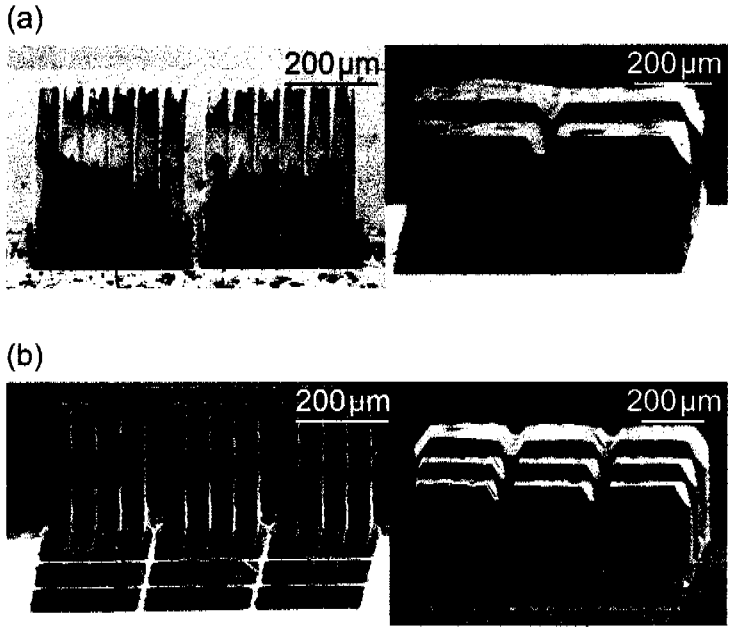

Figure 3-6. SEM micrographs of structures after a DRIE step using 49 by 49 μm^2-sized etch openings (mask level) and a subsequent 20-minute wet etching step in 6-molar KOH at 80 °C. Here a Si-substrate was used. The view angle is from the back side into the etched cavity. (a) Part of a 2 x 2 array. Each single structure has 6 x 6 etch openings and 5 µm width of the separation walls. The spacing of the subunits is 51 µm. (b) 3 x 3 array, where each single structure has 4 x 4 etch openings separated by 5 µm walls. The structure spacing is 54 µm.

The walls between the unity etch openings (49 by 49 μm^2) of the mask were 5 µm in Figure 3-6, whereas the spacing between the different micromachined structures of the array was 51 µm and 54 µm, respectively.

3.2.3.3 Wet Etching and ECE

After the DRIE step, the bare Si-substrate was etched for 20 min in 6-molar KOH at 80 °C. The results are shown in Figure 3-6 (right side). As can be seen, the narrow silicon pillars and separation walls between the unity etch openings have been completely removed, whereas other, wider separation walls partly remained.

The same process has been performed for the CMOS wafers. For the anisotropic wet etching the ECE network on the wafer has been connected in a 4EC configuration before the wafer holder is immersed into the KOH. After the etch stop is reached, the wafer is further etched for another 5-10 minutes to ensure the complete removal of the grid structures. The over-etching also levels out etching depth variations after the DRIE, which are caused by a non-uniformity of the wafer thickness. Figure 3-7 shows a plot of the etching current, I_{CE}, between the p-substrate and the counter electrode versus time during the wet etching phase of the combined process. The current peak in an ECE process is usually clearly detectable, when the etch stop is reached the current

drops almost immediately. For the combined DRIE/ECE process, however, the peak is wide (Figure 3-7) owing to the separation walls remaining after the DRIE. The ongoing lateral etching keeps the I_{CE} current at a high level for extended times.

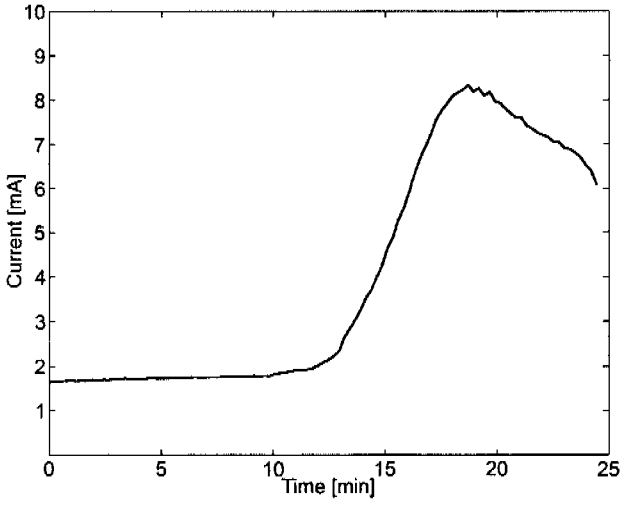

Figure 3-7. Etch current, I_{CE}, versus etching time during the final KOH etching of silicon using the 4EC setup.

SEM micrographs of the micromachined features of a CMOS wafer after the ECE-assisted KOH wet etching are shown in Figure 3-8. Due to the high aspect ratio (wafer thickness of 380 µm) and the angle, from which the micrographs were taken, the dimensions appear to be distorted. The scale bar relates to the structures at the bottom of the etch pit.

In Figure 3-8 (a), a 2 x 2 membrane array with suspended n-wells that are electrically and thermally decoupled from the substrate silicon is shown. 51-µm-wide silicon bridges have been left between the membranes of the array. They are connected to the bulk silicon and provide good mechanical stability to the array. These silicon bridges also feature a high thermal conductivity and act, owing to their connection to the bulk wafer, as heat sinks. The membranes themselves show a very even n-well island bottom. In Figure 3-8 (b) a 3 x 3 array of poly-silicon membranes without any n-well, is shown. In this case, the wet etching stops at the thermal oxide of the CMOS layer stack.

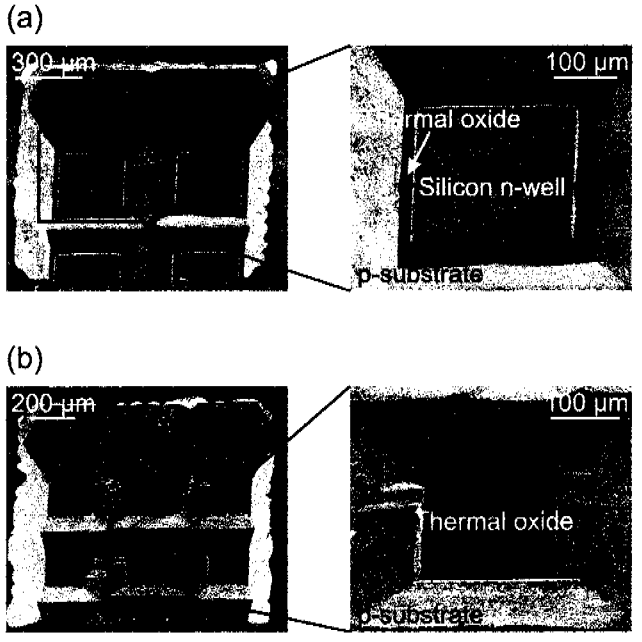

Figure 3-8. SEM micrographs of the structures as in Figure 3-6 on a CMOS-MPW upon 10-minutes over-etching after the ECE etch stop has been reached. Etching was performed in 6-molar KOH at 80 °C. Due to the high aspect ratio and the angle, from which the micrograph was taken, the dimensions seem to be distorted. The scale bar relates to the structures at the bottom of the etch pits.

The thickness of the n-well-based silicon membranes is approximately 5 µm. This is more than the nominal implantation depth of the n-well and is a consequence of the depletion region as discussed earlier.

3.2.3.4 Limitations

The packing density of the etching features is limited by the resolution of the photolithography and also by the barreling effects occuring during the DRIE. The width of the separation walls on the thick photoresist will be narrower as on the mask owing to the considerable radiation dose required for exposure. If the silicon separation walls are punctured during the dry etching step, the area of the etch pit becomes larger, and the etching rate increases drastically. This may lead to a destruction of the n-wells and the devices on the wafer.

The packing density of neighboring micromechanical structures in, e.g., membrane arrays, is limited by the horizontal wet etching rate of the sidewalls of the DRIE-etched pits, which is similar to the vertical wet etching rate. If silicon bridges between the structures are needed as a mechanical support or as heat sinks, care has to be taken to have wide enough separation walls. In practice, the wall width should be larger than twice the lateral under-etching distance. For a complete removal of any silicon feature on the membrane, the maximum width of the grid walls should be less than the

intended etching depth of the ECE process. A further limitation is imposed by the interrelation between the grid width and the DRIE etching depth. Any irregularity on the n-well surface influences the depletion region of the pn-junction and, thus, affects the etching of the p-silicon and the smoothness of the n-well.

3.2.3.5 Discussion

It is evident from Figure 3-6 (left side) that the undercutting of the mask during the DRIE process is considerable owing to the long etching time. Since the silicon surrounding the etch pits is etched away in the subsequent wet etching process step, this strong under-cutting does not pose a problem. Barreling is neither a concern, since the separation walls have been chosen quite wide. Also, non-idealities at the bottom of the etch pit, such as trenching and silicon grass, are removed by the KOH. Further, the non-uniformity of the etching depth over the wafer area is evened out during the wet etching step using an electrochemical or a silicon oxide etch stop so that a time-consuming process tuning is not needed. Any ICP reactor offered by a foundry can be used for the DRIE process step after the etching rate for deep RIE etching has been assessed. A possible problem may arise from the DC bias voltage that is used to clamp the wafer to the chuck during DRIE. CMOS electronics can suffer breakthroughs in the transistor gate oxide. This may lead to problems especially in high-end CMOS processes with smaller feature sizes (0.35 µm or 0.6 µm) than the one used in this work. The devices of the 0.8-µm CMOS MPWs did not show any degradation in the transistor performance.

The silicon separation walls have been completely removed during the wet etching step when the walls are less than 10 µm thick, as can be seen in Figure 3-6. Thicker separation walls can be used, in case smooth silicon surfaces are not necessary. The removal of the walls depend on two factors: (i) the pit spacing on the mask and (ii) the etching depth of the DRIE step. A longer KOH etching time is needed to etch away wider grid walls.

The fabrication process combining DRIE and ECE for the release of membrane-based sensors and sensor arrays as presented in this chapter has been demonstrated to be flexible and allows to accommodate micromachined features of different size on the same wafer. The necessary adjustments can be done on the mask level in subdividing the membrane subunits into a grid pattern of "smallest common area units". The separation of the grid openings is adaptable to the respective target membrane size, after taking into account the etching time of the final wet etching ECE process. Single membranes or membrane arrays featuring sizes from 0.01 mm^2 to 2.2 mm^2 have been fabricated on the same wafer using the combination of etching techniques.

3.3 Experimental Setup and Procedures

3.3.1 Sensitive Layers and Deposition

After completion of the CMOS process and the post-CMOS micromachining, and after packaging, the polymer films that act as chemically sensitive layers have been deposited onto the sensor structures by means of spray-coating using an airbrush (Badger, Model 200-F, Franklin Park, IL, USA). The airbrush has been fixed at a distance of 10 cm from the chip. A specially designed silicon shadow mask that also can be precisely aligned with the packaged chip has been used to cover the circuitry as well as the calorimetric and capacitive reference sensors. Only the sensing elements of the system were exposed during spray coating.

A wide range of partial selectivities and sorption properties can be covered by careful selection of the polymeric coating materials. The microsensors were coated with the nonpolar poly(dimethylsiloxane), (PDMS, Supelco, Bellefonte, PA, USA), the slightly polar polymers poly(cyanopropylmethylsiloxane), (PCPMS, Supelco, Bellefonte, PA, USA - 10% cyano groups) and poly(etherurethane) (PEUT, Thermedics Inc., Woburn, MA, USA), and the more pronouncedly polar polymers ethyl cellulose (EC, Sigma-Aldrich, Buchs, Switzerland), and poly(epichlorohydrin) (PECH, Sigma-Aldrich, Buchs, Switzerland). The polymers were dissolved in dichloromethane (concentration: 4 mg/ml). The solutions were then sprayed onto the cleaned devices using pure nitrogen as a carrier gas.

The polymer layer thickness was optically measured and ranged between 1.9 μm and 2.1 μm, which is thick enough to ensure that the space of electrical field lines extending from the electrodes of the capacitive microsensor is completely filled with polymer. This was important to exclude swelling effects from contributing to the capacitive sensor signals so that only the changes in the dielectric coefficients were measured [70]. After deposition the polymer coatings were cured in a saturated dichloromethane atmosphere for 2 minutes so that smooth layers on the sensing elements were obtained.

3.3.2 Gas Manifold

For gas tests, the CMOS chips were mounted on dual-in-line packages and then clamped onto the measurement chamber of a computer-controlled gas manifold. Measuring physisorption-induced calorimetric transients requires a careful design of the gas manifold so that the signal dynamics reflect the analyte sorption and heat exchange characteristics rather than the gas flow dynamics of the setup. Therefore, all gas switching processes must be fast in comparison to the analyte sorption dynamics. To this end, a manifold and flow setup (Figure 3-1) was designed, the most important features of which include a cross-over flow architecture by use of a fast cross-over 4-way valve, matched flow resistances of the two output gas lines of the 4-way valve, and a small tubing volume between the valve and the sensor measurement chamber.

The cross-over flow architecture has two input gas lines, one supplying pure carrier gas and the other supplying carrier gas with defined doses of the volatile analyte, and two output gas lines, one leading to the measurement chamber, the other leading directly to the exhaust. This architecture offers the advantage that both input and both output flows are continuously streaming and the build-up time of a certain analyte concentration does not influence the dynamic sensor responses. With the dosing line being routed to the exhaust (sensors exposed to pure carrier gas), the desired analyte concentration can be adjusted by means of flow controllers. After sufficient time for concentration stabilization, the cross-over valve switches the dosing line to the sensors (carrier gas to the exhaust), which then experience a sudden steep concentration gradient. Using the cross-over architecture, it is hence possible to rapidly switch between pure carrier gas and carrier gas containing a defined concentration of a certain analyte.

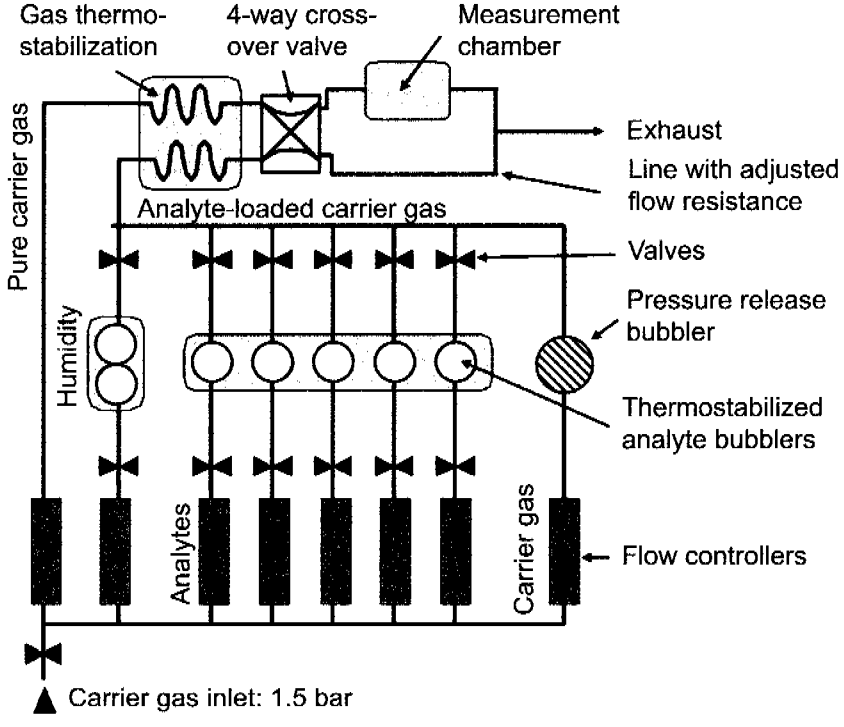

Figure 3-9. Schematic of the gas manifold as designed for fast signal recording.

The valve is a pneumatically driven 4-way cross-over valve (B-43YF2, Whitey, USA) with a switching time of less than half a second (maximum speed: 0.2 s for switching by means of pressured air at 8 bar pressure and 0.3 s for switching back by means of a spring). The fast switching of the valve generates pressure waves in the direction of the measurement chamber but also backwards in the direction of the supply lines and the flow-controllers. On the measurement chamber side the system is open, and no effect on the sensor signal was observed. On the side of the flow controllers, additional measures had to be taken since pressure wave-induced artifacts have been observed: The flow controllers are very sensitive to pressure transients occurring either at their inlet or their outlet so that an additional empty glass bubbler (large diameter and

volume) had to be mounted in between the flow controller for the carrier gas in the dosing line to eliminate these artifacts. Moreover, when switching the 4-way valve, any pressure difference in the two output flow lines affects the gas flow dynamics and, consequently, influences the actual concentrations. Therefore, the output line without measurement chamber was designed to exhibit a flow resistance as similar as possible to that with the measurement chamber, and the two output lines of the 4-way valve fed into the same exhaust line after the measurement chamber.

The overall gas volume between the valve and the sensors was approximately 1.6 ml, which entails a time span of approximately 0.5 s after switching the valve until the gas reaches the sensors at the applied flow rate of 200 ml/min. The flow rate also may influence the dynamic sensor signals in case it is rather low. In pre-studies, the minimum flow rate that did not affect the analyte transients for the given flow setup, was assessed to be 190 ml/min.

The CMOS sensors were mounted in the measurement chamber of the computer-controlled gas manifold. The analyte vapors were generated from specifically developed temperature-controlled (T = 223 to 293 K) vaporizers using synthetic air as a carrier gas, and then diluted as desired using computer-driven mass-flow controllers. The internal volume of these vaporizers, which distribute the liquid over a large-area packed-bed type support to maximize surface-to-volume ratio, was dramatically smaller than that of typical gas-washing bottles ("bubblers") [98]. By using these vaporizers, the noise in the sensor signals caused by concentration fluctuations or aerosol-formation of the liquid analytes is reduced, and the reproducibility of the adjusted gas phase concentrations is significantly enhanced. The vapor-phase concentrations at the respective temperatures were calculated following the Antoine equation [99]. A photoacoustic detector (infrared light for excitation, 1314 Photoacoustic Multi-gas Monitor, Innova Airtec Systems, Denmark) has been used as an independent reference to assess the actual analyte gas phase concentrations.

The sensor measurements were performed in a thermo-regulated chamber at a temperature of 303 K. Both gas streams (pure carrier gas and carrier gas with analyte) were thermostabilized at the measurement chamber temperature before entering the chamber. The response time of the sensors at the given polymer thickness (2 µm) is on the order of a few seconds. Typical experiments consisted of alternating exposures to pure synthetic air and analyte-loaded synthetic air. Exposure times of 10-15 minutes to analyte-loaded gas (to reach thermodynamic equilibrium) were followed by 10-15 minutes purging the chamber with pure synthetic air.

Capacitive and mass-sensitive signals are recorded continuously at rather low temporal resolution since average values for the baseline (zero analyte) and the equilibrium state (defined analyte concentration) are needed for evaluation. The calorimetric sensor relies on transients and provides signals exclusively upon concentration changes. Therefore, the calorimetric recording has to be performed at high time resolution (20 Hz) in two short intervals covering both flanks of the concentration signal, i.e., at the maximum gradient of the analyte concentration. The average peak area of the two transient

signals of the calorimetric transducer (negative upon analyte desorption, positive upon analyte absorption) is then used.

The selected analytes included standard organic solvents and used have been as purchased from Fluka, Buchs, Switzerland without further purification (n-heptane, n-octane, toluene, methanol, propan-1-ol, propan-2-ol, trichloromethane, tetrachloromethane, trichloroethene, and tetrachloroethene).

The enantiomers and the racemic mixtures of the analytes methyl lactate and methyl-(2)-chloropropionate that have been used in chiral discrimination measurements were also purchased from Sigma Aldrich, Buchs, Switzerland.

4 DETECTION AND DISCRIMINATION OF VOLATILE ORGANIC COMPOUNDS

In this chapter, the performance of the single-chip three-transducer CMOS gas sensor microsystem with respect to volatile organic compounds is studied. Several multi-transducer chips have been coated with different partially selective polymers and have then been exposed to different analytes. The sensitivities of the three different transducers coated with various polymers upon exposure to the set of organic compounds have been determined. The obtained sensitivity values have then been normalized with regard to the partition coefficients of the respective polymer/analyte combination to reveal the transducer-specific effects. The results of this investigation show that the three different transducers respond to fundamentally different molecular properties, such as the analyte's molecular mass (mass-sensitive), its dielectric coefficient (capacitive), and its sorption heat (calorimetric) so that correlations between the determined sensitivity values and the different molecular properties of the absorbed analytes could be established [100].

4.1 Experimental

The multi-transducer chips were coated with five different polymers: Poly(dimethylsiloxane), (PDMS), the slightly polar polymers poly(cyanopropylmethylsiloxane), (PCPMS, 10% cyano groups) and poly(etherurethane) (PEUT), as well as the more pronouncedly polar polymers ethyl cellulose (EC), and poly(epichlorohydrin) (PECH), all of which show distinct sorption or physisorption characteristics [49]. The structural formulae of the used polymers are depicted in Figure 4-1 and Figure 4-2; a list with the supplier information can be found in Table A-1.

The thickness of the sensitive layers were between 1.9 µm and 2.1 µm in order to simplify the data interpretation for the capacitive sensor (only changes in the dielectric properties, no swelling effects have to be taken into account) [48, 74]. The polymer-coated sensor systems were then repeatedly exposed (2-3 repetitions) to 8 concentrations steps (4 up, 4 down) of a set of different organic compounds (n-heptane, n-octane, toluene, methanol, propan-1-ol, propan-2-ol, trichloromethane, tetrachloromethane, trichloroethene, and tetrachloroethene) and the response slope, i.e., the sensitivity values were determined and used for the subsequent data interpretation.

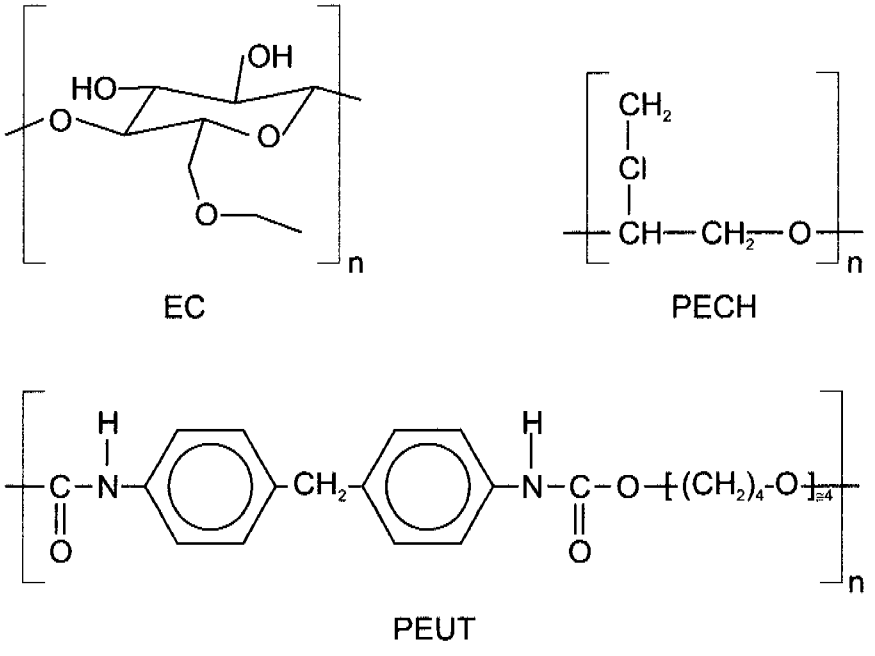

Figure 4-1. Structural formulae of the polymers used.

The sensitivities of the three transducers as determined for each polymer/analyte combination and the average experimental error for the sensitivities (standard deviations) are given in the Appendix (Table A-2 – A-4). The organic volatiles were selected to represent a wide range of molecular properties that can be detected by the different transducers, which include in particular the analyte dielectric constant (capacitor), its molecular weight (cantilever), and the respective heat of vaporization or condensation (calorimeter). The physical properties of all the analytes under investigation are listed in Table 4-1. The analyte concentrations were selected not to exceed a maximum of 2% of the saturation vapor pressure at the respective measurement temperature to ensure conditions of "infinite" dilution (see Table 4-1). In applying these very low analyte concentrations, a linear correlation between sensor response and analyte concentration and a zero intercept have been observed in every case. This is a prerequisite for the calculation of meaningful sensitivities or partition coefficients at "infinite dilution" under the assumption that Henry's Law holds.

Figure 4-2. Structural formulae of the used polysiloxanes.

	Physical properties						
	Sat. vapor pressure	Density	Dielectric coefficient	Molecular weight	Heat of vaporization	Molar volume (liquid phase)	Measurement concentration ranges
	[kPa]	[g/cm^3]	ε	[g/Mol]	[kJ/mol]	[m^3/kmol]	[ppm]
n-Heptane	7.78	0.68	1.92	100.20	36.6	$1.48 \cdot 10^{-01}$	250-6000
n-Octane	2.46	0.70*	1.95	114.23	41.6	$1.64 \cdot 10^{-01}$	250-4800
Toluene	4.90	0.86	2.40	92.14	38.0	$1.07 \cdot 10^{-01}$	250-6000
Methanol	21.86	0.79*	33.00	32.04	38.3	$4.07 \cdot 10^{-02}$	600-6000
Propan-1-ol	3.77	0.80*	20.80	60.10	48.4	$7.52 \cdot 10^{-02}$	250-6000
Propan-2-ol	7.76	0.78*	20.18	60.10	46.2	$7.69 \cdot 10^{-02}$	600-6000
Trichloromethane	32.31	1.47	4.81	119.38	31.5	$8.12 \cdot 10^{-02}$	600-6000
Tetrachloromethane	18.90	1.57	2.24	153.82	32.4	$9.77 \cdot 10^{-02}$	300-6000
Trichloroethene	12.45	1.45	3.40	131.39	34.2	$9.05 \cdot 10^{-02}$	300-6000
Tetrachloroethene	3.15	1.61	2.28	165.83	39.8	$1.03 \cdot 10^{-01}$	300-6000

*Table 4-1. Physical properties of the different analytes at 303 K [101, 102]; (*298 K)*

4.2 Results

4.2.1 Saturation Vapor Pressure Normalization

The aim of these measurements was to demonstrate that the different transducers indeed provide complementary information on the various organic volatiles, and that the information can be used for an analyte characterization according to its physical properties. At a first glance the sensitivity patterns obtained from the different transducers show distinct characteristics so that the use of different transducer types obviously provides complementary information. The sensitivity patterns for PEUT are displayed in Figure 4-3. For a more detailed investigation, however, it is necessary to find a way to systematically compare the signals or sensitivities yielded by the three different transducers for the different polymers. A first factor that affects the direct comparison of the different analyte sensor signals or sensitivities is of thermodynamic nature and is based on the fact that the sensor responses or the physisorption extent largely depend on the analyte saturation vapor pressure: The lower the analyte saturation vapor pressure, the larger are in general the signal intensities. As an example, the analyte n-octane produces for the same analyte concentration always a considerably larger signal on the capacitive transducer than n-heptane (Table A-4, Appendix), though the dielectric coefficient of both molecules is approximately the same (Table 4-1). This is a consequence of the lower saturation vapor pressure or the higher boiling point of n-octane. Therefore a first-order approach to enable a signal or sensitivity data comparison includes the normalization with respect to the analyte saturation vapor pressure. Since the partitioning extent is inversely proportional to the saturation vapor pressure, the sensitivities have to be multiplied with the analyte saturation vapor pressure.

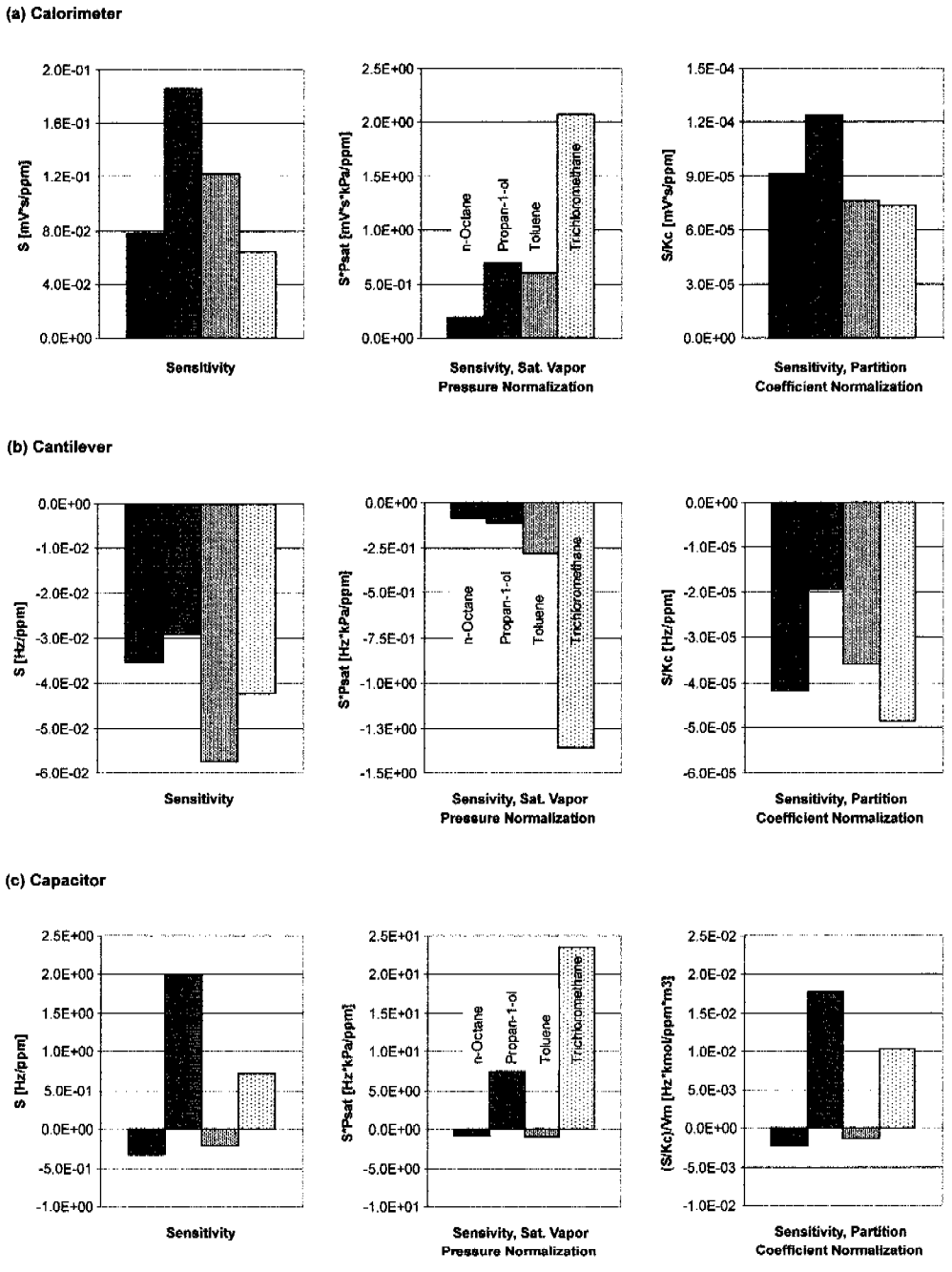

Figure 4-3. Bar graphs representing the sensitivity patterns, the sensitivities as normalized with regard to the saturation vapor pressure and the sensitivities as normalized with regard to the partition coefficients for the three different transducers: (a) calorimetric, (b) mass-sensitive, and (c) capacitive. The polymer coating was PEUT at 303 K, the analytes included n-octane, toluene, propan-1-ol, and trichloromethane.

This normalization takes into account the interaction of the analyte molecules among themselves, i.e., inter-analyte interactions. The effect of this normalization can be seen in Figure 4-3 for the slightly polar and rubbery polymer poly(etherurethane), PEUT.

4.2.2 Partition Coefficient Normalization

The normalization with regard to the saturation vapor pressure is, however, not yet sufficient. One has also to take into account the analyte/matrix interactions, i.e., the polymer or matrix selectivity [49, 103]. A polar polymer will always preferentially absorb polar molecules, whereas a nonpolar polymer will feature an increased partitioning of nonpolar analyte molecules according to the rule "like dissolves like". The consequence is that, e.g., in using a nonpolar polymer on a capacitive sensor, a less polar analyte may be sorbed to a larger extent and produce a larger signal than a rather polar analyte, which nevertheless features a higher dielectric coefficient. Therefore a better normalization is with respect to the partition coefficient, i.e., the sensitivity value is divided by the partition coefficient. The partition coefficient is a dimensionless thermodynamic equilibrium constant and is characteristic for a given volatile/polymer combination (Eq. 2-1). The partition coefficient, K_c, itself is inversely proportional to the saturation vapor pressure or proportional to the boiling temperature and vaporization enthalpy [49]. The partition coefficient takes into account not only the analyte/analyte interactions but also the polymer/analyte interactions. In this context it has to be noted that the overall process of analyte sorption from the gas into the polymeric phase is often modeled as two separate steps: Condensation of the analyte into the liquid state, and mixing of this liquid with the polymer in a dissolution process. This model is for conceptual purposes only, i.e., condensation is not occurring in reality since the measurements are usually performed at extremely low analyte concentrations (infinite dilution).

By normalizing the sensitivities with regard to the partition coefficients all effects related to analyte absorption are accounted for, and the characteristics of the different transducers should become clearly visible. As can be seen in Figure 4-3, deviations between saturation vapor pressure normalization and partition coefficient normalization occur in the case that the nature of the analyte/analyte interactions is significantly different from the nature of the polymer/analyte interactions (the sorption matrix PEUT is slightly polar, $\varepsilon = 4.8$).

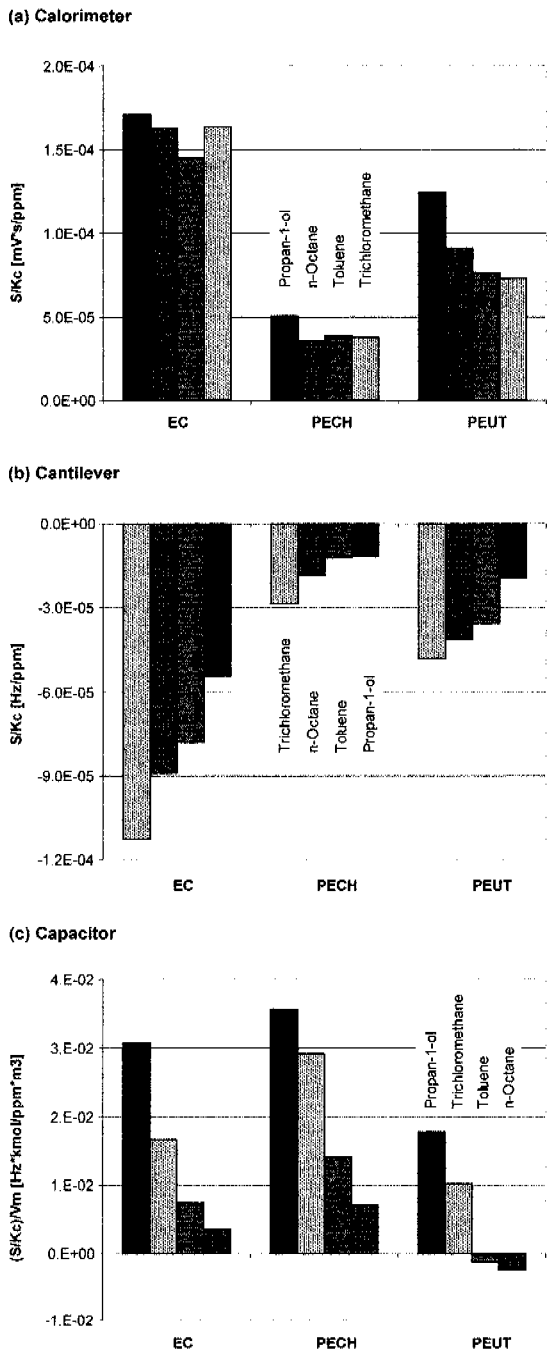

Figure 4-4. Bar graphs representing the S/K_c-values at 303 K as extracted from Table 4-4. Four different analytes (n-octane, toluene, propan-1-ol, and trichloromethane) were detected with three different polymers (EC, PECH, and PEUT). The analytes have been ordered with regard to the decisive molecular property for the respective transducer: (a) decreasing heat of vaporization for the calorimeter, (b) decreasing molecular weight for the cantilever, and (c) decreasing analyte dielectric coefficient for the capacitor.

	Partition coefficients K_i		
	EC	PECH	PEUT
n-Octane	620	430	850
Toluene	830	1370	1610
Propan-1-ol	840	400	1500
Trichloromethane	500	280	870

Table 4-2. Partition coefficients of different analytes in EC, PECH, and PEUT at 303 K [49, 72, 104]

Figure 4-3 shows the normalization results for analytes of different polarity (n-octane, propan-1-ol, toluene, and trichloromethane) in the PEUT polymer matrix. The analytes are ordered with respect to their saturation vapor pressure. Highly volatile compounds, e.g. trichloromethane, featuring a high saturation vapor pressure generate much lower sensor responses than analytes of low volatility, such as n-octane, at comparable concentrations. As already discussed, this is a consequence of the fact that the signal is inversely proportional to the saturation vapor pressure [49, 103]. For partition coefficient normalization the sensitivity values have been divided by the respective partition coefficients for each volatile/polymer combination, which have been previously determined and are listed in Table 4-2 and Table 4-3 [49, 72, 104].

The next step is now to compare the sensitivities that have been normalized with regard to the partition coefficients for the different transducers. The sensitivity equations of the different transducers are given in Chapter 2 (Eqs. 2-3, 2-4, 2-6). For all transducers the geometric factors, G, remain constant, since always the same transducer design is used throughout the measurements. The same holds for the layer thickness, which is almost identical for all devices and polymers and ranges between 1.9 and 2.1 µm. The normalized sensitivity, S/K_c, is, in the case of the calorimetric sensor, proportional to the sorption heat (Eq. 2-3), $H_{sorption}$, in the case of the cantilever proportional to the molecular mass (Eq. 2-4), M_A, and, in the case of the capacitor, it is proportional to the difference of the dielectric coefficients of analyte and polymer (Eqs. 2-5, 2-6). In the case of the capacitive sensor the volume fraction occupied by the analyte molecules is the decisive parameter rather than the number of molecules.

The detection or transduction process is split in two parts (i) the absorption or partitioning, which is the same for all transducers for a given polymer and (ii) the transducer-specific part, which includes the measurand detected by the respective transducer such as sorption heat, molecular mass and dielectric properties.

	Partition coefficients K_c	
	PCPMS	PDMS
n-Heptane	670	800
n-Octane	1830	2200
Toluene	1220	1200
Propan-1-ol	530	250
Propan-2-ol	235	140
Trichloromethane	340	260
Tetrachloromethane	420	450
Tetrachloroethene	1540	1600

Table 4-3. Partition coefficients of different analytes in PCPMS and PDMS at 303 K [49, 72, 104]

The selected analytes, the characteristic properties of which are sufficiently different, should therefore reflect in the measured S/K_c-values and there should be a systematic order in the S/K_c-values with respect to the transducer-specific measurand. For example, for a given polymer the order in the calorimeter S/K_c-values should approximately reflect the analyte vaporization heat, the order in the cantilever values should be according to the analyte molecular mass, and the order of the capacitive values should reflect the analyte dielectric properties or dielectric coefficient (see Eqs. 2-3, 2-4, 2-6).

4.2.3 Discussion

The numerical S/K_c-values for a set of four analytes and three different polymers as well as a set of eight different analytes and two polysiloxanes are listed in Table 4-4 and Table 4-5. For immediate recognition and better visualization the S/K_c-values are ordered with respect to the transducer-specific measurand displayed as bar graphs for the different transducers and polymers in Figure 4-4 (a)-(c) and Figure 4-5 (a)-(c).

	Calorimeter S/K_c [mV·s/ppm]			Cantilever S/K_c [Hz/ppm]			Capacitor $(S/K_c)/V_m$ [Hz·kmol/ppm·m^3]		
	EC	PECH	PEUT	EC	PECH	PEUT	EC	PECH	PEUT
n-Octane	1.63E-04	3.51E-05	9.09E-05	-8.92E-05	-1.84E-05	-4.16E-05	3.59E-03	7.21E-03	-2.30E-03
Toluene	1.45E-04	3.83E-05	7.62E-05	-7.78E-05	-1.21E-05	-3.57E-05	7.60E-03	1.40E-02	-1.21E-03
Propan-1-ol	1.71E-04	5.06E-05	1.24E-04	-5.46E-05	-1.15E-05	-1.94E-05	3.07E-02	3.58E-02	1.77E-02
Trichloro-methane	1.64E-04	3.78E-05	7.37E-05	-1.13E-04	-2.86E-05	-4.84E-05	1.65E-02	2.92E-02	1.03E-02

Table 4-4. Sensitivities as normalized with regard to the partition coefficients, K_c, for EC, PECH, and PEUT for the analytes n-octane, toluene, propan-1-ol, and trichloromethane.

Figure 4-4 (a) shows the calorimetric results for the three different polymers EC, PECH, and PEUT. The calorimetric transducer detects the heat budget changes during the physisorption process, which is positive in the case of analyte absorption and negative upon analyte desorption. The averaged values of both peak integrals (ab- and desorption, see Figure 2-4) have been used for evaluation. The analyte bars are displayed in the order of decreasing vaporization heat, i.e., the bar length or S/K_c-values should decrease from left to right (propan-1-ol, 48.4 kJ/mol; n-octane, 41.6 kJ/mol; toluene, 38.0 kJ/mol; trichloromethane, 31.5 kJ/mol). Within experimental error (see Table A-2 to Table A-4) this holds true for all three polymers. Slight deviations occur, in particular for trichloromethane and EC. There are several possible reasons for that. One reason is certainly due to the fact that the analyte order is according to the heats of vaporization since the sorption heats (heat of vaporization/condensation plus heat of mixing) are not accessible for these polymers (values are available for PDMS, see also discussion there). This means that any change in the heat budget due to polymer/analyte interaction is not accounted for a ranking based on the vaporization heat of the analytes. Another reason may be a consequence of the nature of the calorimetric transducer and the overall lower sensitivity of this transducer. The calorimetric transducer detects fast changes in analyte concentrations as it responds only to concentration transients (see Figure 2-4): Any slow change will produce rather low if any signals. This means that analytes with fast absorption/desorption characteristics may produce relatively larger signals than low-volatility analytes, which may explain the comparably large S/K_c-value of trichloromethane. Moreover, possible changes of the heat conduction through the polymer/analyte composite to the transducer elements (thermocouples), and the fluctuations in the gas flow also constitute sources of experimental variability. As already mentioned in the transducer description, the limit of detection of the calorimetric transducer is not as favorable as for the other transducers so that some variability in the results also is a consequence of the rather low signal levels.

The resonant cantilever is sensitive to the molecular weight of the volatile compounds (Eq. 2-4). The sensor responses are frequency decreases or negative frequency shifts since the resonance frequency drops upon mass loadings as a consequence of analyte absorption in the polymer layer (see Figure 2-6). The S/K_c-values are grouped according to the molecular mass of the analytes: Trichloromethane (119.38 g/mol), n-octane (114.23 g/mol), toluene (92.14 g/mol), and propan-1-ol (60.10 g/mol). The trend (decrease) in the S/K_c-values is consistent with the decreasing molecular mass (Figure 4-4 (b)). The mass-sensitive cantilever is a transducer, the signals of which usually can be interpreted very straightforward.

The last of the three transducers is the capacitive sensor (see Figure 2-8). As has been stated before and described in detail in Ref. [74], analytes with a lower dielectric constant than that of the polymer should produce negative signals, whereas analytes with a larger dielectric constant than that of the polymer should produce positive signals (see Eqs. 2-5, 2-6). Propan-1-ol has the largest dielectric coefficient (20.45), followed by trichloromethane (4.81), toluene (2.38), and n-octane (1.95). The dielectric coefficients of the polymers are 3.4 for EC, 7.4 for PECH, and 4.8 for PEUT. The general signal

trend for all three polymers follows the order of the dielectric coefficients of the analytes: Decrease from propan-1-ol, via trichloromethane, and toluene to n-octane (Figure 4-4 (c)). However, only the PEUT-coated sensors show negative responses for analytes with a dielectric constant that is lower than that of the polymer. This is consistent with observations in previous studies [70, 73, 74]. The exact reasons for this behavior are yet unknown. A possible explanation may be derived from the nature of the different polymers. It seems that the more soft and rubbery the polymers are, the more pronounced is the effect of the sign of the difference of the dielectric coefficients of analyte and polymer. The glass transition temperatures of the three polymers are 233 K for PEUT, 251 K for PECH and 316 K for EC. The polysiloxanes feature even lower glass transition temperatures in the range of approximately 150 K. Low-modulus, rubbery polymers are normally considered to have large segmental mobility and rapid segmental relaxation times so that the free volume in the polymer is rather small. Analyte molecules can penetrate the polymer matrix, but will replace chain segments and such alter the dielectric properties (Figure 4-2). Larger analyte dielectric coefficients will produce a composite dielectric coefficient increase, whereas lower analyte dielectric coefficients will yield a composite dielectric coefficient decrease as expected. For PECH it has been reported that this polymer has an exceedingly open structure of the polymer [105]. The presence of the Cl-group in conjunction with the long alkyl chain on the adjacent backbone carbon forces the polymer backbone into a conformation that confers rather extraordinary rigidity to the chain and loose interactive packing. The resulting polymer features a large amount of excess volume so that the analyte molecules may fill this excess volume upon incorporation in the composite matrix without replacing polymer units (Figure 4-1). This could explain that the composite dielectric constant increases regardless the ratio of dielectric coefficients of analyte and polymer. Similar considerations also can be applied to EC, another rather rigid polymer structure with large excess volume. This explanation is further supported by the comparably large diffusivities of analytes, e.g., in PECH, which have been ascribed to the loose packing of the PECH chains, which presumably permits relatively easy passage of analyte molecules without requiring significant cooperative movement of polymer chain segments [73, 105]. The results for a set of 8 analytes (propan-1-ol, propan-2-ol, tetrachloromethane, trichloromethane, tetrachloroethene, n-heptane, n-octane, toluene) using PCPMS and PDMS as sensitive layers are given in Table 4-5 and displayed in Figure 4-5 (a)-(c). The partition coefficients for each polymer/analyte combination are given in Table 4-2 and Table 4-3. The molecular structures of both polymers are almost identical – the poly(cyanopropylmethylsiloxane) features 10% cyano groups that replace the respective methyl groups of the poly(dimethylsiloxane). Thus, the resulting sensitivity patterns are expected not to be too different for both polymers.

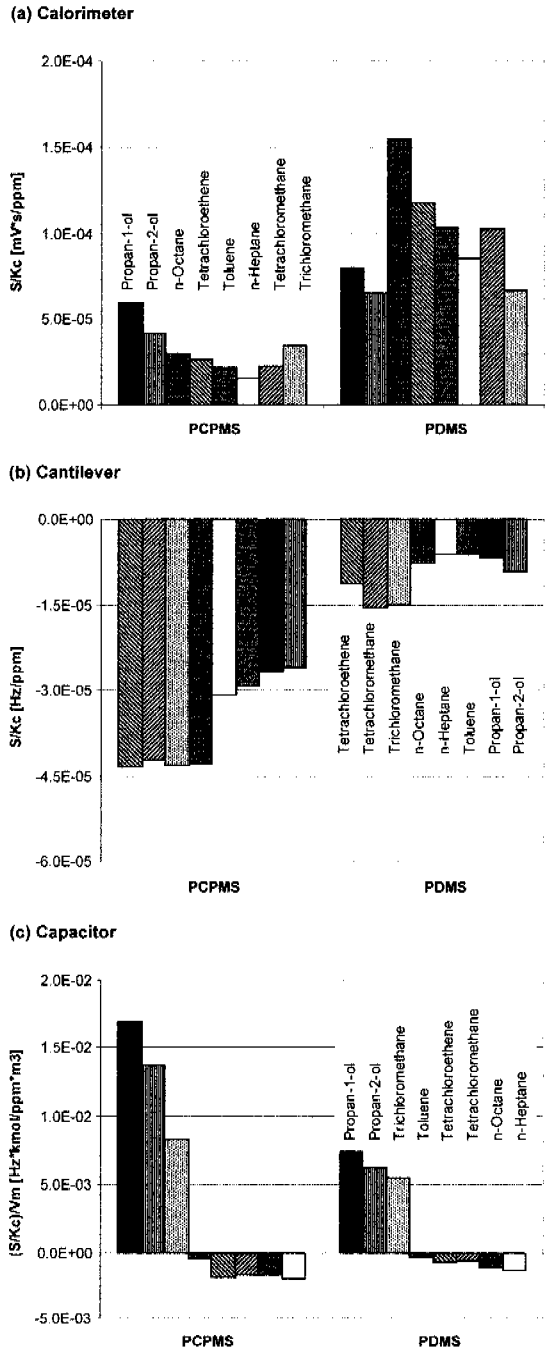

Figure 4-5. Bar graphs representing the S/K_c-values at 303 K as extracted from Table 4-5. Eight different analytes (n-heptane, n-octane, toluene, propan-1-ol, propan-2-ol, trichloromethane, tetrachloromethane, and tetrachloroethene) have been measured using the polymers PCPMS and PDMS. The analytes have been ordered with regard to the decisive molecular property for the respective transducer: (a) decreasing heat of vaporization for the calorimeter, (b) decreasing molecular weight for the cantilever, and (c) decreasing analyte dielectric coefficient for the capacitor.

The normalized sensitivities of the calorimetric sensor are displayed in Figure 4-5. The ordering is again according to decreasing heat of vaporization. In general the normalized sensitivities follow, within experimental error, the trend of decreasing vaporization heat with the exception of the alcohols in PDMS. This can be ascribed to the already mentioned fact that the vaporization heat is used for classification, which implies the assumption that the analyte interacts with a matrix that is of similar nature than the analyte itself, which definitely does not hold for alcohols absorbed in, or interacting with a nonpolar matrix like PDMS. PDMS does not offer the possibility of dipole/dipole interactions and does not permit related molecular ordering effects so that less heat will be released upon absorption or abstracted during desorption. For PDMS, the mixing enthalpies have been measured for several analytes at 298 K, they amount to 15.2 kJ/mol for propan-1-ol, 3.3 kJ/mol for trichloromethane, 0.6 kJ/mol for toluene and 0.7 kJ/mol for n-octane [49]. All mixing is endothermic and entropy-driven. The heat of mixing is the larger the more the analyte properties (e.g., dipole moment) deviate from those of the polymer sorption matrix. The heat of mixing has to be added to the heat of condensation, or its negative value has to be added to the heat of vaporization [49]. The heat of condensation of, e.g., propan-1-ol is reduced by 15.2 kJ/mol mixing heat, i.e., the heat needed to force the polar analyte into the nonpolar polymer, to an overall sorption heat of 33.2 kJ/mol. This shifts the analyte bar in Figure 4-5 (a) to the right in the region of tetrachloromethane. The value of trichloromethane is reduced by 3 kJ/mol, which does not change anything in Figure 4-5 (a). The mixing heats of toluene and n-octane are expectedly much smaller since both, matrix and analyte have similar nonpolar characteristics. Similar considerations can be applied to the other polymers, the mixing heat values of which, however, are not known. In any event the heat of mixing contribution will become significant in the case that the analyte and polymer characteristics significantly diverge. This adds to the fact that molecules exhibiting characteristics largely different from that of the sorption matrix feature, in most cases, poor solubility and comparably low signal levels in the respective polymer (alcohols in PDMS, see Table 4-3), which entails larger experimental errors [49, 53, 74]. Trichloromethane again shows a bit too large signals in PCPMS that can be explained in analogy to Figure 4-3 (a).

The normalized cantilever sensitivities are ordered with respect to the analyte molecular mass as given in Table 4-1. In contrast to the calorimetric and the capacitive sensor, the alcohols are here at the low end since they provide low cantilever signal owing to their comparably low molecular mass. The S/K_c-values by and large reflect the trend of decreasing molecular mass within the ranges of experimental error (Figure 4-5 (b)). Only propan-2-ol sticks a bit out for both polysiloxanes. The experimental error for the alcohols is, however rather large since alcohols show little solubility in the polysiloxanes and, additionally, have a low molecular mass so the signal levels are really low in comparison to the other analytes (see, e.g., alcohol partition coefficients in Table 4-3).

	Calorimeter S/K_c [mV·s/ppm]		Cantilever S/K_c [Hz/ppm]		Capacitor $(S/K_c)/V_m$ [Hz·kmol/ppm·m^3]	
	PCPMS	PDMS	PCPMS	PDMS	PCPMS	PDMS
n-Heptane	1.60E-05	8.53E-05	-3.10E-05	-6.25E-06	-1.96E-03	-1.37E-03
n-Octane	2.98E-05	1.54E-04	-4.31E-05	-7.77E-06	-1.67E-03	-1.16E-03
Toluene	2.22E-05	1.04E-04	-2.93E-05	-6.08E-06	-4.16E-04	-3.28E-04
Propan-1-ol	5.95E-05	7.98E-05	-2.66E-05	-6.80E-06	1.69E-02	7.38E-03
Propan-2-ol	4.15E-05	6.48E-05	-2.60E-05	-9.29E-06	1.37E-02	6.22E-03
Trichloro-methane	3.43E-05	6.66E-05	-4.32E-05	-1.50E-05	8.34E-03	5.47E-03
Tetrachloro-methane	2.25E-05	1.03E-04	-4.24E-05	-1.56E-05	-1.64E-03	-6.19E-04
Tetrachloro-ethene	2.65E-05	1.18E-04	-4.36E-05	-1.13E-05	-1.80E-03	-6.91E-04

Table 4-5. Sensitivities as normalized with regard to the partition coefficients, K_c, for PDMS and PCPMS

The capacitive sensor results are displayed in Figure 4-5 (c), the organic compounds are arranged according to the value of their dielectric constant (decreasing from left to right). The analyte sensitivities decrease of the reduced sensitivity is consistent with the theory. Deviations are within the range of experimental error. The alcohols, which both have a large dielectric constant, show remarkably high signal levels, in particular in comparison to the mass-sensitive transducer. A transition from positive to negative signals can be found between trichloromethane (4.81) and toluene (2.40) since PDMS and the slightly more polar PCPMS have a dielectric coefficient in the range of 2.8 (PDMS) and 3.4 (PCPMS). The siloxanes are both rubbery, low-modulus polymers so that the considerations as discussed for PEUT apply.

4.3 Conclusion

Extensive measurements with a CMOS-based multi-transducer chip comprising a capacitive, a mass-sensitive and a calorimetric sensor have been performed. The microsensor system chips have been coated with different polymers (EC, PECH, PEUT, PCPMS, and PDMS) and exposed to different sets of volatile organic compounds. The sensitivities for the different polymer/analyte combinations have been determined simultaneously for all three different transducers.

The simultaneous recording from the different transducers causes a unique response pattern for each volatile compound. Due to their fundamentally different transduction principles, the sensors do, within experimental error, indeed respond to the diverse physical properties of the analytes such as the molecular weight, the dielectric constant, and the heat of vaporization, which forms part of the mixing enthalpy. This becomes clearly visible by normalizing the sensor sensitivities with regard to the partition coefficient, i.e., separating the partitioning contribution from the specific transducer contribution of the sensor response (Figure 4-4 and Figure 4-5). The analyte signals tend to be rather low in case the physical properties of the sorption matrix (polymer) and that of the analyte largely differ. This poses particular challenges for the calorimetric transducer, where the contribution of the mixing heat to the overall sorption heat can become significant since it is rather difficult to get the respective mixing heat values (see discussion in the context of Figure 4-5 (a)).

5 DETECTION AND DISCRIMINATION OF ENANTIOMERS

Most of the biochemical systems functioning in living organisms involve chiral interactions resulting from different stereochemistry of numerous biologically compounds. This includes, e.g., amino acids and sugars, and hence peptides, proteins, and polysaccharides. Enzymatical reactions, the functioning of transmitters and receptors, and some of the metabolic pathways are stereoselective [21]. The enantioselective synthesis or the discrimination of enantiomers has become important for different biological processes, but also for the production of food additives, pesticides, and pharmaceuticals, where only one of the enantiomers may have the desired effect. Enantiomerically pure pharmaceuticals such as Imovane® make up for almost 50% of all drug products worldwide with increasing tendency [22-24].

Enantiomers of the same compound are difficult to differentiate with "common" physicochemical methods, due to their principally identical physical and chemical properties. Over the last thirty years different methods have been developed to perform the determination and the separation of enantiomers of various classes of chemical compounds [21, 25, 26]. The developed methods are mainly based on the usage of matrices that contain enantioselective molecules or receptors [21, 25, 27-30]. The need for "enantiopure" substances and thus for fast and reliable discrimination methods has increased with the growing field of applications.

In this chapter the capability of the multi-transducer gas sensing system to discriminate enantiomers will be demonstrated. In the following section the properties of enantiomers, enantioselective receptors and the common methods for chiral discrimination and separation will be briefly described. A thermodynamic model will be introduced to evaluate and compare the results of the three different transducers. The measurements have been performed with different pure enantiomers and the respective racemic mixtures using different enantioselective matrices. For evaluation and better comparability, the same set of measurements has been performed with conventional methods for chiral discrimination and separation: Gas chromatography (GC) and nuclear magnetic resonance (NMR).

5.1 Chiral Discrimination and Separation – An Overview

5.1.1 Enantiomers

Chiral molecules or enantiomers are two stereoisomers that constitute image and mirror image. There is no symmetry operation that can convey one of the enantiomers into its mirror image. Every stereocenter in one enantiomer has the opposite configuration in the other (Figure 5-1). Two enantiomers have, when present in a symmetric environment, identical physical and chemical properties except their ability to rotate plane-polarized light by equal amounts but in opposite directions [106, 107].

Figure 5-1. Molecular structures of the enantiomers of methyl lactate.

There are several conventions used for naming chiral compounds, all displayed as a prefix before the chemical name of the substance.

(+)- or (-)- is based on the substance's ability to rotate polarized light. If an isomer rotates the plane clockwise the isomer is labeled (+)- or *d-* for *dextrorotatory*, which means "right turn". Its counterpart has the prefix (-)- or *l- levorotatory* ("left turn").

The D- versus L- convention is also known as Fischer projection. It is based on the geometry of each enantiomer, with the version synthesized from naturally occurring (+)-glyceraldehyde being considered the D-form. The D-/L- labeling is unrelated to (+)-/(-)-; it does not indicate, which enantiomer is dextrorotatory and which is levorotatory. Rather, it says that the compound's stereochemistry is related to that of the dextrorotatory or levorotatory enantiomer of glyceraldehyde.

The (R)-/(S)- nomenclature is based on the actual geometry of each enantiomer, using the Cahn-Ingold-Prelog priority rules to classify the form. Each chiral center is labeled (R)- or (S)- according to a system, by which its four ligands are each assigned a *priority* based on atomic number. If the center is oriented so that the lowest-priority is pointed away from the viewer, the viewer will see two possibilities: A clockwise traversal of the remaining three ligands in decreasing or in increasing order. In the first case, the center is labeled (R)-, in thee second, it is (S)- (compare with Figure 5-1 and Figure 5-2).

The (+)-/(-)-convention is the only one based on optical properties. The other two conventions rely on the actual geometry of each enantiomer. But there is no correspondence between any convention.

More often these enantiomers appear not in the pure form but in racemic mixtures, which consist of equal amounts of both stereoisomers. In this case the substance is optically inactive, i.e., the net rotation of the plane-polarized light is zero. If in a chemical substance one enantiomer is present in a larger fraction than the other a ratio for the enantiomeric excess (ee) is usually given. Unlike the racemic mixture such a substance will show net optical rotation at polarized light depending on which enantiomer contributes the larger fraction. To distinguish these mixtures from the homochiral molecules the prefix is a combination of that of both enantiomers, e.g. (±)-.

Figure 5-2. Molecular structures of (S)-methyl-2-chloropropionate and (R)-methyl-2-chloropropionate

Most biologically active molecules are chiral: Amino acids, sugars and also macromolecules like enzymes and receptors. For amino acids typically the L-form is present, whereas sugars have a D-form. As a result, different enantiomers of a compound may have substantially different biological effects. The flavoring agent limonene, e.g., is perceived differently by the human nose, which contains chiral olfactory receptors. Whereas the (S)-enantiomer is associated with mint, the (R)-molecule is perceived as a citrus fruit-type smell [108]. Because numerous biological processes rely on enantiomeric interaction, many chiral drugs must be made with high enantiomeric purity due to potential side-effects of the other enantiomer. Advances in chemical engineering have made it economical for pharmaceutical manufacturers to market the individual enantiomers. Thalidomide® is an example of a racemic drug, in which one enantiomer produces a therapeutically effect (against morning sickness), whereas the other is toxic and has a teratogenic side-effect. Unfortunately, in this case administering just one of the enantiomers to a pregnant patient would still be dangerous as the two enantiomers are racemized in the body.

5.1.2 Chiral Receptors - Cyclodextrins

Chiral recognition is based on the ability of a receptor molecule to form a complex preferentially with one of the enantiomers of a chiral molecule. The higher the difference of the affinity of the receptor to the different enantiomers the better is the chiral discrimination efficiency. Besides approaches based on molecular imprinted polymers (MIPs) [109, 110] most receptors used for chiral recognition are based on macrocyclic structures [27, 45, 111], such as calixarenes, fullerenes, crown-ethers, macrocyclic antibiotics, transition metal complexes, chiral crown ethers, proteins, and cyclodextrins [24]. Cyclodextrins and their derivatives are the most widely used receptors for chiral separation methods (see following section). The reason is the relatively simple production, the associated low costs, and the respective chiral recognition features [26, 45].

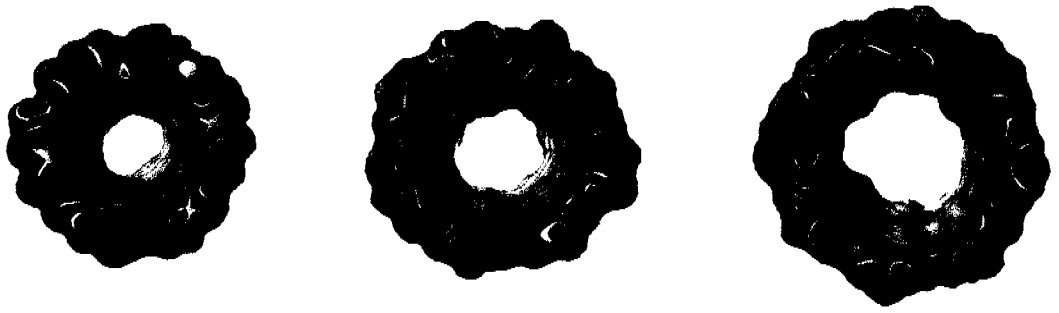

Figure 5-3. Native α-, β-, and γ-cyclodextrins modeled with MolCad [106].

Cyclodextrins (sometimes called cycloamyloses) are cyclic oligomers composed of 5 or more α-D-glucopyranoside units, which are bound via a α-(1,4) glucosydic linkage. Cyclodextrins (or short CDs) are produced by the enzymatic degradation of starch by cyclodextrin glycosyltransferase (CGTase), an α-amylase found in microorganisms [112]. The three main types of cyclic molecules produced by this method are α-, β-, and γ-cyclodextrins consisting of 6, 7, or 8 units, respectively. These "native" cyclodextrins represent rather rigid toroids (Figure 5-3). The primary (smaller opening) and the secondary hydroxyl groups (wide rim) are exposed and readily accessible [45, 106, 112].

	α-Cyclodextrin	β-Cyclodextrin	γ-Cyclodextrin
Number of glucose units	6	7	8
Molecular weight [g/mol]	972	1135	1297
Heigth of torus [10^{-10} m]	7.9 ± 0.1	7.9 ± 0.1	7.9 ± 0.1
Cavity diameter [10^{-10} m]	4.7 – 5.3	6.0 – 6.5	7.5 - 8.3
Cavity volume [$(10^{-10}$ m$)^3$]	174	262	427
Solubility in water [g/l]	142	18.5	232
Number of chiral recognition sites	30	35	40

Table 5-1. Physical properties of native α-, β-, and γ-cyclodextrins [112, 113].

The interior of the toroids is not hydrophobic, but considerably less hydrophilic than an aqueous environment and, thus, able to host even highly hydrophobic molecules (e.g. esters), whereas the exterior is sufficiently hydrophilic to impart cyclodextrins water solubility. Depending on the size of the macrocycle the solubility varies. The solubility of the β-cyclodextrin is smallest (compare Table 5-1), which can be explained by its different intramolecular hydrogen-bonding between the hydroxyl groups [114]. The propensity of native cyclodextrins to form inclusion complexes with organic molecules has made them attractive for applications in different fields, e.g., food industry, cosmetics, agriculture and especially in the pharmaceutical industry. The

mechanism is such that a guest molecule is included into the more hydrophobic open cavity and interacts via hydrogen bonds, dipole/dipole or ionic interaction with the groups on the rim of the cyclodextrin toroid [21].

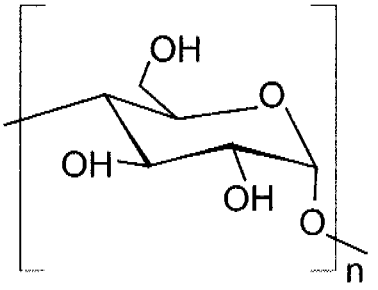

Figure 5-4. D-glucopyranoside unit of a native cyclodextrin.

By essence cyclodextrins are chiral host molecules and even native cyclodextrins are able to form diastereomeric complexes with chiral guests [115]. The reason is the different interaction of the enantiomers of a chiral molecule with the cyclodextrin: One enantiomer is bound more tightly to the cyclodextrin forming a complex of higher stability, whereas the other is loosely connected, and the interaction can be broken up more easily [45]. The stability difference between the complexes formed by the two enantiomers defines the efficiency of the chiral discrimination process. For most enantiomer/cyclodextrin complexes the hydrogen bonds constitute the key interaction that enables a reversible host/guest complex formation. The broad chiral recognition capability of cyclodextrins is based on several phenomena [116]. Additionally to their numerous chiral centers – five in every glucose unit – every chiral center in a glucose unit has a different orientation and is at a different distance from the neighboring atoms.

Cyclodextrins have been chemically modified by substituting the free hydroxyl groups (example in Figure 5-5) with other functional groups (e.g. alkyl-, amino-, pentyl-groups) [114, 117]. This improves the physicochemical properties of the macrocycle, such as its solubility, but also enhances the selectivity towards a certain enantiomer. These modified cyclodextrins exhibit more variability in their shape than the native cyclodextrins, so that they can interact more intimately with the analyte. This "induced fit" mechanism enhances the chiral selectivity of these modified cyclodextrins [26]. As the glucose units do not deviate from their ring formation, the geometrical preferences of the modified cyclodextrin are mainly driven by the conformation of the macrocycle and its side chains [118-120]. Results based on molecular dynamic simulations indicate that the major contribution to the host/guest interaction and enantiomer discrimination is due to the inclusion of the analyte into the cyclodextrin cavity. But it was also shown that the interaction between the enantiomer and the macromolecule can also occur on the surface of the cyclodextrin [26, 118, 119, 121, 122]. Most frequently the "host/guest" ratio is 1:1, but also other ratios of are known [112].

It was found that mixtures of cyclodextrin derivatives with achiral silicone polymers lead to an improved efficiency and an increased working temperature range for some separation methods [111, 116, 123]. The relatively low polarity of the silicone matrix allows for the analysis of polar enantiomers without derivatization and for low analysis temperatures with higher selectivity. The solubility of the chiral selector in the siloxanes is limited, and a leveling off of the chiral selectivity of these matrices have been observed with increasing concentration of the chiral selector [124, 125].

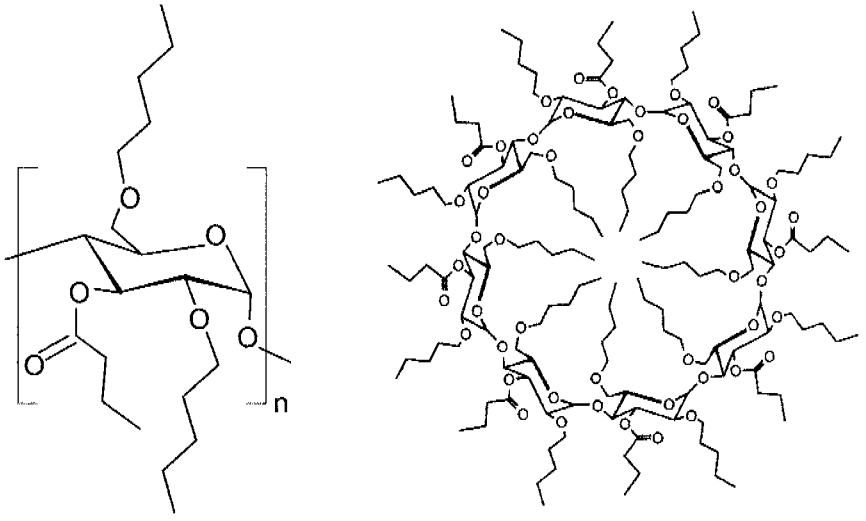

Figure 5-5. Structure of the cyclodextrin derivative and molecular structure of a octakis(3-O-butanoyl-2,6-di-O-n-pentyl)-γ-cyclodextrin.

5.1.3 Methods for Chiral Separation and Discrimination

Over the last three decades different methods have been developed for chiral separation. The separation methods can be applied in liquid phase and gas phase. Depending on the chiral component and the enantioselective interaction, a chiral separation can be either carried out directly, based on the formation of a reversible diastereomeric complex, or indirectly by using chiral derivatization reagents to form diastereomeric pairs [21, 24, 26, 126]. Currently, the direct approach is more commonly used, which entails the use of a chiral selector as a mobile or stationary phase. The indirect way has the disadvantage of requiring additional procedures, but, in some cases, the detection sensitivity can be increased by adding, e.g. fluorophores [24].

The most common methods for chiral separation include electrophoresis and chromatographic techniques [24, 26, 27, 112]. The systems based on electrophoresis are targeted at liquid phase application and make use of an electrical field to separate molecules according to their charge and frictional forces, which leads to differences in their migration speed. The analytes are injected into columns or plates coated with a liquid or viscous enantioselective electrolyte. The most common technique is the capillary electrophoresis (CE) [26]. The chromatography is a separation method that exploits differences in the partitioning behavior of the chiral analyte in a mobile phase and a

stationary phase. The molecules in the eluent may interact with the stationary phase according to their relative solubility, their charge or, as it is also the case for enantiomers, different interaction strength with the stationary phase. The analytes are retained to a different extent (retention) with the stationary phase and, thus, eluted separately. Common chromatography methods include: Gas chromatography (GC), high-performance liquid chromatography (HPLC), thin layer chromatography (TLC), supercritical fluid chromatography (SFC), countercurrent chromatography (CCC), simulated moving bed (SMB) chromatography, and free solution capillary electrophoresis (FSEC) [21, 24, 26, 27, 45, 111]. Capillary electrochromatography (CEC) and micellar electrokinetic chromatography (MEKC) [127] combine the methods of HPLC and CE; the chiral selector can be present in either the mobile or the stationary phase.

Chromatographic and electromigration techniques are predominantly used for the quality control of enantiomeric purity after synthesis to check for racemization processes for pharmaceutical quality control, clinical diagnostics, and environmental monitoring. Besides the cyclodextrins other enantioselective receptors, such as chiral micelles and crown ethers, are used.

Additional analysis techniques include nuclear magnetic resonance (NMR), surface plasmon resonance (SPR), resonance Raman spectroscopy (RRS), laser-induced fluorescence (LIF), reflectometric interference spectroscopy (RIfS), and reversed-polarity capillary zone electrophoresis (CZE) [45].

Over the last decade a lot of effort has been put into miniaturizing techniques for chiral separation and chiral detection, with the aim to reduce the instrument size, the reagent consumption and, consequently, the costs of operation. Moreover, the separation/detection speed and the sample throughput can be increased by the use of microsystems. The most promising approach for chiral separation is the microchip electrophoresis (MCE) relying on the same principles and techniques as the classical CE on a micromachined planar devices [31-34]. Other methods for on-line analysis include miniaturized immunosensors [35-38] and gas sensors [21, 35]. In most cases, the sensors rely on only one transducing principle, such as optical [36], amperometric [39], potentiometric [40, 41] or mass-sensitive transduction [42-44]. The mass-sensitive devices, e.g., quartz crystal microbalances and surface acoustic wave sensors, have been extensively used in the past for chiral detection in the gas phase [45].

A viable approach includes the detection of chiral molecules with multiple different sensors simultaneously to receive more information about the target analyte. The three different sensors of the multi-transducer gas sensor system introduced previously (Chapter 2 and 4) respond to fundamentally different molecular properties, such as the analyte's molecular mass (mass-sensitive), its dielectric coefficient (capacitive), and its sorption heat (calorimetric). The enantioselective coating consists of modified cyclodextrins dissolved in a poly(dimethylsiloxane) matrix.

In the result section the results for chiral discrimination of the enantiomers of methyl lactate and methyl-2-chloropropionate will be detailed and subsequently evaluated.

5.2 Absorption Model and Experimental Setup

5.2.1 Absorption Model and Chiral Discrimination Factor

The following absorption model was introduced by K. Bodenhöfer *et al.* [125]. It has been developed for the chiral discrimination in gas phase using an enantioselective-coated thickness-shear mode resonator (TSMR). The model takes into account the different interactions taking place in the sensitive layer. The enantioselective layer is composed of modified cyclodextrins dissolved in an achiral, nonpolar polymer matrix. The model considers three different types of adsorption sites and interactions: Preferential and nonspecific sorption sites at the receptor molecule (cyclodextrin) and dispersion interactions with the polymer matrix. Adsorption takes place simultaneously at all three different sites (two at receptor, one in the polymer), so that a superposition of the individual sorption mechanisms results.

In a first assumption the sensor response (e.g., frequency shift), and consequently the overall interaction between analyte molecule and sensing layer, is considered to consist of two principally independent contributions taking place at different types of absorption sites:

$$\Delta f_{sum} = \Delta f_{spec} + \Delta f_{nonspec}$$

Eq. 5-1

Here, Δf_{spec} represents the sensor response due to a specific or preferential interaction between analyte molecules and the cage-type recognition sites. $\Delta f_{nonspec}$ includes the sensor response upon different nonpreferential interactions. The nonspecific response includes the nonspecific interactions between analyte molecule and nonpreferential sites at the cyclodextrin interaction and the interaction between analyte molecule and polymer matrix. This model does not necessarily imply that the two nonpreferential interactions are identical.

Assuming that the chiral interaction occurs at the specific absorption sites Eq. 5-1 can be written as:

$$\Delta f_{sum} = \Delta f_{chiral} + \Delta f_{achiral}$$

Eq. 5-2

It has been demonstrated that each recognition or specific site of the γ-cyclodextrin derivative interacts with just one analyte molecule [125]. The number of macrocycles within the polymer layer is limited. Hence, the maximum occupation is reached when all available preferential sites are occupied. This corresponds to a coverage $\theta = 1$. A Langmuir-type behavior, describing the absorption of one layer of analyte molecules, is used to model this preferential absorption under assumption that no mutual interac-

tion between the absorbed molecules themselves occurs. The chiral contribution to the sensor response, Δf_{chiral}, hence depends on the coverage, θ, and on the analyte concentration, c. The Langmuir-type equation was used:

$$\Delta f_{chiral} = K_{chiral} \cdot \theta(c) = K_{chiral} \cdot \frac{K' \cdot c}{1 + K' \cdot c}$$

Eq. 5-3

where $K' = k_{ad}/k_{de}$ and denotes the ratio of the kinetic constants of the adsorption and desorption process of the chiral molecule at/from the recognition site. K' determines the initial curvature of the sensor response and is a superposition of the contributions of the analyte partitioning at the preferential sites and the specific recognition interactions. K_{chiral} corresponds to a sensor signal at complete coverage, $\theta = 1$, of the enantioselective sites. The dimension of K' is ppm^{-1} or l/µg, depending on what concentration scale has been used. K_{chiral} has the dimension of the sensor read-out signal, such as Hz for the cantilever and capacitor (frequency conversion of capacitance values) and mV·s for the calorimeter[1].

It should be noted that the number of achiral absorption sites is unlimited in contrast to the chiral recognition sites. Therefore, a Henry-type linear correlation between sensor signal and analyte concentration is assumed. This is observed in most cases of nonspecific sorption of analyte molecules into polymer matrices (compare Chapter 4) for concentration ranges [128] for which Henry's law still holds.

$$\Delta f_{achiral}(c) = K_{achiral} \cdot c$$

Eq. 5-4

Here $K_{achiral}$ corresponds to the linear part of the sensor response slope for higher analyte concentrations. The dimension of this constant also depends on the sensor type: Hz/ppm for the mass-sensitive and capacitive device and mV·s/ppm in the case of the calorimeter.

Eq. 5-4 includes all achiral contributions (polymer matrix and cyclodextrin) to the overall sorption. The overall sensor response within the range within which Henry's law holds, is then given by

$$\Delta f_{sum}(c) = \Delta f_{chiral}(c) + \Delta f_{achiral}(c) = K_{chiral} \cdot \frac{K' \cdot c}{1 + K' \cdot c} + K_{achiral} \cdot c$$

Eq. 5-5

[1] It will be discussed in the "result" section (Section 5.3), to which extent such thermodynamic model can be qualified to the responses of the different transducers mentioned here.

The sensor responses versus analyte concentrations according to the model are plotted in Figure 5-6. The superposition of a Langmuir-type from (Δf_{chiral}) with a dispersion form ($\Delta f_{achiral}$) is displayed. For simplicity reasons, frequency shifts have been taken as sensor signals.

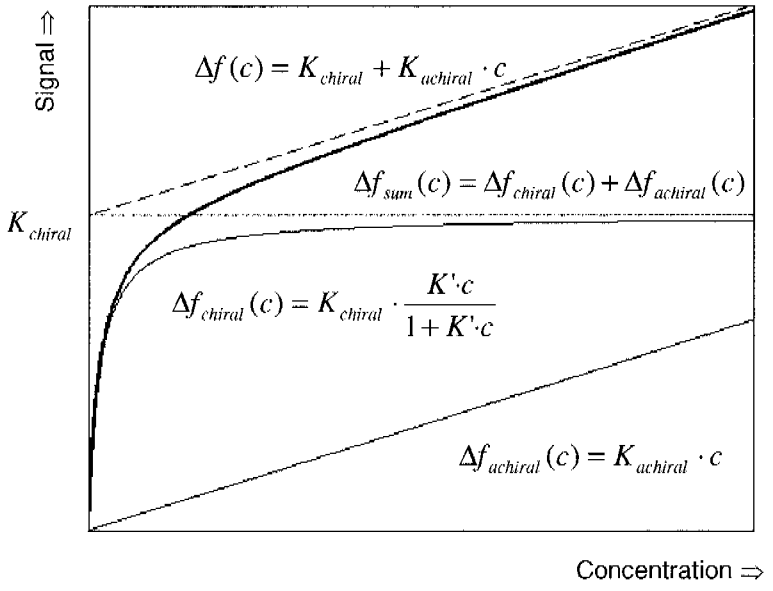

Figure 5-6. Sensor responses, $\Delta f_{sum}(c)$, versus analyte concentration according to the model. Superposition of a Langmuir term, $\Delta f_{chiral}(c)$, and a dispersion term, $\Delta f_{achiral}(c)$.

The initial slope of the response curve depends on the three coefficients K_{chiral}, $K_{achiral}$, and K' and can be calculated from the following equation:

$$\Delta f_{sum}'(c) = \frac{K_{chiral} \cdot K'}{(1 + K' \cdot c)^2} + K_{achiral} \quad \text{with} \quad \Delta f_{sum}'(0) = K_{chiral} \cdot K' + K_{achiral}$$

Eq. 5-6

For low analyte concentrations the specific or chiral interactions dominate ($K_{chiral} \cdot K' > K_{achiral}$), which is a consequence of the stronger interaction of preferred analyte molecule with the recognition sites.

For both enantiomers the measurement conditions, i.e., analyte saturation vapor pressure, and its physical properties are identical. Since also the number of available recognition sites remains constant, K_{chiral} has to be identical for both enantiomers of a chiral molecule. The same holds for $K_{achiral}$, which describes the behavior of chiral molecules in an achiral environment.

The difference in the sorption behavior and hence the sensor responses to the optical antipodes is therefore characterized by K'. The larger K' ($K' = k_{ad}/k_{de}$), the faster a

complete occupation of the specific sites is reached. The stronger interacting enantiomer shows the larger K'-value.

Enantioselectivity is related to the difference of the Gibbs energy of both enantiomers, $\Delta\Delta G$, which can be correlated with the chiral discrimination factor α:

$$-\Delta\Delta G^{0} = RT \cdot \ln \alpha$$

Eq. 5-7

Here, $\Delta\Delta G^{0}$ is the difference between the free enthalpies of both enantiomers for the transition from the gas phase into the liquid phase (sorption in sensitive layer or interaction with receptor). T is the absolute temperature and R is the universal gas constant. The equation is simplified and only includes enthalpy constitutions of the chiral interaction [129].

In standard gas chromatography the chiral discrimination factor, α, is defined as the ratio of two net retention times:

$$\alpha = \frac{t_R - t_0}{t_S - t_0} \quad \text{for } t_R > t_S \qquad \text{resp.} \qquad \alpha = \frac{t_S - t_0}{t_R - t_0} \quad \text{for } t_S > t_R$$

Eq. 5-8

where $t_{R/S}$ is the retention time of the respective enantiomer and t_0 is the dead time of the chromatography column. This equation is valid for undiluted chiral selectors [111, 129]. In case of diluted selector systems, such as cyclodextrins in a polymer matrix, the discrimination is dependent of the receptor concentration or the receptor activity, a_A. The retention of the analyte depends on two contributions: The chiral interaction with the selector molecule and an unspecific interaction with the achiral polymer matrix. The strength of the chiral interaction differs for both enantiomers, whereas the achiral interaction is identical. For the chiral discrimination the unspecific contributions can be neglected:

$$\alpha_{diluted} = \frac{K_R \cdot a_A + 1}{K_S \cdot a_A + 1} = \frac{R'_R + 1}{R'_S + 1}$$

Eq. 5-9

Here, $K_{R/S}$ is the distribution ratio (partition coefficient) of the chiral analyte in the gas and the liquid phase, and $R'_{R/S}$ describes the retention increment of the respective enantiomer. According to this equation the optimum of the chiral discrimination is reached at low analyte concentrations, where the chemical complexation prevails. A detailed derivation for the calculation of the retention increment is described in literature [111, 129]. However, some of the considerations, such as migration time, are applicable to the detection of enantiomers with chemical sensors.

As a consequence of the above introduced absorption model the discrimination factor α depends on the relative concentration ratio of recognition sites in the stationary phase (cyclodextrin molecules) and the analyte molecules in the gas phase [125].

$$\alpha_{sensor}(c) = \frac{\Delta f_{sum(S)}(c)}{\Delta f_{sum(R)}(c)} = \frac{K_{chiral} \cdot \theta_S(c) + K_{achiral} \cdot c}{K_{chiral} \cdot \theta_R(c) + K_{achiral} \cdot c} = \frac{K_{chiral} \cdot \frac{K'_S \cdot c}{1 + K'_S \cdot c} + K_{achiral} \cdot c}{K_{chiral} \cdot \frac{K'_R \cdot c}{1 + K'_R \cdot c} + K_{achiral} \cdot c}$$

Eq. 5-10

For high analyte concentrations there will be no chiral discrimination ($\alpha \rightarrow 1$), since $\theta_S(c)$ and $\theta_R(c)$ in the numerator and dominator of Eq. 5-10 will both simultaneously become 1, when all the receptor sites are fully covered ($\theta_S(c)$, $\theta_R(c) \rightarrow 1$).

The limit of α for infinite dilution can be derived from applying de L'Hôpital's rule (Eq. 5-11).

$$\lim_{x \to 0} \frac{f(x)}{g(x)} = \lim_{x \to 0} \frac{f'(x)}{g'(x)}$$

Eq. 5-11

The maximum value for the chiral discrimination factor, α, can thus be calculated as:

$$\alpha_{max} = \lim_{c \to 0} \alpha(c) = \lim_{c \to 0} \frac{\frac{K_{chiral} \cdot K'_S}{(1 + K'_S \cdot c)^2} + K_{achiral}}{\frac{K_{chiral} \cdot K'_R}{(1 + K'_R \cdot c)^2} + K_{achiral}} = \frac{K_{chiral} \cdot K'_S + K_{achiral}}{K_{chiral} \cdot K'_R + K_{achiral}}$$

Eq. 5-12

The experimentally measured sensor responses were fitted according to the above detailed absorption model and the respective equations. Each sensor curve was fitted separately using a MatLab® program. The parameters K', K_{chiral}, and $K_{achiral}$ were calculated by minimizing the absolute error on the data set.

The extracted parameters were used to determine the quality of chiral discrimination for each sensor type and analyte/receptor combination. The results will be detailed in Section 5.3.2.

5.2.2 Chiral Selectors: Cyclodextrins

The gas sensor microsystem was already successfully used for the detection of volatile organic compounds in air with commercially available, achiral polymers (e.g., PDMS, PEUT, EC) as sensitive layers and has been described in Chapter 4. Here, an enantioselective additive is necessary for the detection and discrimination of enantiomers. A modified cyclodextrin (octakis(3-O-butanoyl-2,6-di-O-pentyl)-γ-cyclodextrin), which showed consistent results in gas chromatography [123, 130] and for mass-sensitive gas microsensors [43, 125] has been chosen.

For chiral discrimination experiments a mixture of the modified cyclodextrins and a polymer with nonpolar properties, here poly(dimethylsiloxane), of 50% (w/w) was used utilizing dichloromethane as a solvent. On the one hand the mixture enables a discrimination of the respective enantiomers at 90% of the possible maximum achievable with the pure compound [125]. On the other hand the mixture shows a strong substrate adhesion and provides sufficient stability of the enantioselective mixture on the sensing elements.

For determining the influence of the receptor ring size on the selectivity the measurements were performed with three different cyclodextrins (α-, β-, and γ-CD): Hexakis(3-O-butanoyl-2,6-di-O-n-pentyl)-α-cyclodextrin, heptakis(3-O-butanoyl-2,6-di-O-n-pentyl)-β-cyclodextrin, and octakis(3-O-butanoyl-2,6-di-O-n-pentyl)-γ-cyclodextrin. The glucose ring of these derivatives exhibit a slightly polar, lipophilic behavior, whereas the side chains have nonpolar properties [118, 131]. The structure of a glucose unit and the ring-formation of a γ-cyclodextrin is depicted in Figure 5-5. These cyclodextrin derivatives were synthesized and provided by A. Bogdanski [132] and show an excellent selectivity for a variety of chiral molecules [118, 125]. The γ-cyclodextrin derivative is commercially available as Lipodex E© (Macherey-Nagel).

The synthesis of the cyclodextrin derivatives is performed in two steps: The carbon atoms at the positions C(2) and C(6) of the native α-, -β, and γ-cyclodextrins are pentylized with 1-bromopentane (pentyl bromide) and pulverized sodium hydroxide in dimethyl sulfoxide at room temperature. This step is followed by replacing the hydroxyl group of the carbon atom at the third position of the saccharide molecule with an O-butanoyl group. This is done with a mixture of butyric acid anhydride and 4-(dimethylamino)-pyridine in triethylamine (for pH stabilization) at a temperature of 100 °C. More information on the modification of cyclodextrins and the influence on the selectivity of the macrocycles towards certain chiral molecules can be found in literature [114, 117, 133].

The chiral polymer mixtures as well as two achiral polymers serving as control experiments (poly(dimethylsiloxane) and poly(etherurethane)) have been deposited onto the transducer structures by spray-coating (see Section 3.3.1). The thicknesses of all sensitive layers were approximately 4 µm to avoid the contribution of swelling effects in the case of the interdigitated capacitor.

	Physical Properties					Measurement concentration ranges	
	Sat. vapor pressure [kPa]	Density [g/cm^3]	Molecular weight [g/Mol]	Boiling point [°C]	Molar volume [m^3/kmol]	[µg/l]	[ppm]
Methyl lactate	0.83	1.09	104.10	144	$9.55 \cdot 10^{-2}$	40-3300	10-800
Methyl-2-chloro-propionate	1.55	1.08	122.55	133	$1.14 \cdot 10^{-1}$	100-7800	20-1600

Table 5-2. Physical properties of the investigated analytes and the concentration ranges for the measurements [125, 134, 135].

For the measurements two different analytes (the respective (S)-enantiomer, the (R)-enantiomer and the racemic mixture) both based on propionic acids were chosen: Methyl lactate (methyl 2-hydroxypropionate) and methyl-2-chloropropionate. Since these analytes are commercially available, comprehensive sets of measurements could be performed (product information, see Table A-5). Both analytes are rather similar in their molecular structure but differ in either the methyl-group or the chlorine atom bound to the second carbon atom in the molecule (Figure 5-1 and Figure 5-2). As mentioned before, the stereoisomer chiral molecules are identical in their physical properties and not distinguishable in an achiral environment. Unfortunately the information on the physical properties that is available in literature [43, 125, 136] is limited. The coefficients for the Antoine equation, and thus the saturation vapor pressure, and the molar volume of the analytes were calculated based on measurements as published by K. Bodenhöfer *et al.* [125]. The physical properties and the used analyte concentrations ranges are listed in Table 5-2. The measurement setup has been detailed in Section 3.3.2.

To cover a wide range of analyte concentrations, several measurement series, using different mass-flow controllers, have been performed. The measurements have then been arranged with regard to the analyte concentrations and the overlap helped to set up sensor response plots versus analyte concentrations over a larger range.

5.3 Results

5.3.1 Preparatory Investigation of Material Properties

5.3.1.1 Determination of the Dielectric Constants

No values of the dielectric constants were available in literature for the enantiomers and the enantioselective polymers used in this work. As described in the previous chapter the physisorption of a certain analyte, e.g. n-octane, into different polymers causes different sensor signals. This is due to the different polymer/analyte interactions. To perform any data interpretation in the case of the capacitive sensor, it is necessary to precisely know the dielectric coefficients of the analytes and the polymers or cyclodextrin.

The usual operation mode of a capacitive sensor is the detection of analyte in air by means of a chemically sensitive layer. The change of the overall capacitance upon the absorption of the analyte is then measured. Alternatively, the capacitor may also be used to directly determine the dielectric constant of a pure liquid or a polymer sample. For this purpose, a drop of the liquid or a thick layer of a sample was applied onto an array of five uncoated interdigitated sensor structures and the change of the overall sensor capacitance was measured [72]. This method was used to determine the dielectric constants of the analytes methyl lactate and methyl-2-chloropropionate, as well as that of the pure cyclodextrins and the cyclodextrin/polymers composites.

In order to establish correlation between the capacitance and the dielectric constants, ε, a calibration curve with analytes of precisely known dielectric coefficient values was recorded (see Figure 5-8).

	Dielectric constant ε (25°C)
Toluene	2.38
Ethyl acetate	6.02
Dichloromethane	8.93
2-Butanol	16.56
Propan-2-ol	19.92

Table 5-3. Relative dielectric constants of the volatile organic compounds used for the calibration of the capacitive sensor to determine the dielectric coefficients of liquid analytes [102].

The liquid organic compounds were dropped onto the surface of the uncoated capacitive sensors by a pipette. For an accurate detection of the dielectric constant the amount of applied analyte has to completely fill the volume of the capacitor's electrical field [72]. Since rather volatile compounds evaporate rapidly, the coated chip was sealed with an inert and easily removable tape (Parafilm®, Mercateo). Due to this,

enclosure temperature and atmosphere around the capacitive sensor were kept stable for several minutes. After determining the frequency shift the remaining solvent was removed by using a tissue. By constantly monitoring the sensor response it was possible to confirm the complete removal of analyte residues before performing another measurement; the read-out frequency returns to the original value of the uncoated sensor before the experiment. The measurement temperature was 25 °C.

An equation for the fitting of the sensor responses was derived from the simplified equivalent circuit as shown in Figure 5-7.

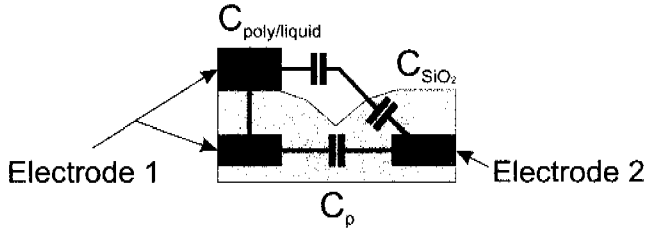

Figure 5-7. Sensor capacitance and simplified equivalent circuit.

The capacitances of the polymer or the liquid analyte, $C_{poly/liquid}$, and of the intermetal oxide, C_{SiO2}, are electrically connected in series. The resulting capacitance is connected in parallel with C_p, which describes the coupling between the two electrodes through the intermetal oxide (see Figure 5-7). The equivalent circuit yields the following equation:

$$C(\varepsilon) = C_p + \frac{C_{poly/liquid} \cdot C_{SiO_2}}{C_{poly/liquid} + C_{SiO_2}}$$

Eq. 5-13

As stated before, the frequency signal of the capacitive sensor is proportional to the overall sensor capacitance, C. The capacitance of the coating, $C_{poly/liquid}$, in Figure 5-7 can be expressed as a product of the analyte dielectric constant, ε, and the capacitance of an identical capacitor without any coating, C_0.

This leads to following equation for the curve fit:

$$f \propto C(\varepsilon) = k + \frac{1}{\frac{1}{C_{SiO_2}} + \frac{1}{\varepsilon \cdot C_0}}$$

Eq. 5-14

Here, k is a factor for the capacitive sensor offset. It includes the capacitance, C_p, of the sensing and the reference capacitor, and those of the feedback capacitors in the sigma-delta-converter circuitry [75]. The second term includes a serial combination of

the capacitances C_{SiO2} and $C_{poly/liquid}$. A more detailed description of the relation between the frequency shift and the capacitance change will be given in the subsequent section. The complete derivation of Eq. 5-14 can be found in literature [72].

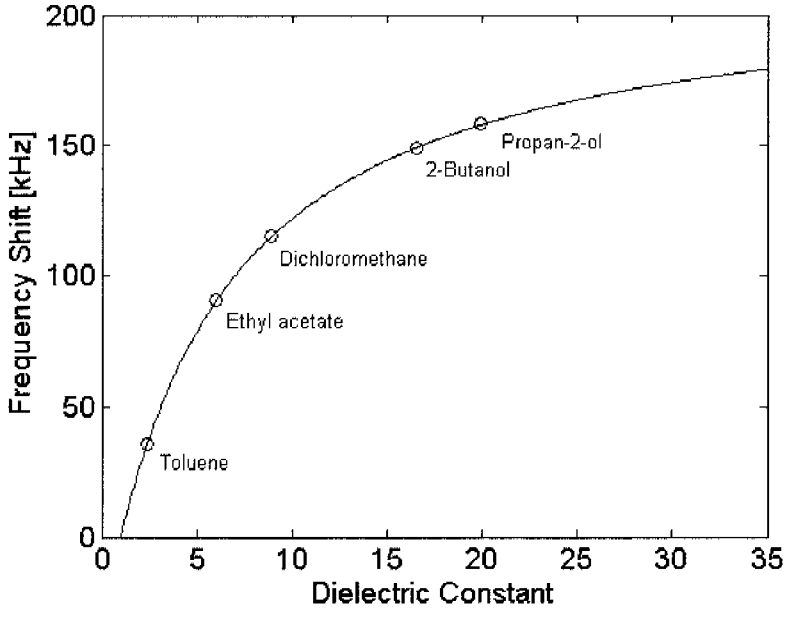

Figure 5-8. Sensor signals upon exposure to liquid analytes of defined dielectric constant and the respective fits (solid line).

For the determination of the dielectric constants of methyl lactate and methyl-2-chloropropionate, the liquid analytes have been applied to the capacitor structure as described before. The cyclodextrins and the cyclodextrin/PDMS mixtures were dissolved in dichloromethane to enable the deposition on the capacitor surface. After the coating procedure the chip was then placed in a vacuum for several minutes to evaporate the solvent and to eliminate its possible disturbance on the sensor signal. After measuring a substance the chip was carefully rinsed with different solvents (dichloromethane and trichloromethane) until the read-out signal coincided with the original value of the uncoated capacitor.

Figure 5-8 shows the calibration measurement results. Here, the frequency shift upon sample exposure is plotted versus the relative dielectric constant. The extracted fitting parameters were used to determine the unknown dielectric constants of the enantiomers and the enantioselective coatings by solving Eq. 5-14 for ε.

The results are listed in Table 5-4. It was found that the dielectric constants of the enantiomeric analytes are rather high: Methyl-2-chloropropionate has a value of $\varepsilon = 15.0$ and methyl lactate features an $\varepsilon = 31.1$. For the pure cyclodextrins the dielectric coefficient values are found to be about 4. The β-cyclodextrin with an uneven number of seven molecules in the ring has the highest dielectric constant of $\varepsilon = 4.15$, followed by α-cyclodextrin ($\varepsilon = 4.12$) and γ-cyclodextrin ($\varepsilon = 4.07$). Due to the lower dielectric

constant of PDMS ($\varepsilon = 2.8$), mixing the respective cyclodextrins with the polysiloxane at 50% (w/w) reduces the composite dielectric value to $\varepsilon = 3.08$-3.21. The dielectric constant of β-cyclodextrin/PDMS is, again, higher than that of other two cyclodextrins in PDMS.

	Dielectric constant ε (25°C)
Methyl lactate	31.11 ± 2.56
Methyl-2-chloropropionate	15.02 ± 0.23
α-Cyclodextrin (pure)	4.12 ± 0.48
β-Cyclodextrin (pure)	4.15 ± 0.13
γ-Cyclodextrin (pure)	4.07 ± 0.58
α-Cyclodextrin/PDMS (50% w/w)	3.10 ± 0.04
β-Cyclodextrin/PDMS (50% w/w)	3.21 ± 0.06
γ-Cyclodextrin/PDMS (50% w/w)	3.08 ± 0.03

Table 5-4. Dielectric constants and the calculated standard deviations of the enantiomers, cyclodextrins and the cyclodextrin/PDMS composites as determined by means of a capacitor array.

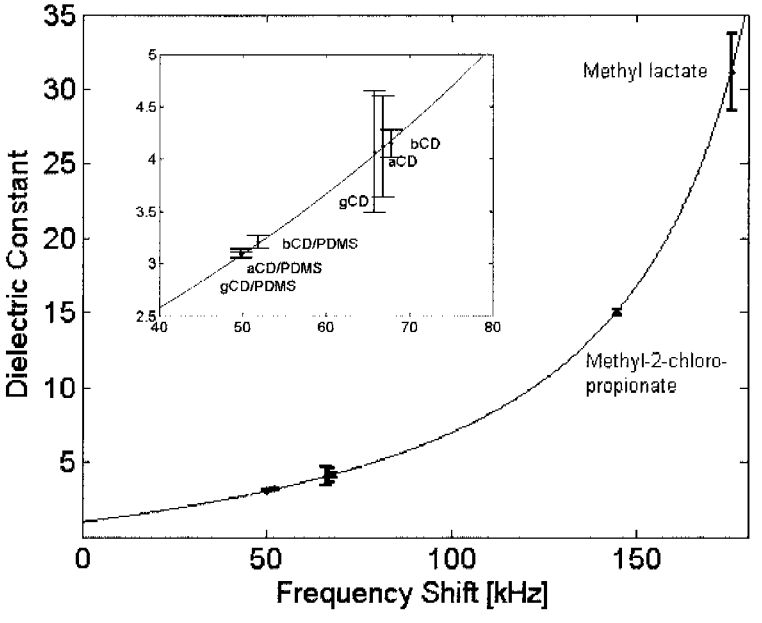

Figure 5-9. Dielectric constants of the chiral analytes, the α-, β-, γ-cyclodextrins (aCD, bCD and gCD) and the 50% CD/PDMS combinations. The solid line represents the calibration curve.

Figure 5-9 depicts the calculated dielectric constants of the substances listed in Table 5-4 as a function of the frequency shift. The sensor calibration curve is represented by the solid lines in Figure 5-8 and Figure 5-9.

5.3.1.2 Relation of Frequency Shift to Capacitance Change

The capacitance change upon analyte absorption within a polymer is in the atto-Farad range. A second-order sigma-delta-modulator (ΣΔ-modulator) differential measurement with the polymer-coated sensing-capacitor, C_S, and a passivated reference, C_{ref}, is used to assess such minute capacitance changes [67, 75]. With the preset reference and feedback capacitances a change in the output signal Δf_{out} can be directly assigned to a change in the sensor capacitance, ΔC_S, via:

$$\Delta C_S = \frac{2 \cdot C_{fb}}{f_{clk}} \cdot \Delta f_{out} \approx 5.25 \frac{aF}{Hz} \cdot \Delta f_{out}$$

Eq. 5-15

For an uncoated sensing capacitor the absolute value of the interdigitated capacitors (C_S and C_{ref}) is approximately 8 pF [75], which is mainly due to the parallel capacitance, C_p, through the intermetal oxide (compare Figure 5-7). The fraction of the overall capacitance resulting from the sensitive polymer layer is only in the low pico-Farad range. To estimate the additional capacitance of the polymer layer the output frequency of a capacitor on a multi-transducer chip was measured before and after applying the polymer layer of γ-cyclodextrin/PDMS (50% (w/w)). A frequency shift of Δf_{out} = 151,5 kHz was determined, which corresponds accordingly to Eq. 5-15, to a capacitance of only 0.8 pF. The total capacitance of the polymer layer amounts to $C_{coating}$ = 1,68 pF after introducing a correction factor ε - 1 in Eq. 5-15, which relates the capacitance of the coated device to that of an "air-filled" uncoated sensor (Figure 5-7). Since the dielectric constant of the different cyclodextrin/PDMS layers are very similar to that of the polymer alone (see following section) their capacitance contribution should be similar.

5.3.2 Characterization of Different Enantioselective Composites

5.3.2.1 Enantiomers in an Achiral Environment

Two different achiral polymers were applied as sensitive layers for comparison with the results of the enantioselective coatings. The nonpolar PDMS and the slightly polar PEUT were used as an achiral sorption matrix. The two polymers show distinct sorption or physisorption characteristics (compare with Chapter 4). Two differently coated multi-sensor chips, one with an achiral and the other with an enantioselective coating, have then been measured in parallel. The sensor systems were exposed to different analytes: The two enantiomers of (i) methyl lactate and (ii) methyl-2-chloropropionate, as well as the standard organic volatiles n-octane and propan-1-ol. Linear sorption behavior, which is typical for a nonspecific physisorption process, was found for all analytes. As expected, the sensors showed no discrimination of the enantiomers of the chiral molecules, since their physical properties are identical. The measured sensitivi-

ties and the respective standard deviations for the different polymer/analyte combinations are listed in Table 5-5.

	Calorimeter		Cantilever		Capacitor	
	Sensitivity [mV·s/ppm]		Sensitivity [Hz/ppm]		Sensitivity [Hz/ppm]	
	PDMS	PEUT	PDMS	PEUT	PDMS	PEUT
n-Octane	$4.11 \cdot 10^{-1} \pm 1.13 \cdot 10^{-2}$	$2.10 \cdot 10^{-1} \pm 3.80 \cdot 10^{-2}$	$5.36 \cdot 10^{-2} \pm 8.32 \cdot 10^{-3}$	$2.08 \cdot 10^{-2} \pm 5.65 \cdot 10^{-5}$	$-4.44 \cdot 10^{-1} \pm 1.80 \cdot 10^{-2}$	$-5.01 \cdot 10^{-1} \pm 6.97 \cdot 10^{-2}$
Propan-1-ol	$4.45 \cdot 10^{-2} \pm 7.84 \cdot 10^{-3}$	$3.40 \cdot 10^{-1} \pm 4.18 \cdot 10^{-2}$	$3.88 \cdot 10^{-3} \pm 1.15 \cdot 10^{-3}$	$1.83 \cdot 10^{-2} \pm 6.69 \cdot 10^{-4}$	$1.72 \cdot 10^{-1} \pm 1.11 \cdot 10^{-2}$	$1.86 \pm 1.42 \cdot 10^{-1}$
Methyl lactate	$3.03 \cdot 10^{-1} \pm 3.34 \cdot 10^{-2}$	$7.02 \cdot 10^{-1} \pm 6.35 \cdot 10^{-2}$	$1.56 \cdot 10^{-2} \pm 4.95 \cdot 10^{-3}$	$7.01 \cdot 10^{-2} \pm 1.55 \cdot 10^{-3}$	$1.09 \pm 1.57 \cdot 10^{-1}$	$6.54 \pm 5.39 \cdot 10^{-1}$
Methyl-2-chloro-propionate	$3.05 \cdot 10^{-1} \pm 6.12 \cdot 10^{-2}$	$6.58 \cdot 10^{-1} \pm 2.90 \cdot 10^{-2}$	$4.41 \cdot 10^{-2} \pm 1.13 \cdot 10^{-3}$	$7.06 \cdot 10^{-2} \pm 2.34 \cdot 10^{-4}$	$1.38 \pm 6.89 \cdot 10^{-2}$	$3.66 \pm 3.58 \cdot 10^{-2}$

Table 5-5. Measured sensitivities and their standard deviations for volatile organic compounds and chiral analytes using the achiral polymers PDMS and PEUT.

In an achiral environment the enantiomers behave like any other analyte undergoing a physisorption process (compare Chapter 4): A polar molecule will always be preferentially absorbed in a polar polymer and a nonpolar polymer features an increased partitioning of nonpolar analyte molecules. This also holds true for these measurements, and for the capacitive sensor the polymer/analyte correlation is very clear: The more polar methyl lactate with a dielectric constant of 31 generates a larger signal in the slightly more polar PEUT in comparison to methyl-2-chloropropionate with a dielectric constant of $\varepsilon = 15$. The chloropropionate, in turn, causes higher signals in the nonpolar PDMS.

The partition coefficients of the enantiomer/polymer combinations have not been determined during the course of this thesis. However, the order of magnitude can be estimated based on the partition coefficients for the organic compound/polymer combinations (Table 4-2 and 4-3) and the known physical properties of the analytes. From the measured sensitivities given in Table 5-5 it can be derived that the partition coefficients of the chiral compounds in PEUT are larger than those of the standard organic volatiles (n-octane $K_c = 850$ and propan-1-ol $K_c = 1500$). For methyl lactate they are 3-4 times higher and of methyl-2-chloropropionate twice as high than those of propan-1-ol, which is in agreement with literature values [125]. The estimated partition coefficient of methyl lactate in PDMS is approximately 3-4 times larger and that of methyl-2-chloropropionate approximately 8 times larger than that of propan-1-ol ($K_c = 250$), which is slightly less than the values reported in literature [125].

5.3.2.2 Absorption of Standard Organic Solvents in Enantioselective Composites

Two standard solvents, n-octane and propan-1-ol, were tested with the different enantioselectively coated multi-sensor chips and served as control analytes. The enantioselective coatings consisted of a composite of either the α-, β- or γ-cyclodextrin derivative and of PDMS at a weight ratio of 50% (w/w). The concentration range for the organic compounds was 30-1200 ppm.

All transducers showed a linear dependence of the sensor signal on the analyte concentration upon exposure to the achiral volatile organic compounds. This linear sorption behavior (Henry sorption) is characteristic for physisorption and indicates a nonselective interaction between the analyte and the sensitive layer. It was found that the presence of the enantioselective receptors in the polymer increases the overall partitioning of the volatile organic analytes in the composite sensitive layer. One possible reason for this phenomenon was given in Chapter 4: The presence of the bulky supramolecular cyclodextrin molecules may increase the free volume within the polymer matrix and may enable an easier incorporation of the analyte molecules in the sorption matrix. Besides the increased free volume, the higher partitioning may also be a consequence of the presence of the macrocycles that serve as additional nonspecific sorption sites [125]. For the calorimetric and the mass-sensitive sensor this assumption is substantiated by an increasing sensitivity towards volatile organic compounds with increasing size of the cyclodextrin molecule (Table 5-6).

The measurements with the capacitive sensor support the assumption that both, the increase of the free volume and the presence of the enantioselective receptors that serve as additional nonspecific sites, are responsible for the sensitivity increase. For the pure rubbery polymers PDMS and PEUT (Table 5-5) it was shown that the absorption of analytes featuring a lower dielectric constant (e.g. n-octane) than that of the sensitive polymer leads to a capacitance decrease, whereas analytes with a higher dielectric constant than that of the polymer produce a capacitance increase (thick layers, compare Section 2.3.3). Polymers with an open structure and a large free volume, such as EC and PECH (Chapter 4), show a positive signal regardless of the analyte dielectric constant. In the case of the enantioselective coatings also the latter effect occurs: The absorption of n-octane ($\varepsilon = 1.95$) causes an increase of the layer capacitance, even though the constant of the enantioselective coating is higher than that of the analyte ($\varepsilon = 3.1$). The sensitivities in Table 5-6 show the effects of the cyclodextrin acting as additional nonspecific sites. For both organic compounds the calorimeter and the cantilever show an enhanced sensitivity with increasing size of the cyclodextrin molecule, which can be ascribed to the additional free volume in the sorption matrix. The capacitive sensor shows the strongest response upon absorption of organic compounds in the β-cyclodextrin derivative/PDMS coating. This finding will be discussed in detail in the following sections.

	Calorimeter			Cantilever			Capacitor		
	Sensitivity [mV·s/ppm]			Sensitivity [Hz/ppm]			Sensitivity [Hz/ppm]		
	α-CD/ PDMS	β-CD/ PDMS	γ-CD/ PDMS	α-CD/ PDMS	β-CD/ PDMS	γ-CD/ PDMS	α-CD/ PDMS	β-CD/ PDMS	γ-CD/ PDMS
n-Octane	$2.05 \cdot 10^{-1} \pm 3.17 \cdot 10^{-2}$	$2.59 \cdot 10^{-1} \pm 3.65 \cdot 10^{-2}$	$5.65 \cdot 10^{-1} \pm 6.82 \cdot 10^{-2}$	$3.20 \cdot 10^{-2} \pm 5.75 \cdot 10^{-3}$	$3.48 \cdot 10^{-2} \pm 8.72 \cdot 10^{-3}$	$5.78 \cdot 10^{-2} \pm 1.65 \cdot 10^{-2}$	$8.68 \cdot 10^{-1} \pm 3.15 \cdot 10^{-1}$	$1.21 \pm 2.14 \cdot 10^{-1}$	$5.87 \cdot 10^{-1} \pm 1.39 \cdot 10^{-1}$
Propan-1-ol	$5.97 \cdot 10^{-2} \pm 6.74 \cdot 10^{-3}$	$1.09 \cdot 10^{-1} \pm 3.99 \cdot 10^{-2}$	$4.78 \cdot 10^{-1} \pm 3.85 \cdot 10^{-2}$	$2.69 \cdot 10^{-3} \pm 1.34 \cdot 10^{-3}$	$1.33 \cdot 10^{-2} \pm 5.17 \cdot 10^{-3}$	$2.62 \cdot 10^{-2} \pm 4.03 \cdot 10^{-3}$	$1.56 \pm 2.00 \cdot 10^{-1}$	$1.96 \pm 8.06 \cdot 10^{-2}$	$1.77 \pm 6.84 \cdot 10^{-1}$

Table 5-6. Sensitivities to the volatile organic compounds n-octane and propan-1-ol using different enantioselective coatings.

5.3.2.3 α-Cyclodextrin

Even though α-cyclodextrins show little enantioselectivity [120, 131] and are, therefore, rarely used for chiral separation, a sensor chip was coated with a 4-µm-thick layer of hexakis(3-O-butanoyl-2,6-di-O-pentyl)-α-cyclodextrin/PDMS (50% (w/w)). Measurements were conducted for comparison with the other enantioselective coatings. The sensor system was exposed to the enantiomers of methyl lactate and methyl-2-chloropropionate, as well as the volatile organic compounds n-octane and propan-1-ol (see previous section). The concentration ranges for the chiral substances are given in Table 5-2.

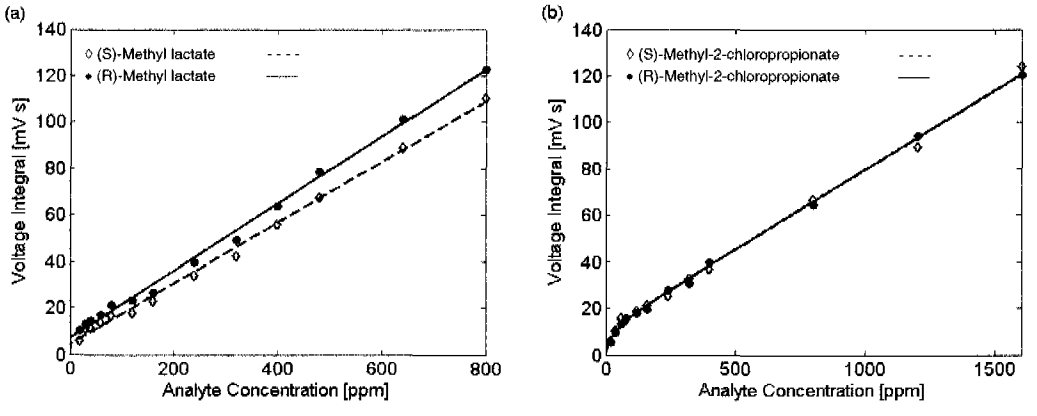

Figure 5-10. Sensor response versus analyte concentration of the calorimetric sensor coated with α-cyclodextrin/PDMS (50% (w/w)) upon exposure to (a) the two enantiomers of methyl lactate and (b) those of methyl-2-chloropropionate. The plotted lines provide a guide to the eye.

The working principle of the calorimetric transducer has been extensively described in Chapter 2. Here, the averaged values of the absorption and desorption peak integrals have been used for data evaluation. In Figure 5-10 the response of the calorimetric sensor upon exposure to the different enantiomers are displayed as heating power values versus analyte concentration. For the enantiomers of methyl lactate (Figure

5-10 (a)) the sensor showed linear sorption behavior as known from standard physisorption processes. It is evident that (R)-methyl lactate was preferentially absorbed in comparison to the other enantiomer. The calorimetric transducer did not show any discrimination of the enantiomers of methyl-2-chloropropionate as displayed in Figure 5-10 (b). The lack of a pronounced curvature of the graph, which would indicate a selective or preferential interaction, obviates the application of the absorption model for measurements with the α-cyclodextrin derivative. Therefore, the ratio of the linear response slopes upon dosing the enantiomers was used as a measure for chiral discrimination, so that a discrimination factor of 1.07 for methyl lactate was obtained, whereas no discrimination between the enantiomers of methyl-2-chloropropionate was detected ($\alpha \approx 1$).

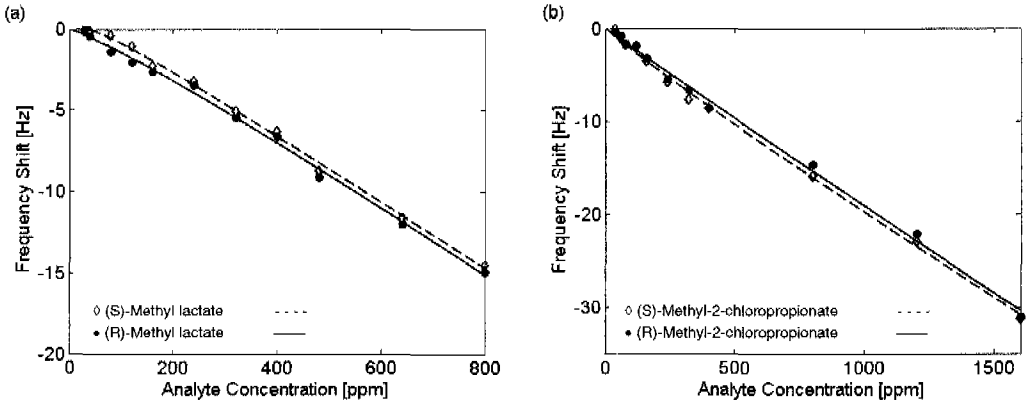

Figure 5-11. Sensor response versus analyte concentration of the mass-sensitive cantilever coated with α-cyclodextrin/PDMS (50% (w/w)) upon exposure to (a) the enantiomers of methyl lactate and (b) those of methyl-2-chloropropionate.

The linear sensor responses of the mass-sensitive cantilever for the enantiomers of methyl lactate and methyl-2-chloropropionate are plotted in Figure 5-11 (a) and Figure 5-11 (b), respectively. This transducer also evidenced only little preference of the sorption matrix for one of the enantiomers of both chiral substances. For methyl lactate a slightly higher signal was read out for the (R)-molecule, whereas for methyl-2-chloropropionate the (S)-enantiomer generated a marginally higher frequency shift. The chiral discrimination as determined by comparing the response slopes yielded values of 1.07 for methyl lactate. The chiral discrimination factor for the enantiomers of methyl-2-chloropropinate produced a value of 1.04 and is within the experimental error of the measurements. Therefore, a chiral discrimination was not possible for this substance.

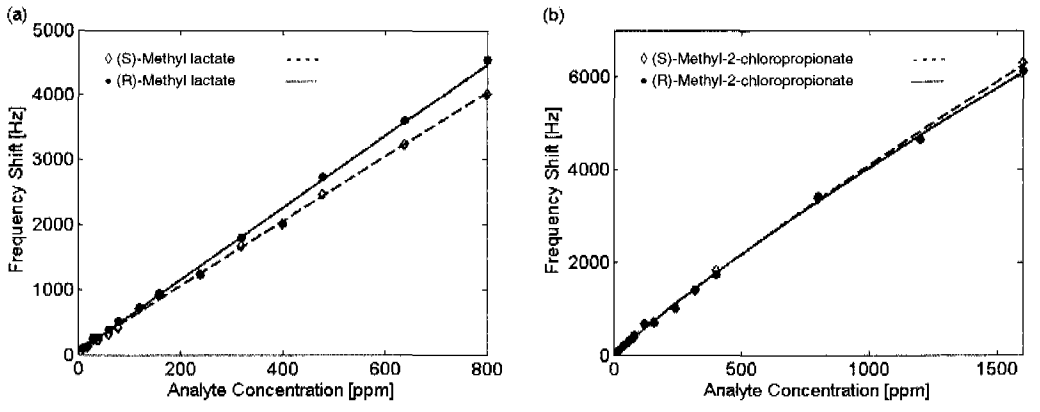

Figure 5-12. Sensor response versus analyte concentration of the capacitive sensor coated with α-cyclodextrin/PDMS (50% (w/w)) upon exposure to (a) the enantiomers of methyl lactate and (b) those of methyl-2-chloropropionate. The plotted lines serve as guides to the eye.

The measurement results of the capacitive sensor are consistent with those of the two other transducers: A slight preference of (R)-methyl lactate compared as to the (S)-enantiomer and no identifiable preference for any of the enantiomers of methyl-2-chloropropionate. As the graphs show linear characteristics the determined sensitivities were used as a measure for the chiral discrimination, which yields in an α of 1.13 for methyl lactate, whereas only little discrimination of the enantiomers of methyl-2-chloropropionate was observed.

All three sensor types show approximately linear response characteristics upon exposure to the chiral substances. This indicates none or only a very little specific interaction between the enantioselective cyclodextrin and the chiral analyte molecules. The results are in agreement with comparable measurements performed with the gas chromatography: The chiral discrimination factor for the enantiomers of methyl lactate yielded a value of 1.03, whereas no discrimination for the enantiomers of the chloropropionate was possible ($\alpha = 1$).

5.3.2.4 β-Cyclodextrin

The native β-cyclodextrin and, particularly, its derivatives are often used for chiral separation and discrimination in CE, CEC, GC, HPLC, SFC, and TLC. They are suitable materials for the separation of chiral amines, amino acids, ketones, lactones, sulfoxides, and sulfinate esters [27, 131].

For a comprehensive study a multi-sensor system chip was coated with a sensitive layer of heptakis(3-O-butanoyl-2,6-di-O-pentyl)-β-cyclodextrin/PDMS (50% (w/w)) and exposed to different concentrations of the enantiomers of methyl-2-chloropropionate. The sensor responses to the chiral substances evidence an enantioselective interaction, which is further supported by the response curvature. The curves are depicted in Figure 5-13 (a)-(c). Here, all three transducers show a preferential absorption of (S)-methyl-2-chloropropionate in comparison to the (R)-enantiomer. This

result coincides with NMR measurements that describe a preferential interaction of (S)-methyl-2-chloropropionate using a similar β-cyclodextrin derivative (heptakis(3-O-acetyl-2,6-di-O-pentyl)-β-cyclodextrin) [137].

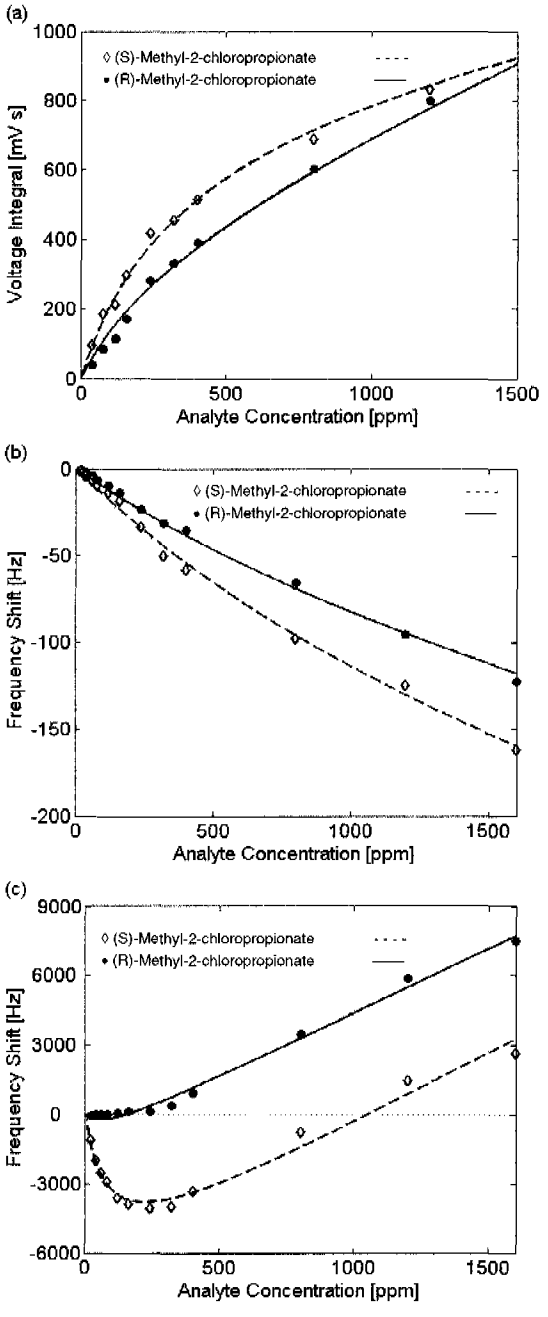

Figure 5-13. Sensor response versus analyte concentration for the calorimetric (a), the mass-sensitive (b), and the capacitive sensor (c) upon exposure to (S)- and (R)-methyl-2-chloropropionate. The coating is a 4-μm-thick β-cyclodextrin/PDMS (50% (w/w)) matrix. The plotted lines serve as guides to the eye.

Nevertheless, the absorption model as presented in Section 5.2.1 was not applicable and yielded a large error. This is due to the fact that, according to the model, an enantioselective interaction between analyte molecule and recognition site is only visible in the initial Langmuirian-type adsorption and desorption process (K'). The sensor responses should be very similar in their Henry-type nonspecific sorption ($K_{achiral}$) and the chiral contribution (K_{chiral}) for both enantiomers. This also implies a convergence of both signals at high analyte concentrations, when the specific sites are completely covered ($\theta = 1$), and when the nonspecific sorption dominates (Section 5.2.1).

The calorimetric sensor response (Figure 5-13 (a)) shows the described behavior. Whereas the mass-sensitive cantilever displays a nonlinear absorption behavior with only little bending. Here, the sensor response curves diverge at higher concentrations (Figure 5-13 (b)).

The signals for the capacitor are depicted in Figure 5-13 (c). The capacitive sensor shows the most pronounced effects upon exposure to the enantiomers. At low concentration the capacitance, which is proportional to the frequency shift, even decreases. This effect is then reversed at higher analyte concentrations. For (S)-methyl-2-chloropropionate this effect is more pronounced: The most negative sensor response value is reached at approximately 240 ppm, and then the capacitance increases continuously with analyte concentration (influence of the nonspecific sorption). At a (S)-methyl-2-chloropropionate concentration of about 1000 ppm the capacitor signal then becomes positive. The capacitor initially shows a similar response to the second enantiomer, (R)-methyl-2-chloropropionate, but displays a capacitance increase already at concentrations larger than 40 ppm.

The chiral receptor/analyte interaction and the underlying absorption and partitioning thermodynamics are certainly identical for all three sensors. The mass-sensitive cantilever is probably most closely related to the partitioning of the analyte in the enantioselective coating.

The output signal of the calorimeter and even more obviously of the capacitive sensor, however, are a convolution of the sorption thermodynamics and the sensor-specific transduction principle.

For the capacitive transduction, it is assumed that the intimate interaction of one of the enantiomers with the β-cyclodextrin causes a short-range-ordering of the molecules within the diastereomeric complex. This is then detected as a decrease of the overall dielectric constant of this complex with regard to its components (compare Chapter 2). The more intimate the chiral interaction, the more pronounced is this effect. However, the response contribution of the nonspecific sorption outweighs this ordering-induced response effects after full coverage of the recognition sites, and then, the overall capacitance increases due to the larger dielectric constant of the analyte ($\varepsilon \approx 15$) in comparison to that of the sorption matrix ($\varepsilon \approx 3.2$). A more detailed analysis of the capacitive signal will be given in the subsequent section for the γ-cyclodextrin derivative.

As explained above, the absorption model could not be directly applied to the transducer responses. As a measure for the chiral discrimination, the sensitivity ratios of the respective enantiomers were calculated for a defined, low concentration of 40 ppm. The determined discrimination factor α for the calorimeter and the mass-sensitive cantilever showed values of 2.4 and 2.0, respectively. At this concentration the capacitor provided a much higher discrimination factor of 114.2.

Comparative gas chromatographic measurements yielded a chiral discrimination factor of 1.57 for the enantiomers of methyl-2-chloropropionate, clearly showing a preferential absorption of the (S)-enantiomer.

5.3.2.5 γ-Cyclodextrin

Besides the β-cyclodextrins the larger γ-cyclodextrins and their derivatives are the most popular macrocycles for chiral separation [24, 27, 115]. The octakis(3-O-butanoyl-2,6-di-O-pentyl)-γ-cyclodextrin used here features properties that allow for the separation of a broad range of substances [138]. This cyclodextrin derivative is commercially available under the name of Lipodex E© for GC-applications (Macherey-Nagel).

The possibility of using cyclodextrins for the discrimination of enantiomers by means of gas microsensors has been first demonstrated by J. Ide *et al.* [139]. K. Bodenhöfer *et al.* further exploited the research on thickness-shear mode resonators (TSMR) using octakis(3-O-butanoyl-2,6-di-O-pentyl)-γ-cyclodextrin dissolved in PDMS as an enantioselective coating [44, 125, 140].

Based on these results, octakis(3-O-butanoyl-2,6-di-O-pentyl)-γ-cyclodextrin/PDMS (50% (w/w)) was chosen here again as an enantioselective layer to discriminate the enantiomers of methyl lactate and methyl-2-chloropropionate. The thickness of the enantioselective layer as used for this study was approximately 4 µm. The absorption model developed by K. Bodenhöfer [125] that has been detailed in Section 5.2.1 was used to also evaluate the results of the multi-transducer gas sensor system.

5.3.2.5.1 Homochiral Analytes

The calorimetric sensor relies on transient signals. It detects the release or the absorption of heat on the coated membrane, which is induced by the enthalpy changes during the absorption or desorption of analyte molecules in the sensitive layer (Chapter 2). Figure 5-14 displays the measured thermovoltages of the calorimetric sensor upon exposure to both enantiomers of methyl lactate. Here, the concentration range was 40-160 ppm applied in equidistant steps. For the absorption and the desorption process the sensor shows higher signals for the preferentially incorporated (R)-methyl lactate. The preferentially absorbed enantiomer generates a more sorption heat of one enantiomer than the less preferred analyte at the same concentration. The larger sorption heat is probably due to two effects: A larger enrichment of the preferred enantiomer and the release of more heat upon formation of the somewhat stronger diastereomeric complex.

It was found that, in comparison to the physisorption of standard organic compounds (Section 5.3.2.2), the desorption of the enantiomers generates higher signals and the thermal transient duration is longer. The higher peaks and the longer duration of, e.g., the desorption process indicate that more heat has to be abstracted from the environment to dissociate the diastereomeric complexes. This applies to a larger extent to the retention of the preferred enantiomer, which forms a more stable complex with the cyclodextrin receptor. On the other hand, the absorption time constants of both enantiomers are comparable.

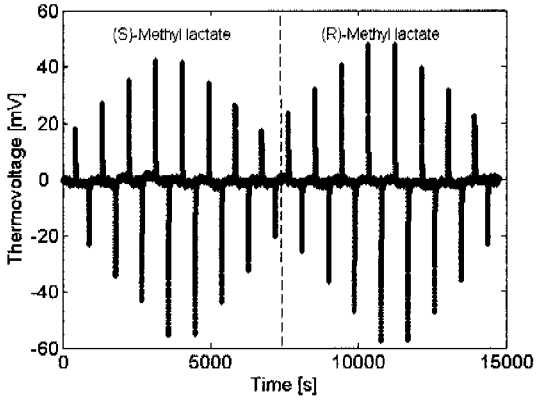

Figure 5-14. Measured signals of the calorimetric sensor upon exposure to (S)-methyl lactate and (R)-methyl lactate at concentrations of 40-160 ppm in equidistant steps.

Therefore, only the signal integrals of the absorption process were used for data evaluation and not, as before, the averaged values of the absorption and desorption peak integrals.

Figure 5-15 (a) and (b) depict the thermovoltage integrals in dependence of the analyte concentrations for the enantiomers of methyl lactate and methyl-2-chloropropionate, respectively. The pronounced curvatures of all responses suggest a stronger interaction in comparison to the previously described α- and β-cyclodextrins. The sensor detects a preferential absorption of (R)-methyl lactate and (S)-methyl-2-chloropropionate. The chloropropionate generates higher signals as has been shown in literature [43, 125, 140].

The absorption and desorption characteristics (e.g., long desorption time) of the analytes in the enantioselective coating suggests that not only the partitioning but also the different enantiomer/receptor-complexation heats significantly contribute to the sensor signal. Hence, the absorption model presented in Section 5.2.1 cannot be directly applied to the calorimeter data, since only the thermodynamics are considered in this model. Nevertheless, an analysis according to this model was attempted.

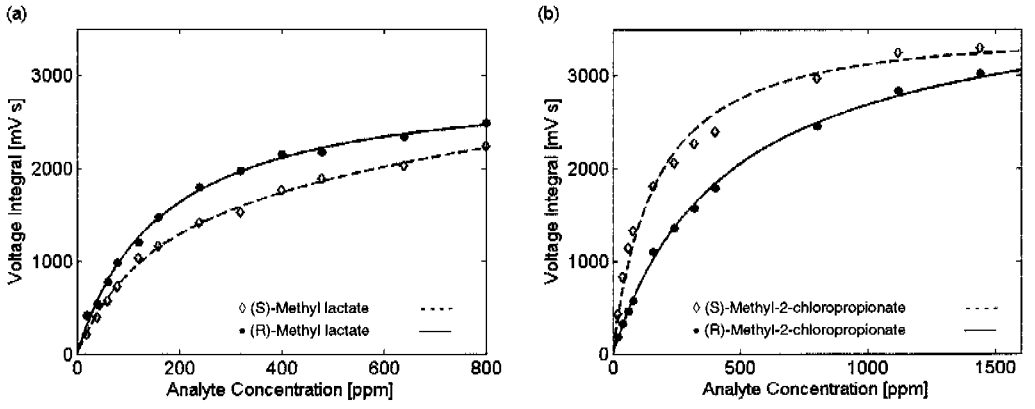

Figure 5-15. Measurement results of the calorimetric sensor: Integrated thermovoltage (absorption peak only) versus analyte concentration for (S)- and (R)-methyl lactate (a) and the enantiomers of methyl-2-chloropropionate (b). The respective fits are displayed as dashed and solid lines.

The evaluation of the data and the extraction of the fitting parameters were done with a MatLab® program: The parameters K', K_{chiral} and $K_{achiral}$ were extracted from the measured signals using a least-mean-square fit. The results are given in Table 5-7. From the results but also from the plots in Figure 5-15 it can be concluded that the main contribution to the sensor signal is the preferential or chiral interaction (K_{chiral}). The nonspecific absorption, which prevails at higher concentrations, adds only little to the low-concentration signals. From the extracted parameter values the discrimination factor can be calculated according to Eq. 5-12. For the discrimination of the enantiomers of methyl lactate a factor $\alpha_{R/S} = 1.53$ has been determined and for methyl-2-chloropropionate the calculated value is $\alpha_{S/R} = 2.49$.

	Calorimeter			
	(S)-Methyl lactate	(R)-Methyl lactate	(S)-Methyl-2-chloropropionate	(R)-Methyl-2-chloropropionate
K' [ppm^{-1}]	$4.13 \cdot 10^{-3}$	$6.31 \cdot 10^{-3}$	$5.88 \cdot 10^{-3}$	$2.35 \cdot 10^{-3}$
K_{chiral} [mV·s]	2900		3730	
$K_{achiral}$ [mV·s/ppm]	$6.61 \cdot 10^{-2}$		$6.73 \cdot 10^{-2}$	
Discrimination factor α	1.53		2.49	
Average relative error [%]	0.46	0.44	0.97	0.31

	Mass-sensitive Cantilever			
	(S)-Methyl lactate	(R)-Methyl lactate	(S)-Methyl-2-chloropropionate	(R)-Methyl-2-chloropropionate
K' [ppm^{-1}]	$6.57 \cdot 10^{-3}$	$2.17 \cdot 10^{-2}$	$1.00 \cdot 10^{-2}$	$1.86 \cdot 10^{-3}$
K_{chiral} [Hz]	-18.9		-34.1	
$K_{achiral}$ [Hz/ppm]	$-4.15 \cdot 10^{-2}$		$-2.93 \cdot 10^{-2}$	
Discrimination factor α	2.73		3.99	
Average relative error [%]	2.80	2.49	1.67	1.94

	Capacitor			
	(S)-Methyl lactate	(R)-Methyl lactate	(S)-Methyl-2-chloropropionate	(R)-Methyl-2-chloropropionate
K' [ppm^{-1}]	$1.92 \cdot 10^{-3}$	$2.74 \cdot 10^{-2}$	$1.84 \cdot 10^{-2}$	$8.67 \cdot 10^{-4}$
K_{chiral} [Hz]	± 996		± 244	
$K_{achiral}$ [Hz/ppm]	5.72		5.53	
Discrimination factor α	4.33		6.59	
Average relative error [%]	1.85	2.66	14.84	9.43

Table 5-7. Characteristic parameters of combined fits: K', K_{chiral}, $K_{achiral}$, and calculated discrimination factor, α, for the enantiomers of methyl lactate and methyl-2-chloropropionate as determined with the different sensor types coated with octakis(3-O-butanoyl-2,6-di-O-n-pentyl)-γ-cyclodextrin/ PDMS (50% (w/w)).

An example measurement of the mass-sensitive cantilever is depicted in Figure 5-16 for methyl lactate at concentrations of 10, 20, 30, and 40 ppm. The negative frequency shift of the resonating cantilever is a consequence of the increase of the oscillating mass. Since the molecular weight of both methyl lactate enantiomers is identical, the higher signal for the preferentially absorbed enantiomer results from a higher partitioning.

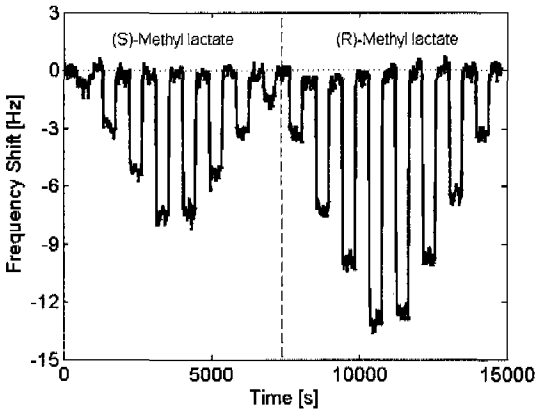

Figure 5-16. Measurement signals of the mass-sensitive cantilever upon exposure to concentrations of 10-40 ppm of (S)-methyl lactate and (R)-methyl lactate.

The measured frequency shifts and the respective curve fittings are depicted in Figure 5-17. Again, a preferential absorption of the (R)-methyl lactate and the (S)-methyl-2-chloropropionate is evident.

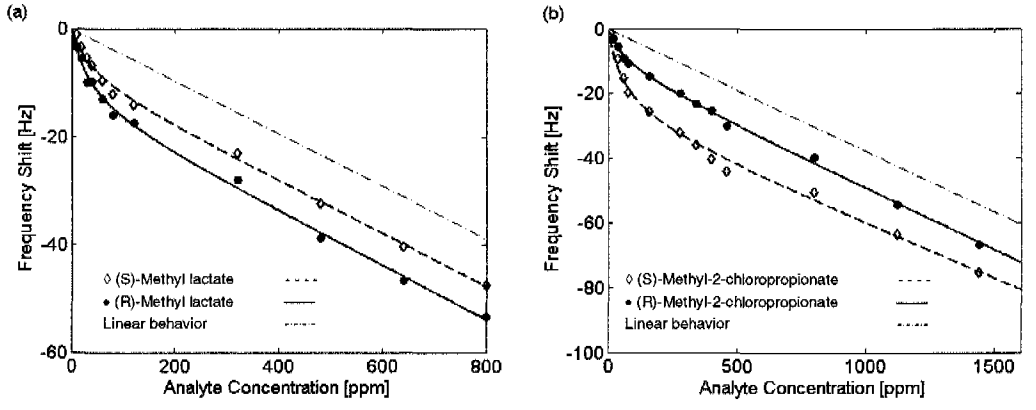

Figure 5-17. Measurement results of the mass-sensitive cantilever: Frequency shift versus analyte concentration for (S)- and (R)-methyl lactate (a) and the enantiomers of methyl-2-chloropropionate (b). The respective fits are displayed as dashed and solid lines. The dashed/dotted line marks a corresponding linear, unspecific analyte absorption.

There is no chiral discrimination possible, e.g., the chiral discrimination factor, α, equals unity ($\alpha \rightarrow 1$) at higher concentrations, where the unspecific absorption is predominant. According to Eq. 5-10 of the absorption model, this implies that the (S)- and (R)-analyte signal adopt the same linear sorption isotherm for high concentrations. A convergence of the chloropropionate response curves can be seen in Figure 5-17 (b), but the applied concentrations are still too low to clearly see the isotherm coincidence.

The extracted fitting parameters allow for the calculation of the discrimination factors, α, which are 2.73 in the case of the methyl lactate enantiomers and 3.99 for the chloropropionate (Table 5-7).

The capacitive transducer detects changes of the dielectric constant of the composite sensitive layer upon analyte absorption, which changes of the overall layer capacitance.

In the context of the capacitive measurements with the β-cyclodextrin derivative (Section 5.3.2.4) it was shown that the aspects that additional aspects have to be taken into account for capacitive enantioselective measurements. The sensor responses upon dosage of the two enantiomers of a specific analyte can be vastly different, although the relative dielectric constants of both chiral molecules are identical (Section 5.3.1.1). This behavior has been ascribed to the fact that one of the enantiomers interacts more intensely with the receptor, which leads to short-range-ordering effects and a lower dielectric coefficient of the analyte/receptor complex in comparison to that of the analyte or receptor alone.

At low concentration, where mainly the specific interaction between analyte and macrocycle occurs, the less preferred enantiomer causes positive sensor signals (capacitance increase), whereas the preferentially absorbed molecule generates a negative response. The explanation for this behavior is that the formation of the tighter diastereomeric complex of recognition site and preferred enantiomer causes a close-proximity ordering effect.

Figure 5-18 displays the capacitor response to the nonpreferred (S)-methyl lactate and the preferentially absorbed (R)-enantiomer at a concentration range from 10 to 400 ppm. Whereas the absorption of (S)-methyl lactate always generates a capacitance increase, the preferentially sorbed enantiomer causes a decrease up to a concentration of about 100 ppm (full occupation of the macrocycles). Then, the sensor signal returns in the range of a positive frequency shift; the unspecific sorption and thus the larger analyte dielectric constant prevails over the effect of the short-range-ordering. The effect of this "short-range-ordering" is so strong that it entails higher absolute signal values in comparison to the nonpreferentially absorbed analyte at the initial low concentrations.

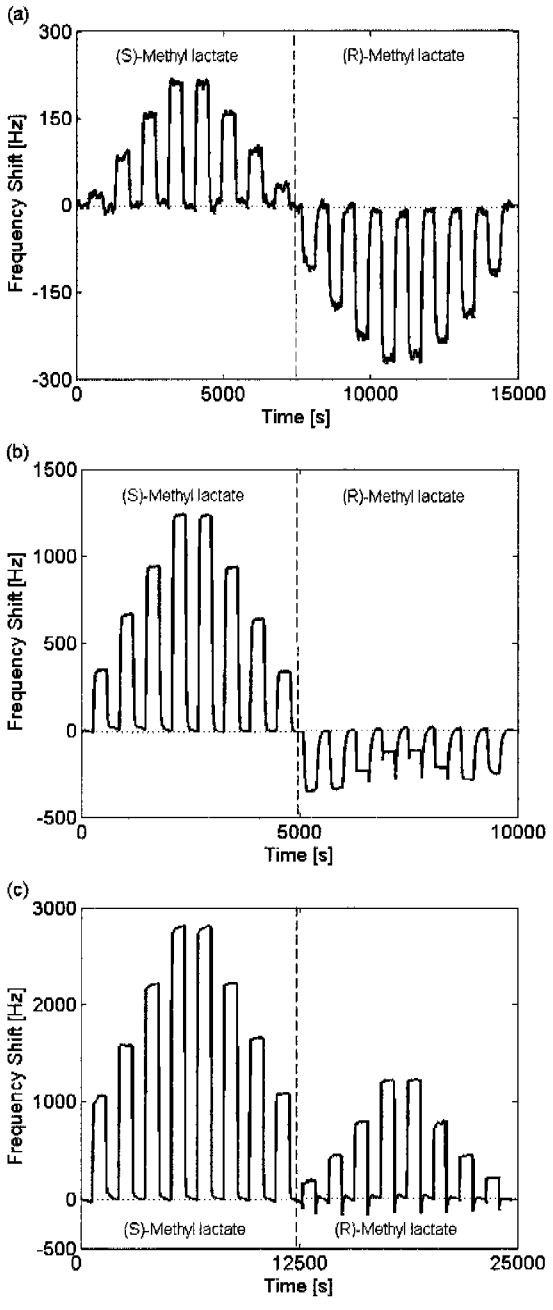

Figure 5-18. Signals of the capacitive sensor upon exposure to the enantiomers of methyl lactate at concentrations of (a) 10-40 ppm, (b) 40-160 ppm, and (c) 160-400 ppm.

Only the steady-state signals have been examined so far. But as is displayed in Figure 5-18 for methyl lactate and Figure 5-19 for methyl-2-chloropropionate, the sensor dynamics upon absorption and desorption of the preferred analyte also contain valuable information. At concentrations, where the nonspecific absorption of the analyte within the sensitive layer becomes predominant, the capacitor first exhibits a transient, very short signal decrease (down peak) followed by a capacitance increase. This indicates,

in my opinion, that the specific recognition sites are covered first and then, after full coverage of these sites, the nonspecific sorption takes place and determines the signal since the analyte concentrations are rather high. With increasing analyte concentrations, however, this "down peak" becomes less pronounced (Figure 5-19). This implies a simultaneous specific and nonspecific sorption behavior at a supply of a large number of analyte molecules. Upon desorption of the analyte from the enantio-selective matrix the sensor response shows another particularity. Independent of the analyte concentration, which is higher than that needed for full coverage of all recognition sites, the capacitor always shows a distinctive down-peak for the pure enantiomer. It can be concluded that the desorption time constant of the nonspecifically embedded molecules is significantly lower than that of the preferentially bound analyte molecules. The high stability of the diastereomeric complex prevents the immediate dissociation of the molecules. These results correlate with the previously mentioned findings for the calorimetric sensor.

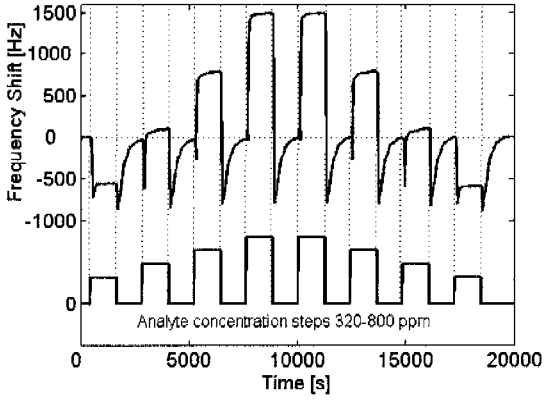

Figure 5-19. Sensor response of the capacitor coated with modified γ-cyclodextrin/PDMS (50% (w/w)) upon dosage of 320, 480, 640, and 800 ppm (S)-methyl-2-chloropropionate.

It was observed that the desorption time constant of the preferentially absorbed (S)-methyl-2-chloropropionate is larger than that of the (R)-methyl lactate. This may be a consequence of the more stable diastereomeric complex in the case of the chloropropionate. Further and more detailed investigations of the absorption and desorption kinetics will be the topic of future work. Additional measurements at a higher sampling frequency will provide more information on the dynamic behavior.

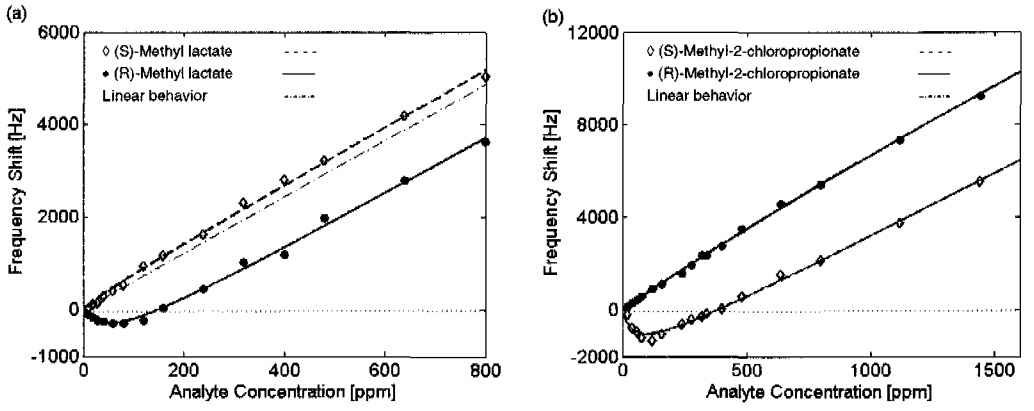

Figure 5-20. Experimental results and model fits of the capacitive sensor responses in dependence of the analyte concentration for (S)- and (R)-methyl lactate (a) and the enantiomers of methyl-2-chloropropionate (b). The model fits are displayed as dashed and solid lines. The dashed/dotted line indicates a linear, unspecific analyte absorption behavior.

Only the steady-state signals of the capacitive sensor were used for data evaluation and for applying the absorption model. Figure 5-20 (a) and (b) show the results and the individual fits for the pure enantiomers of methyl lactate and methyl-2-chloropropionate, respectively. It should be noted that for each fit the parameters K', K_{chiral}, $K_{achiral}$ have been individually optimized. The preferred enantiomers (R)-methyl lactate and (S)-methyl-2-chloropropionate display the lowest signal at a concentration of 100 ppm. This indicates that at this analyte concentration all of the specific recognition sites are occupied ($\theta = 1$). Again, a stronger interaction of the (S)-methyl-2-chloropropionate and the macrocycle in comparison to the (R)-methyl lactate is apparent. At full coverage of the recognition sites the sensor signal of the (S)-chloropropionate analyte is about five times larger than that of the (R)-methyl lactate. With higher analyte concentrations the sensor signal then increases steadily, which can be attributed to the increasing unspecific sorption of the analyte molecules. For high analyte concentrations the sensor seemingly shows higher signals for the nonpreferred enantiomer, but one has to keep in mind that the short-rang-ordering effects reduce the overall signal for the preferentially absorbed analyte.

Since all of the sensors are coated with the same material, the thermodynamic considerations of the absorption model are valid for all transducers. However, in particular for the capacitive sensor the measured signal represents a convolution of the sorption thermodynamics and the close-proximity-effect of the specific analyte/cyclodextrin interaction. This ordering effect largely influences the sensor signal and is specific for the applied transduction principle. From Figure 5-20 it is obvious that the absorption model is not directly applicable for this case. Nevertheless, a combined fit for both enantiomer signals was performed (Table 5-7).

The results of this combined fit show a better chiral interaction (K_{chiral}) for methyl lactate in comparison to the chloro derivative and an error for methyl-2-chloropropionate.

The results, however, contradict the results of the other two transducers and the large error implies a bad fit. The bad fit and the strange results are a consequence of the application of a combined fit, for which it is assumed that both response curves will coincide for rather large analyte concentrations. This, however, will not be the case. Due to the initial negative signal swing for the preferentially absorbed enantiomer, the response graphs will never coincide, but run in parallel for high concentrations. Therefore individual fits are the solution of choice for the capacitor in contrast to the other two transducers, for which the combined fit is applicable, since the prerequisites are met (see Figure 5-15 and Figure 5-17).

The chiral discrimination factors, α, were nevertheless calculated for the combined fit and yielded a value of 4.33 for methyl lactate and 6.59 for methyl-2-chloropropionate.

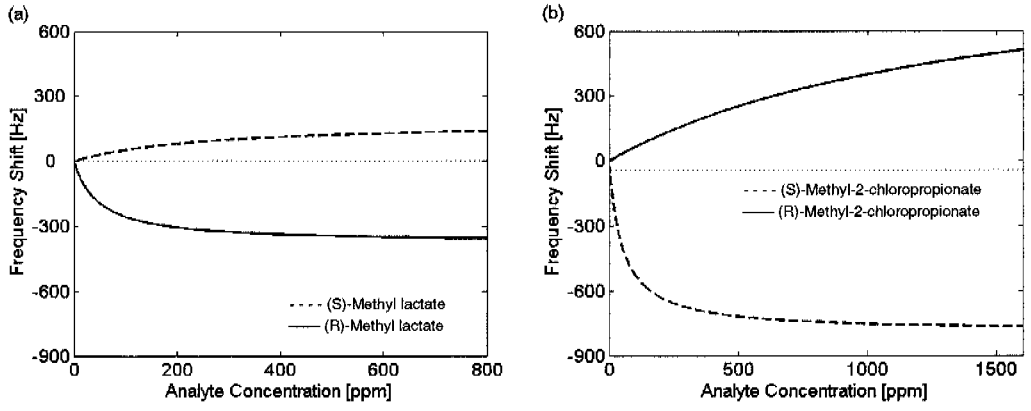

Figure 5-21. Modeled $\Delta f_{chiral}(c)$ part for the individually fitted analyte responses. The (S)-enantiomers of methyl lactate and methyl-2-chloropropionate are represented by dashed lines, the (R)-analytes by solid lines.

Based on the individual fits, the sensor response ($\Delta f_{sum}(c)$) has been divided into two parts: One part represents only the chiral interaction ($\Delta f_{chiral}(c)$) and the other part corresponds to the unspecific, Henry-type analyte sorption ($\Delta f_{achiral}(c)$) (see Section 5.2.1).

Using the fit parameters, the Langmuirian contribution to the sensor signals has been calculated backwards and is displayed as a graph frequency shift versus analyte concentration in Figure 5-21 for both chiral analytes.

It is obvious that the short-range-ordering causes a significantly higher sensor response (absolute value) than the interaction with the nonpreferentially sorbed enantiomer. This can be concluded from the initial curvature (K') and the sensor signal at full occupation of the receptor sites (K_{chiral}). As a measure for this "sensitivity enhancement", which is a consequence of the transduction principle, the chiral discrimination factors, α, were determined according to Eq. 5-12 of the absorption model, using the parameters of the individual fits. The discrimination factors were 4.71 for methyl lactate and 51.8 for methyl-2-chloropropionate.

In summary, the absorption model was only directly applicable to the mass-sensitive cantilever, since the signals of this sensor reflect the model thermodynamics. In Eq. 5-7 the correlation of the chiral discrimination factor, α, and the difference of the Gibbs energy of both enantiomers ($\Delta\Delta G$) was shown. The calculated α-values correspond to a difference of the Gibbs energy of $\Delta\Delta G = 2.53$ kJ/mol for the enantiomers of methyl lactate and 3.49 kJ/mol for methyl-2-chloropropionate upon transition from the gas to the liquid phase (polymer sorption).

The three investigated enantioselective coatings were identical in their compositions (cyclodextrin derivative and PDMS at 50% (w/w) but different in the size of the dissolved cyclodextrin ring: α-cyclodextrin consists of six α-D-glucopyranoside units, the β-cyclodextrin of seven and the γ-cyclodextrin is an eight-unit ring molecule.

Comparing the sensor responses using these three different coatings, it was found that the enantioselectivity as well as the sensitivity to the organic compounds of the calorimetric and the mass-sensitive transducer increased with the size of the cyclodextrin. The capacitive sensor, on the other hand, showed the strongest response upon dosage of the enantiomers and volatile organic compounds for the β-cyclodextrin derivative. Based on previous considerations, it is clear that the short-range-ordering seems to be particularly strong for the β-cyclodextrin. However, at this point it cannot be clarified, whether such more "intimate" interaction is due to the smaller cavity (assuming inclusion of the analyte molecule) or to other effects of the glucose units and side chains. Nevertheless, the γ-cyclodextrin derivative is the most interesting for chiral discrimination, since it allows for an immediate distinction of the less preferred and preferentially sorbed enantiomer at low analyte concentrations by means of a positive versus a negative sensor response.

A decrease in enantioselectivity of the coating over time was noticeable for all three transducers. For the resonating cantilever the loss in sensitivity is not uncommon: A lot of the polymer volume shifts from the tip of the cantilever towards the base, due to the cantilever oscillation and the elasticity of the polymer coating. This causes a decrease of the resonance frequency and, thus, the cantilever sensitivity. The other two transducers also showed a decrease in enantioselectivity. This is probably a result of the so-called "self-inclusion", which was explored by A. Mele [118] for the γ-cyclodextrin derivative. One of the mobile 6-O-pentyl chains connected to the secondary rim of the glucose unit (Figure 5-5) inserts into the inner part of the cavity and remains there. This chain thus inhibits the analyte molecules interaction inside the cyclodextrin forms. It was also shown that the mobility and the interaction participation of the side chains strongly depend on the temperature. At room temperature (measurement temperature 303 K) the macrocycle dynamics are rather slow in comparison to the elevated temperatures used in GC (60-80 °C), which renders the insertion of a pentyl chain less probable.

5.3.2.5.2 Racemic Mixtures

A racemate is a mixture of equal amounts of left- and right-handed enantiomers of a chiral molecule. It is optically inactive, because the two optical isomers rotate plane-polarised light to the same extent in opposite directions so that a net rotation of zero results.

The measurements of the racemic mixtures of methyl lactate and methyl-2-chloropropionate were performed with the modified γ-cyclodextrin/PDMS-coated multi-sensor chip. For the calorimetric sensor only the signals upon analyte absorption were taken into account to compare the results with the measurements of the pure enantiomers. In the case of the capacitor and the cantilever the steady-state signals were analysed.

Applying a certain racemate concentration means that half of the analyte amount consists of the (S)-enantiomer and the other half of the (R)-analyte. All sensors showed upon exposure to the racemic mixture a signal that represents approximately a "mean value" of the signals upon exposure to the pure enantiomers rather than a superposition of the signals of both enantiomers at half the concentration. This suggests that not all receptor sites are occupied by the "preferentially absorbed" enantiomer, but that there is a competitive process for sorption at the preferential sites of the dextrin molecules. In Figure 5-22 (a) an example measurement of the calorimetric sensor is depicted.

In the case of the capacitor the stronger sensor response to the preferentially absorbed enantiomer causes a decrease of the overall layer capacitance (Figure 5-22 (b)) at low concentrations. The short-range-ordering of the preferentially absorbed enantiomer predominantly contributes to the resulting signal, which also can be seen for the signals of the racemic mixture. At higher analyte concentrations the signal is dominated by the unspecific analyte absorption (Henry absorption) so that the sensor response upon racemic exposure coincides with the "mean value" of both pure enantiomers.

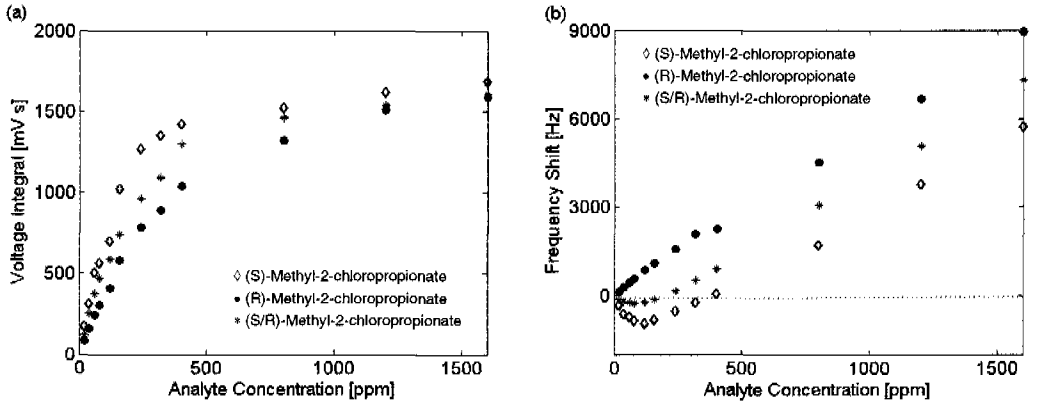

Figure 5-22. Comparison of the measurements of the pure enantiomers of methyl-2-chloropropionate and the racemic mixture of (a) the calorimeter and (b) the capacitive sensor.

As mentioned before, only the steady-state signals of the capacitive sensor were taken into account for the data evaluation. The dynamic signals of the capacitor contain information about the absorption and desorption characteristics, which can be seen in Figure 5-23. For better comparison Figure 5-23 (a) shows the sensor signals upon exposure to the preferentially sorbed (S)-methyl-2-chloropropionate and to the respective (R)-enantiomer in a concentration range of 40-160 ppm. From the measurements of the pure (S)-enantiomer the analyte concentration at full receptor coverage can be determined to be approximately 100 ppm. In Figure 5-23 (a) it can be seen that the capacitor response is either from the beginning positive (nonpreferred analyte) or initially negative (preferentially absorbed analyte) (compare Section 5.3.2.5.1). The absorption of the racemic mixture (Figure 5-23 (b)), however, shows a different dynamic behavior. At low overall analyte concentrations, where the analyte molecules prevalently interact with the specific reception sites, the capacitance initially sharply increases. With increasing exposure time of the analyte a maximum is reached and, thereafter, the capacitance decreases and reaches an equilibrium value. This indicates that first the Henry-type absorption of the less preferred enantiomer ((R)-methyl-2-chloropropionate or (S)-methyl lactate) occurs. The absorption and desorption of the preferentially sorbed enantiomer is slower, which also suggests a stronger interaction between the cyclodextrin and the preferred enantiomer. Upon switching off the analyte supply there is a strong overshoot in the negative signal direction indicating slower desorption of the preferentially absorbed (S)-chloropropionate or (R)-methyl lactate, which obviously forms a stronger complex with the cyclodextrin.

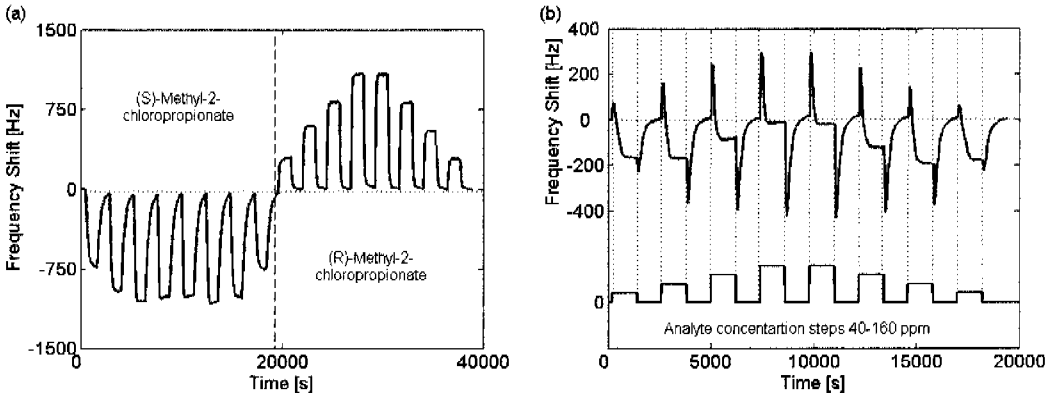

Figure 5-23. Sensor response of the capacitor upon exposure to (a) (S)-methyl-2-chloropropionate and the (R)-enantiomer at concentrations of 40-160 ppm and (b) to only the racemic mixture at concentrations of 40, 80, 120, 160 ppm. The concentration steps are indicated by dotted lines.

On the basis of the measurement results of the pure enantiomers and the transient signals upon exposure to the racemic mixtures it can be concluded that there is a competitive interaction with the nonpreferentially absorbed enantiomer and the preferred enantiomer competing for the specific absorption sites of the cyclodextrin. This behavior is also observed at higher analyte concentrations, where the overall sensor response is

then dominated by the unspecific absorption. It seems to be the case that the nonpreferentially sorbed enantiomer is initially faster to interact with the cyclodextrin and that there is a certain kinetic barrier for the preferred enantiomer. The preferred enantiomer, however, subsequently replaces most of the nonpreferred mirror-image molecules, since it forms a more stable complex with the cyclodextrin as is obvious from GC measurements and sensor measurements. The stability of this complex also entails a comparably slow desorption leading to a negative peak. From the measurements of the pure enantiomers it was shown that the non- or less preferred enantiomer molecules or the preferred enantiomer molecules in nonspecific sites (Figure 5-19) desorb faster than the specifically absorbed analytes, which form a more stable complex with the receptor. This is an indication for the dissociation of the less stable complex taking place first and a stronger retention of the preferred enantiomer at the receptor site (Figure 5-23 (b)).

The coexistence of two complexes of different stability is up to now a hypothesis, but the presented results strongly support this assumption. Results from literature [125, 129] further support this assumption that the occupation of the recognition sites is dependent on the availability and fraction of the two enantiomers in an enantiomeric mixture (statistical distribution). At this point the measurements of mixtures with enantiomeric excess (ee) will have to be conducted to learn more about the mechanisms and dynamics at the receptor sites.

However, it should be noticed that the dynamic sensor response of the γ-cyclodextrin/PDMS coated sensor upon exposure to a racemic mixture or a mixture of the two enantiomers of arbitrary composition contains quantitative information about the concentrations of both enantiomers present in the mixture so that a detection of the enantiomeric purity of a compound of impurities is possible within seconds after the sensor exposure to the respective sample.

5.3.2.5.3 Steric Investigation of the Diastereomeric Complex

Further insight into the interaction between the chiral analytes and the enantioselective sites can be found by means of using thin sensitive layers on the capacitive sensor. The effect, which is used then, is the so-called swelling effect [72]. To measure this effect the sensor was coated with a really thin layer of sensitive material as opposed to the previously performed measurements, where a thick layer of sensitive material was used (see Chapter 4 and above) so that any swelling occurred outside the reach of the electrical field lines and was not detected by the sensor, i.e., did not contribute to the sensor signal. A mixture of the modified γ-cyclodextrin and PDMS (50% (w/w)) was used as enantioselective coating. The thickness of the coating layer was about 1 µm and, thus, the overall layer volume was within the extension of the electrical field generated by the interdigitated capacitor electrodes. The capacitor was exposed to different concentrations of the enantiomers of methyl lactate and methyl-2-chloropropionate.

Upon analyte absorption, the volume of the sensitive matrix increases and this volume increase occurs within the electrical field lines, i.e., air is replaced by the layer/analyte composite. Assuming ideal mixing and low concentrations of the analyte within the sensitive layer, a relative increase of the layer thickness, $\delta h/h$, is directly proportional to the volume fraction of the analyte, φ_A:

$$\frac{\delta h}{h} = \varphi_A$$

Eq. 5-16

For small changes in the layer thickness the change of capacitance can be assumed to be proportional to the volume increase upon analyte absorption. Strictly speaking two effects taking place within the sensitive matrix have to be taken into account: (i) the now predominant swelling and (ii) the change of the layer composite dielectric constant. A more detailed description of the swelling effect can be found in literature [72].

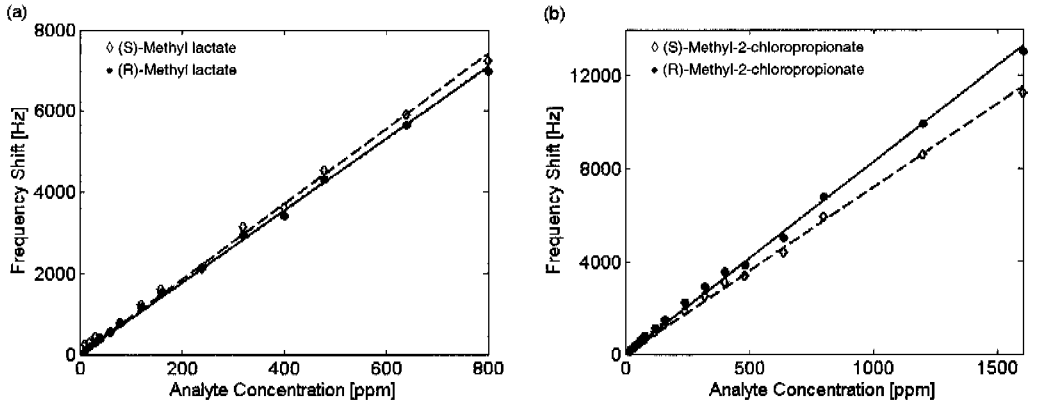

Figure 5-24. Frequency shift of a capacitor coated with a thin enantioselective coating upon analyte absorption of (a) (S)- and (R)-methyl lactate and (b) the enantiomers of methyl-2-chloropropionate.

The sensor response of a capacitor with a thin sensitive layer upon exposure to different analyte concentrations is depicted in Figure 5-24. From the figures it is obvious that the predominant effect is the swelling of the sensitive layer, since there is always a capacitance increase. The occurrence of negative signals, which was pronounced for low enantiomer concentrations in thick layers, is not visible here. The curves show minute curvatures at very low concentrations, suggesting some degree of specific interaction. The sensor signal then increases proportionally to the analyte concentration. This is indicated by the solid and dashed lines in Figure 5-24.

The capacitor yields a higher response for both the nonpreferentially absorbed enantiomers, (S)-methyl lactate and (R)-methyl-2-chloropropionate. One has to bear in mind that the partitioning of these analytes in the enantioselective layer is less in comparison to the preferentially absorbed enantiomers [125]. As mentioned before, the

dissolution of cage-like bulky cyclodextrin molecules increases the amount of excess or free volume in the polymer. The measurements now suggest that despite the lower partitioning, the nonpreferentially absorbed analytes causes more swelling of the enantioselective layer.

These findings confirm the more intimate and closer interaction of the preferred enantiomer with the receptor site. Assuming an inclusion of the chiral molecule in the γ-macrocycle, as it is suggested in literature [43, 118, 120, 131], the preferentially absorbed enantiomer is embedded deeper in the cavity of the cyclodextrin than the less preferred molecule and, thus, requires less space in the surrounding layer matrix. But even when considering only an external interaction of the chiral molecules with the cyclodextrin torus, the measurements would indicate a more intimate, compact diastereomeric complex with the preferentially sorbed enantiomer.

5.4 Comparison of the Results with GC and NMR

For comparison corresponding measurements with the chiral analytes were performed using gas-solid chromatography (GC) and nuclear magnetic resonance (NMR).

5.4.1 Gas Chromatography Measurements

In gas chromatography (GC) the sample is vaporized into the head of a chromatographic column. The flow of an inert gaseous mobile phase is then transporting the sample through the column. In contrast to most other types of chromatography, the mobile carrier phase does not interact with the molecules of the analyte; its only function is to transport the analyte through the column. Gas-solid chromatography, as opposed to gas-liquid chromatography, is based upon a solid stationary phase, on which the analytes are retained as a consequence of physical adsorption. GC is performed with packed, open tubular or capillary columns. For the latter, a thin layer of the adsorbant is immobilized at the inner walls of the capillary [141].

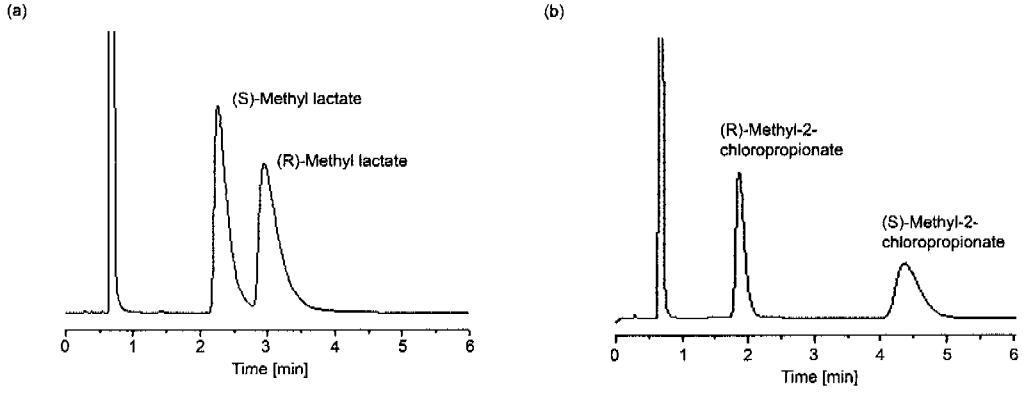

Figure 5-25. Gas chromatographic measurements of (S)- and (R)-methyl lactate (a) and (S)- and (R)-methyl-2-chloropropionate (b). The enantioselective layer is octakis(3-O-butanoyl-2,6-di-O-pentyl)-γ-cyclodextrin/PDMS. The measurements have been performed at a temperature of 60 °C.

Enantioselective receptors, such as cyclodextrins, are used as component of the capillary coating for chiral separations [111]. The interaction of the enantiomer and the receptor results in a different retention time of each analyte: The nonpreferred analyte eludes first, whereas the preferentially adsorbed enantiomer is retained to a larger extent within the column. The examination of the signals (Figure 5-25) reveals a similarity of the GC-peaks to Gaussian curves. The peaks or GC signals result from the superposition of a large number of absorption/desorption processes of the respective enantiomer as the analyte migrates through the column. The retention of an analyte is defined by the time it takes for the analyte peak to reach the detector after injection.

From the ratio of the retention times of two enantiomers the chiral discrimination, α, can be calculated according to Eq. 5-8.

	Chiral discrimination factor α		
	α-Cyclodextrin	β-Cyclodextrin	γ-Cyclodextrin
Methyl lactate	1.03 (S/R)	1.21 (R/S)	1.31 (S/R)
Methyl-2-chloropropionate	1.00 (/)	1.57 (R/S)	2.35 (R/S)

Table 5-8. Chiral discrimination factors, α, and the elution order (in brackets) for the different cyclodextrin/analyte combinations measured with GC.

The measurements were performed using a HP 5890A gas chromatograph with split-injector and flame-ionization-detector (FID). The injector and the detector were operated at temperatures of 200 °C and 250 °C, respectively. The fused-silica-capillaries (Polymicro Technologies, Phoenix, AZ) were 10 m long and had an inner diameter of 250 µm. These capillaries were coated with the enantioselective hexakis-, heptakis-, or octakis(3-O-butanoyl-2,6-di-O-pentyl)-cyclodextrins, which were dissolved in a poly(methyl-methylvinylsiloxane matrix (PS 255, Petrarch Systems Inc., Bristol, PA) at 20% (w/w). For each column the layer thickness was 0.25 µm. During the measurements the temperature of the capillary was 60 °C. A racemic mixture of methyl lactate and methyl-2-chloropropionate was injected into the column using hydrogen as a carrier gas (0.25 bar). Data evaluation was carried out with the program Clarity 2.3 (DataApex Ltd., Prag, CZE).

Figure 5-25 displays the different retention times of the enantiomers of methyl lactate and chloropropionate after passing through a γ-cyclodextrin derivative/PDMS coated column. The graphs show that in the case of methyl lactate the (S)-enantiomer eludes before the (R)-analyte. An inverted elution order and better discrimination occurs for the enantiomers of methyl-2-chloropropionate. The chiral discrimination factors were calculated from the retention times. In Table 5-8 the discrimination factors for all different enantioselective coatings are listed. Overall, the results agree with the measurements as performed with the multi-sensor chip (compare Section 5.3.2.).

One has to bear in mind that the results obtained by GC are the result of multiple interaction processes (thousands of theoretical plates), whereas the measurements performed with the multi-sensor system are a result of only one analyte absorption/desorption step.

As only the chiral discrimination factors obtained by the mass-sensitive cantilever can be considered as thermodynamically controlled and relevant, these values were compared to those of the GC measurements for the γ-cyclodextrin derivative/PDMS coating. The cantilever yields higher values for both analytes: $\alpha = 2.73$ for methyl lactate and $\alpha = 3.99$, whereas the discrimination factors obtained by the GC are 1.31 and 2.35, respectively. Other values for the chiral discrimination of these analytes via GC (at

30 °C) are given in literature [129]: Methyl lactate 1.54 and chloropropionate 4.19. The sensor values correspond quite well to those values.

5.4.2 Results of NMR Spectroscopy

Nuclear magnetic resonance spectroscopy (NMR) is a method, which relies on the magnetic property of an atom nucleus. It is based on absorption measurements of electromagnetic radiation in the radio-frequency region of roughly 4 to 900 MHz. NMR is based on measuring the magnetic field of a nucleus, like that of a hydrogen atom by aligning its spin with an external magnetic field and perturbing this alignment using a constant-frequency electromagnetic field. The response to the perturbing field generates a unique pattern, which is displayed as a frequency spectrum (Fourier transform NMR) [141]. Proton NMR or ^{1}H-NMR is the application of nuclear magnetic resonance spectroscopy to hydrogen, mostly in organic compounds. Simple NMR spectra are recorded in solution. The spectra include information on chemical shifts in the range of +12 to -4 ppm and on spin-spin coupling between the protons. Among other things NMR is used for determination molecular structures (proteins and nucleic acid fragments) and for the analysis of interactions between molecules.

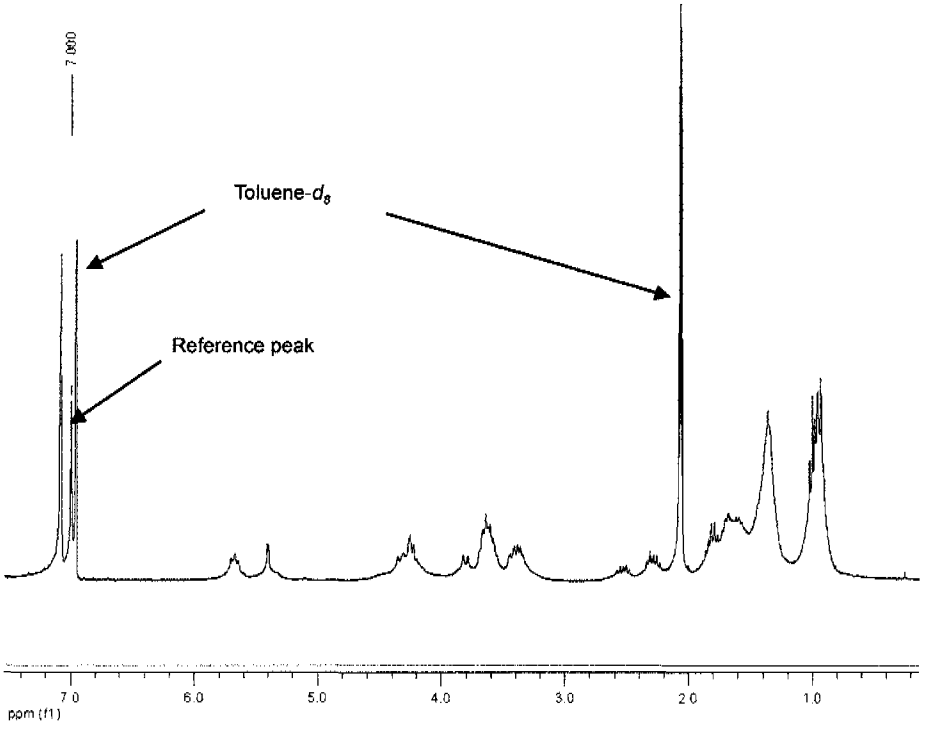

Figure 5-26. Full NMR spectrum of the modified γ-cyclodextrin dissolved in toluene-d_8. The peaks that can be assigned to the solvent are indicated.

The one-dimensional ^{1}H-NMR spectra were measured on a Varian Gemini 300 at 300 MHz (multiplicity, constant coupling J in Hz, number of protons). A deuterated toluene (toluene-d_8, Dr. Glaser AG, Basel; CH) was used as a solvent. The solvent

peak was used as internal reference (Figure 5-26), which was $\delta_H = 7$ ppm for toluene-d_8. The used solvent determines the spectrum of the cyclodextrin, may differ from those recorded with other solvents. The NMR measurements were carried out with the help of H. Dube [142].

The NMR measurements were performed to clarify the interactions between the modified γ-cyclodextrin molecule and the enantiomers. A NMR spectrum contains the information about the substances present in the sample solution and how they interact. If the different sample components do not interact with each other, the spectrum will consist of a superposition of the individual compound spectra (spectrum of the single substances in the solvent). In case a specific interaction, such as complexation, occurs, the resulting spectrum will show changes (shifts) in the peak pattern of the host and the guest molecule. This effect will be more pronounced with increasing analyte (guest) concentration. The shifts are due to reorganizations of the host molecular structure to accommodate the guest.

Using a gradual increase of the analyte concentration a so-called "titration" was performed. The titration describes the addition of a measured quantity of analyte (enantiomer) to a reagent (cyclodextrin) of known concentration. The preparations and all specifications for the titration are given in the Appendix (Table A-6 and Table A-7).

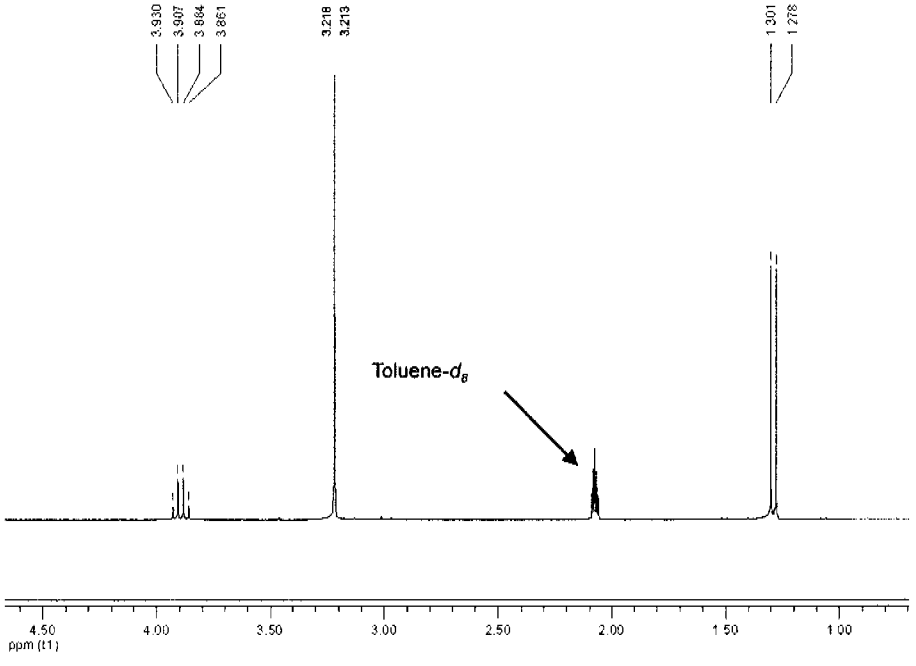

Figure 5-27. NMR spectrum of (S)-methyl-2-chloropropionate dissolved in toluene-d_8. The peaks of the analyte are indicated, and the respective peak assignments are given as ppm-values.

Two NMR control measurements were recorded for later comparison with the resulting spectra. For these measurements the NMR test tube only contained either the pure

octakis(3-O-butanoyl-2,6-di-O-pentyl)-γ-cyclodextrin (Figure 5-26) or the pure enantiomer (Figure 5-27) dissolved in toluene-d_8. It is crucial that the solvent used for the titration solution is the same as that for dissolving the cyclodextrin.

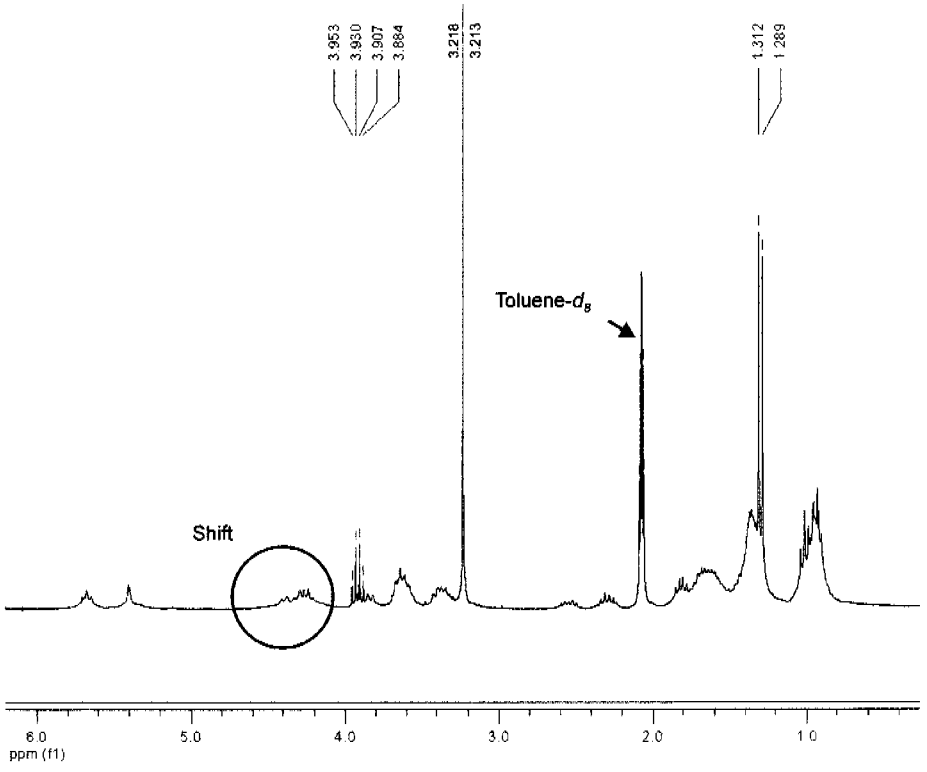

Figure 5-28. NMR spectrum of the titration sample at a 9.5-fold excess of (S)-methyl-2-chloropropionate. The analyte peaks are assigned. Changes in the cyclodextrin spectrum are visible, compare Figure 5-26.

After the control measurements a certain volume of the titration solution (Table A-6 and Table A-7), which contained the dissolved pure enantiomer of either methyl lactate or methyl-2-chloropropionate, was added to the test tube, which initially contained only the dissolved cyclodextrin. With each titration step the ratio of the analyte-to-cyclodextrin concentration was increased, and a NMR measurement was then performed. The titration was continued until the analyte concentration was about 45 times higher than the cyclodextrin concentration. The enantiomer concentration seems to be very high with respect to the cyclodextrin concentration having in mind the 1:1 complexation of enantiomer and cyclodextrin molecule [125]. However, it is important to know that in the liquid environment the receptors (host) also interact with the abundant solvent molecules. A displacement of the toluene by the analyte molecules has to been forced by drastically increasing the enantiomer concentration to observe the interaction effect.

Figure 5-28 displays the NMR spectrum of the test tube solution at an approximately 10-fold excess of (S)-methyl-2-chloropropionate. The spectral lines of (S)-methyl-2-

chloropropionate and that of the solvent are indicated by the assigned values and by labels. The spectrum is a cyclodextrin spectrum. The region marked with a circle indicates the spectrum components of the carbon atoms in 6-, 5- and 4-position in the glucose unit of the cyclodextrin derivative (Figure 5-29).

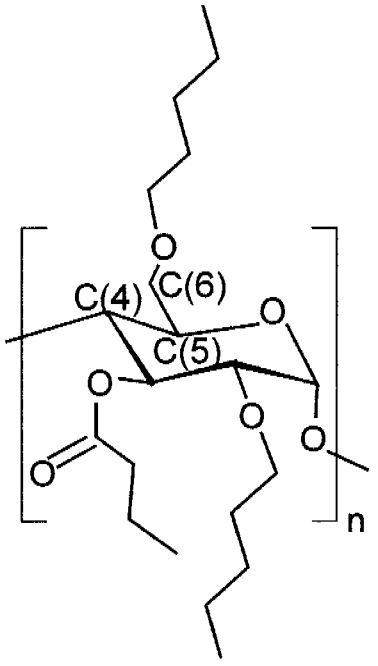

Figure 5-29. Assignment of the carbon molecules in the glucose unit, where the strongest shift during the titration measurements occured.

In Figure 5-30 a close-up of the relevant section is displayed. The upper image (Figure 5-30 (a)) shows the spectrum of the control measurement with the pure cyclodextrin dissolved in toluene. In the lower picture (Figure 5-30 (b)) the spectrum of the same sample with a 44-fold excess of the analyte is depicted. A shift in the molecular "pattern" of the cyclodextrin is distinguishable (for better comparison lines serving as guides to the eye were added). This suggests that indeed the host and the guest molecule form a complex.

The spectrum of the dissolved γ-cyclodextrin without analyte additive (Figure 5-30 (a)) nicely coincides with measurements from literature [118]. A. Mele performed NMR measurements on the very same γ-cyclodextrin derivative using cyclohexan-d_{12} as a solvent. A residual solvent peak is commonly used as internal reference, and the values of the sample spectrum are assigned with regard to this internal reference. Since different solvents were used the spectrum values (location of the peaks) do not exactly coincide. But the spectra resembled each other well enough to use the published assignment data also for the spectra here, so that a correlation of the shifts and the locations of the atoms within the cyclodextrin were possible. According to these data the C(6) atom (compare Figure 5-29) experiences the strongest conformational changes. But also the C(4) and C(5) atoms show shifts upon complexation with the en-

antiomer molecule. The strongest interaction of host and guest takes place at the C(6) location.

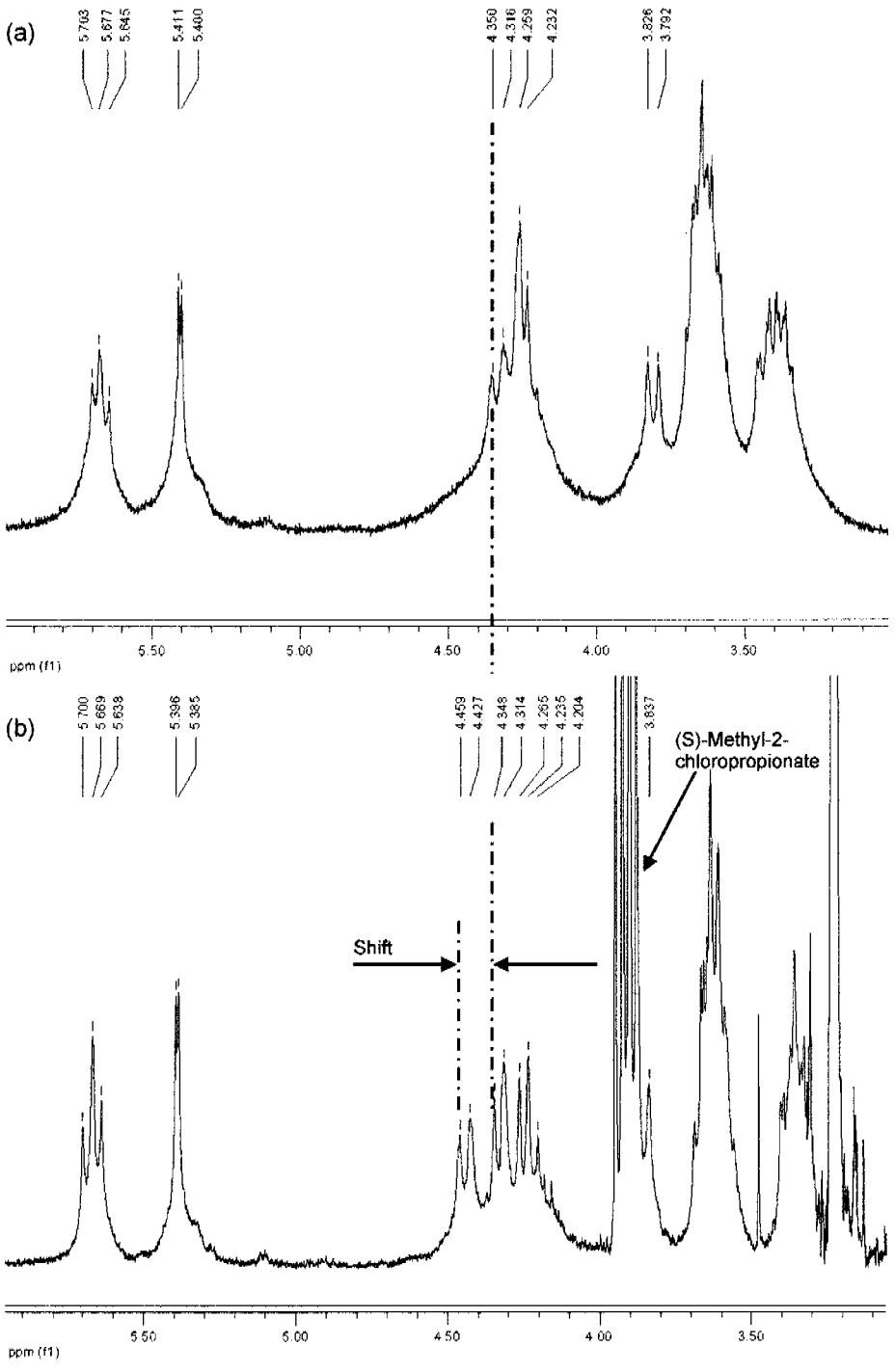

Figure 5-30. Section of the NMR spectrum of (a) the pure γ-cyclodextrin derivative dissolved in toluene-d_8 and (b) after adding a 44-fold excess of (S)-methyl-2-chloropropionate. The spectral shifts can be assigned to interactions at the C(6) atom of the cyclodextrin glucose unit.

The titration measurements were performed for the (S)- and (R)-enantiomers of methyl lactate and methyl-2-chloropropionate. The results are plotted in Figure 5-31 (a) and (b). The results are displayed as frequency shifts with regard to the initial control measurement (only cyclodextrin) versus the concentration ratio of host and guest.

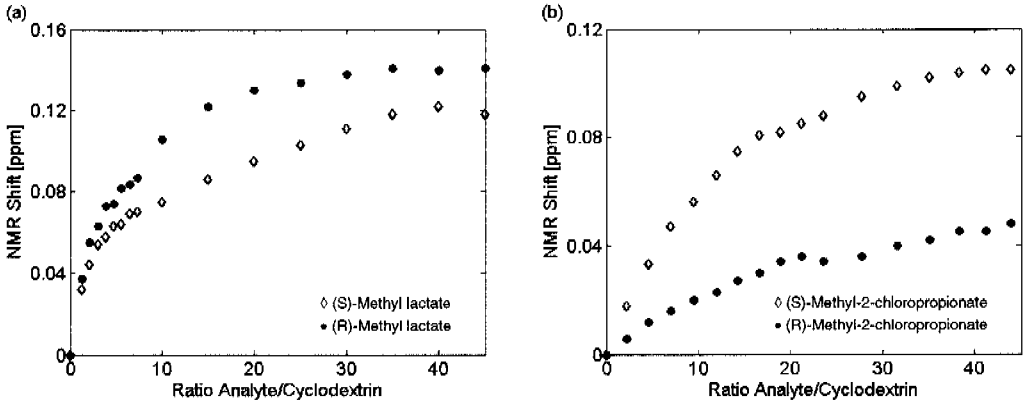

Figure 5-31. Results of NMR titration measurements: Frequency shifts versus ratio of the enantiomer/cyclodextrin concentration for (a) the enantiomers of methyl lactate and (b) (S)- and (R)-methyl-2-chlororpropionate.

The plots evidence that the analytes (R)-methyl lactate and (S)-methyl-2-chloropropionate cause larger conformational changes in the cyclodextrin molecule than the respective other enantiomer. It is noticeable that the shifts generated by the chloropropionates exhibit a larger difference than that of the enantiomers of methyl lactate. The NMR measurements, however, do not give information about the strength or the stability of the complexation; they only confirm that a complexation occurs.

5.5 Conclusion

It was demonstrated that chiral discrimination is possible by means of multi-transducer chip. Different enantioselective coatings were tested, but only the octakis(3-O-butanoyl-2,6-di-O-pentyl)-γ-cyclodextrin/PDMS (50% (w/w)) coating provided stable and reproducible results. The interdigitated capacitor shows direct chiral discrimination via opposite-sign signals for the optical isomers. There was also a distinct signal difference in the transient capacitive signals upon the exposure to the enantiomers. Furthermore, the enantiomeric purity or composition of a sample also can be immediately determined on the basis of the time-dependent capacitive signal.

The capacitive sensor was also used for determining the dielectric constants of the analytes and the enantioselective layers. These values are necessary for a better understanding of the enantiomer and cyclodextrin interaction and were as yet unknown.

The validity of the discrimination results was controlled by conducting GC and NMR measurements using the same enantioselective materials and analytes.

6 CONCLUSION AND OUTLOOK

6.1 Conclusion

The performance of a single-chip, three-transducer CMOS gas sensor microsystem for the detection of volatile organic compounds was studied. Several multi-transducer chips were coated with different partially selective polymers (EC, PECH, PEUT, PCPMS, and PDMS) and were then exposed to different sets of volatile organic compounds. The simultaneous recording from the different transducers caused a unique response pattern for each volatile compound. The normalization of the sensor response with regard to the partition coefficients of the respective polymer/analyte combination, i.e., separating the partitioning contribution to the signal from the specific transducer contribution, revealed the transducer-specific effects. Due to their fundamentally different transduction principles, the sensors indeed responded to the various physical properties of the analytes such as the molecular weight (mass-sensitive), the dielectric coefficient (capacitive), and the sorption heat (calorimetric). Correlations between the determined sensitivity values and the different molecular properties of the absorbed analytes were established.

The applicability of the multi-sensor gas microsystem to chiral discrimination was also demonstrated. Several gas sensor chips were coated with different composites consisting of an enantioselective modified cyclodextrin (α-, β-, and γ-cyclodextrin) and poly(dimethylsiloxane) (PDMS) at 50% (w/w). For the experiments the multi-transducer chips were exposed to the different chiral analytes (the respective (S)-enantiomers, the (R)-enantiomers and the racemic mixtures) of methyl lactate and methyl-2-chloropropionate. It was shown that chiral discrimination by means of the multi-sensor chip was indeed possible. The comparison of the responses of the sensors with the three different enantioselective coatings revealed that the enantioselectivity, as well as the sensitivity increased with the size of the cyclodextrin. The octakis(3-O-butanoyl-2,6-di-O-pentyl)-γ-cyclodextrin/PDMS (50% (w/w)) coating provided the best results. The calorimetric sensor and the mass-sensitive cantilever showed a chiral discrimination according to the respective fundamental transduction principles, i.e., the detection of differences in the sorption heat and mass increase as a consequence of the enhanced partitioning of the preferentially absorbed enantiomer. The capacitive sensor, however, showed more complex effects. It was found that due to the different interaction of the recognition sites (cyclodextrins) with both enantiomers, the sensor shows opposite signal signs for the two optical isomers, i.e., one enantiomer produces a capacitance increase, the other one a decrease, even though both enantiomers exhibit the same dielectric coefficient. We interpret these results by assuming that the complexation of receptor and preferred enantiomer causes a short-range-ordering, which, in turn, changes the overall polarization of the analyte/layer composite. A capacitance decrease is a consequence of strong short-range-orientation and ordering effects, whereas without such ordering effects, capacitance increases are observed. Due to this

distinct signal difference a highly time-resolved dynamic capacitive signal reveals new information on the absorption and desorption behavior of the analyte in the enantioselective layer. Furthermore, the enantiomeric purity of a sample (racemic mixture) has been immediately assessed by observing the time-dependent signal. The capacitive sensor was additionally used for determining the dielectric coefficients of the analytes and the enantioselective layers. The validity of the discrimination experiments performed with the multi-sensor gas system was controlled by conducting GC and NMR measurements using the same enantioselective material and analytes.

In addition to the work with the multi-transducer chip, a novel post-processing approach for the fabrication of low-pitch arrays of silicon membranes on standard CMOS wafers has been developed, which is a combination of deep reactive ion etching (DRIE) and electrochemical etching (ECE) techniques. It provides the possibility of tightly packing micromachined structures using DRIE and the precise etch stop that is attainable using ECE. The concept to use a grid-like masking pattern, which subdivides the micromechanical structures into small subunits of unity size and shape, was introduced. This concept and the combined etching techniques have been demonstrated to allow for the fabrication of membrane-based sensors and sensor arrays featuring different membrane sizes on a single wafer with a well defined etch stop. The combination of a grid-like mask pattern featuring uniform-size etch openings for the DRIE process with a reliable ECE technique allowed to fabricate silicon membranes with sizes ranging from 0.01 mm^2 to 2.2 mm^2. It was shown that the process is easily adaptable to varying membrane sizes. The necessary adjustments can be done on mask level. The goal of the process development as done in this work was to devise a concept for post-processing in a fabless, foundry-based approach, which relies on easily accessible standard processes.

6.2 Outlook

Future research with the single-chip, three-transducer CMOS gas sensor microsystem should focus on specific applications, such as air quality control. The "orthogonality" or complementarity of the information as provided by the system can be used in conjunction with appropriate signal processing and pattern recognition techniques to not only classify single analytes but also to qualify and quantify components of more complex mixtures. Field measurements would require the integration of an array of multi-sensor with different coatings in a hand-held system. The system would have to comprise, e.g., a pump, a filter, and valves, which would allow for sharp concentration gradients to perform a meaningful transient signal analysis as required for the calorimetric sensor. The use and analysis of transient or dynamic signals for the capacitive or mass-sensitive transducer is an additional option for the multi-sensor system in particular since the calorimetric sensors *per se* require a system that provides sharp concentration steps. The analysis of such dynamic sensor signals would allow for gaining

even more information on the detected analytes, as has been demonstrated for the capacitive sensors[2].

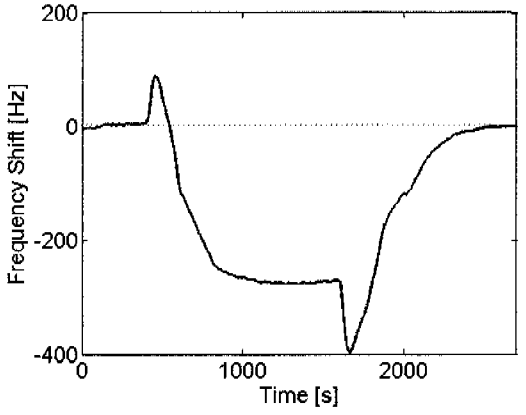

Figure 6-1. Capacitor response upon absorption and desorption of the racemic mixture of 120 ppm methyl-2-chloropropionate.

The interest in fast and reliable systems for chiral discrimination has increased over the last years. Such systems are used not only for the understanding of biological processes, but also in other fields, such as for pharmaceutical, food, and environmental applications. In this thesis the applicability of the single-chip, gas sensor CMOS microsystem to the chiral discrimination of methyl esters was demonstrated. The discrimination of other chiral molecules, such as amines, amino acids, ketones, or lactones would also be possible. Other host/guest interactions could be explored using other receptors, e.g., calixarenes, fullerenes, crown-ethers, or macrocyclic antibiotics, as components of the receptor layer. Due to the opposite sensor response signs as observed for the different enantiomers, especially the capacitor could provide immediate information about the purity of a sample after transient signal analysis (Figure 6-1). Furthermore it could provide more detailed information on the interaction between host and guest molecules, such as binding energies upon analyte desorption. Further experiments with different coatings and analytes and measurements at higher temporal resolution will have to be conducted to explore the full potential of the interdigitated capacitor for the analysis of such host/guest interactions.

[2] Kummer, A. M., Burg, T.P., et al. "*Transient Signal Analysis Using Complementary Metal Oxide Semiconductor Capacitive Chemical Microsensors*", Analytical Chemistry **78** (1), 279-290, 2006

Seite Leer /
Blank leaf

APPENDICES

Chapter 4

	Full name	Supplier	Product code
EC	Ethyl cellulose	Sigma-Aldrich, Buchs, Switzerland	24.749-9
PECH	Poly(epichlorohydrin)	Sigma-Aldrich, Buchs, Switzerland	18.186-2
PEUT	Poly(etherurethane)	Thermedics Inc., Woburn, MA, USA	SG-80A
PCPMS	Poly(cyanopropyl-methylsiloxane)	Supelco, Bellefont, PA, USA	OV-105
PDMS	Poly(dimethylsiloxane)	Supelco, Bellefont, PA, USA	SE-30

Table A-1. Polymers, suppliers, and product codes as used for the VOC detection.

	Calorimeter $\Delta\int U_{th} \cdot ds / \Delta c$ [mV·s/ppm]				
	EC	PCPMS	PDMS	PECH	PEUT
n-Heptane	$3.28 \cdot 10^{-2} \pm 2.86 \cdot 10^{-3}$	$1.08 \cdot 10^{-2} \pm 1.04 \cdot 10^{-3}$	$6.82 \cdot 10^{-2} \pm 2.47 \cdot 10^{-3}$		$1.34 \cdot 10^{-2} \pm 2.78 \cdot 10^{-3}$
n-Octane	$1.01 \cdot 10^{-1} \pm 6.48 \cdot 10^{-3}$	$5.45 \cdot 10^{-2} \pm 1.42 \cdot 10^{-3}$	$3.40 \cdot 10^{-1} \pm 1.15 \cdot 10^{-2}$	$1.51 \cdot 10^{-2} \pm 1.09 \cdot 10^{-3}$	$7.73 \cdot 10^{-2} \pm 6.49 \cdot 10^{-3}$
Toluene	$1.21 \cdot 10^{-1} \pm 1.17 \cdot 10^{-2}$	$2.71 \cdot 10^{-2} \pm 2.76 \cdot 10^{-3}$	$1.24 \cdot 10^{-1} \pm 3.78 \cdot 10^{-3}$	$5.25 \cdot 10^{-2} \pm 4.39 \cdot 10^{-3}$	$1.23 \cdot 10^{-1} \pm 3.61 \cdot 10^{-3}$
Methanol	$2.69 \cdot 10^{-2} \pm 2.19 \cdot 10^{-3}$	$7.15 \cdot 10^{-3} \pm 3.80 \cdot 10^{-4}$			$1.82 \cdot 10^{-2} \pm 5.72 \cdot 10^{-4}$
Propan-1-ol	$1.44 \cdot 10^{-1} \pm 5.81 \cdot 10^{-3}$	$3.16 \cdot 10^{-2} \pm 1.99 \cdot 10^{-3}$	$2.00 \cdot 10^{-2} \pm 1.17 \cdot 10^{-3}$	$2.02 \cdot 10^{-2} \pm 1.00 \cdot 10^{-3}$	$1.86 \cdot 10^{-1} \pm 8.30 \cdot 10^{-3}$
Propan-2-ol	$6.23 \cdot 10^{-2} \pm 2.26 \cdot 10^{-3}$	$9.75 \cdot 10^{-3} \pm 1.25 \cdot 10^{-3}$	$9.07 \cdot 10^{-3} \pm 6.51 \cdot 10^{-4}$		$4.53 \cdot 10^{-2} \pm 9.27 \cdot 10^{-4}$
Trichloromethane	$8.20 \cdot 10^{-2} \pm 5.18 \cdot 10^{-3}$	$1.17 \cdot 10^{-2} \pm 7.19 \cdot 10_{-4}$	$1.73 \cdot 10^{-2} \pm 9.62 \cdot 10^{-4}$	$1.06 \cdot 10^{-2} \pm 1.50 \cdot 10^{-3}$	$6.42 \cdot 10^{-2} \pm 1.91 \cdot 10^{-3}$
Tetrachloro-methane	$2.65 \cdot 10^{-2} \pm 2.83 \cdot 10^{-3}$	$9.45 \cdot 10^{-3} \pm 1.15 \cdot 10^{-3}$	$4.62 \cdot 10^{-2} \pm 5.51 \cdot 10^{-3}$		$3.42 \cdot 10^{-2} \pm 1.03 \cdot 10^{-3}$
Trichloroethene	$1.21 \cdot 10^{-1} \pm 1.46 \cdot 10^{-2}$	$1.48 \cdot 10^{-2} \pm 1.93 \cdot 10^{-3}$	$5.34 \cdot 10^{-2} \pm 5.22 \cdot 10^{-3}$		$6.83 \cdot 10^{-2} \pm 1.49 \cdot 10^{-2}$
Tetrachloroethene	$2.20 \cdot 10^{-1} \pm 4.92 \cdot 10^{-3}$	$4.09 \cdot 10^{-2} \pm 2.34 \cdot 10^{-3}$	$1.88 \cdot 10^{-1} \pm 1.21 v10^{-2}$		$1.78 \cdot 10^{-1} \pm 3.74 \cdot 10^{-3}$
Water	$3.13 \cdot 10^{-2} \pm 3.98 \cdot 10^{-3}$	$7.38 \cdot 10^{-3} \pm 2.52 \cdot 10^{-4}$	$4.48 \cdot 10^{-3} \pm 4.02 \cdot 10^{-4}$		$2.87 \cdot 10^{-2} \pm 9.15 \cdot 10^{-4}$
Ethanol	$4.11 \cdot 10^{-2} \pm 2.08 \cdot 10^{-3}$	$1.02 \cdot 10^{-2} \pm 1.50 \cdot 10^{-4}$			$2.92 \cdot 10^{-2} \pm 1.22 \cdot 10^{-3}$
Ethyl acetate	$4.69 \cdot 10^{-2} \pm 1.92 \cdot 10^{-3}$	$1.58 \cdot 10^{-2} \pm 1.06 \cdot 10^{-3}$	$2.11 \cdot 10^{-2} \pm 1.68 \cdot 10^{-3}$		$2.48 \cdot 10^{-2} \pm 2.06 \cdot 10^{-3}$

Table A-2. Analyte sensitivities and standard deviations as measured with the calorimetric sensor for different polymers.

	Cantilever $\Delta f/\Delta c$ [Hz/ppm]				
	EC	PCPMS	PDMS	PECH	PEUT
n-Heptane	$-2.31 \cdot 10^{-2} \pm 1.16 \cdot 10^{-3}$	$-2.08 \cdot 10^{-2} \pm 2.29 \cdot 10^{-3}$	$-5.00 \cdot 10^{-3} \pm 3.04 \cdot 10^{-4}$	$-2.80 \cdot 10^{-3} \pm 5.79 \cdot 10^{-4}$	$-1.49 \cdot 10^{-2} \pm 7.62 \cdot 10^{-4}$
n-Octane	$-5.53 \cdot 10^{-2} \pm 3.07 \cdot 10^{-3}$	$-7.88 \cdot 10^{-2} \pm 1.14 \cdot 10^{-3}$	$-1.71 \cdot 10^{-2} \pm 1.14 \cdot 10^{-3}$	$-7.90 \cdot 10^{-3} \pm 7.75 \cdot 10^{-4}$	$-3.54 \cdot 10^{-2} \pm 7.68 \cdot 10^{-4}$
Toluene	$-6.46 \cdot 10^{-2} \pm 5.37 \cdot 10^{-3}$	$-3.58 \cdot 10^{-2} \pm 1.84 \cdot 10^{-3}$	$-7.30 \cdot 10^{-3} \pm 3.28 \cdot 10^{-4}$	$-1.66 \cdot 10^{-2} \pm 6.04 \cdot 10^{-4}$	$-5.74 \cdot 10^{-2} \pm 1.04 \cdot 10^{-3}$
Methanol	$-7.30 \cdot 10^{-3} \pm 2.55 \cdot 10^{-4}$	$-3.30 \cdot 10^{-3} \pm 6.40 \cdot 10^{-4}$			$-3.80 \cdot 10^{-3} \pm 4.41 \cdot 10^{-5}$
Propan-1-ol	$-4.59 \cdot 10^{-2} \pm 3.15 \cdot 10^{-4}$	$-1.41 \cdot 10^{-2} \pm 1.25 \cdot 10^{-3}$	$-1.70 \cdot 10^{-3} \pm 2.49 \cdot 10^{-4}$	$-4.60 \cdot 10^{-3} \pm 6.46 \cdot 10^{-4}$	$-2.91 \cdot 10^{-2} \pm 1.97 \cdot 10^{-4}$
Propan-2-ol	$-1.79 \cdot 10^{-2} \pm 1.33 \cdot 10^{-3}$	$-6.10 \cdot 10^{-3} \pm 4.60 \cdot 10^{-4}$	$-1.30 \cdot 10^{-3} \pm 1.42 \cdot 10^{-4}$	$-9.00 \cdot 10^{-4} \pm 3.01 \cdot 10^{-4}$	$-1.35 \cdot 10^{-2} \pm 3.00 \cdot 10^{-5}$
Trichloromethane	$-5.64 \cdot 10^{-2} \pm 2.41 \cdot 10^{-3}$	$-1.47 \cdot 10^{-2} \pm 4.17 \cdot 10^{-4}$	$-3.90 \cdot 10^{-3} \pm 3.29 \cdot 10^{-4}$	$-8.00 \cdot 10^{-3} \pm 3.87 \cdot 10^{-4}$	$-4.21 \cdot 10^{-2} \pm 3.28 \cdot 10^{-4}$
Tetrachloro-methane	$-2.37 \cdot 10^{-2} \pm 2.44 \cdot 10^{-3}$	$-1.78 \cdot 10^{-2} \pm 7.26 \cdot 10^{-4}$	$-7.00 \cdot 10^{-3} \pm 5.28 \cdot 10^{-4}$	$-3.50 \cdot 10^{-3} \pm 5.10 \cdot 10^{-4}$	$-3.20 \cdot 10^{-2} \pm 1.61 \cdot 10^{-4}$
Trichloroethene	$-7.13 \cdot 10^{-2} \pm 3.14 \cdot 10^{-3}$	$-2.35 \cdot 10^{-2} \pm 2.15 \cdot 10^{-3}$	$-4.80 \cdot 10^{-3} \pm 9.32 \cdot 10^{-4}$	$-8.30 \cdot 10^{-3} \pm 7.19 \cdot 10^{-4}$	$-5.03 \cdot 10^{-2} \pm 1.03 \cdot 10^{-2}$
Tetrachloroethene	$-1.27 \cdot 10^{-1} \pm 3.08 \cdot 10^{-3}$	$-6.71 \cdot 10^{-2} \pm 1.24 \cdot 10^{-3}$	$-1.80 \cdot 10^{-2} \pm 8.69 \cdot 10^{-4}$	$-1.94 \cdot 10^{-2} \pm 3.19 \cdot 10^{-3}$	$-1.28 \cdot 10^{-1} \pm 2.31 \cdot 10^{-3}$
Water	$-5.50 \cdot 10^{-3} \pm 2.98 \cdot 10^{-4}$	$-3.55 \cdot 10^{-3} \pm 1.29 \cdot 10^{-3}$	$-1.45 \cdot 10^{-3} \pm 8.88 \cdot 10^{-5}$		$-2.70 \cdot 10^{-3} \pm 4.96 \cdot 10^{-5}$
Ethanol	$-1.27 \cdot 10^{-2} \pm 8.65 \cdot 10^{-4}$	$-6.45E \cdot 10^{-3} \pm 3.40 \cdot 10^{-4}$	$-1.10 \cdot 10^{-3} \pm 1.52 \cdot 10^{-4}$		$-8.50 \cdot 10^{-3} \pm 1.29 \cdot 10^{-4}$
Ethyl acetate	$-2.98 \cdot 10^{-2} \pm 3.40 \cdot 10^{-4}$	$-1.31 \cdot 10^{-2} \pm 5.11 \cdot 10^{-4}$	$-2.30 \cdot 10^{-3} \pm 7.52 \cdot 10^{-4}$	$-4.70 \cdot 10^{-3} \pm 1.26 \cdot 10^{-3}$	$-1.48 \cdot 10^{-2} \pm 6.34 \cdot 10^{-4}$

Table A-3. Analyte sensitivities and standard deviations as measured with the mass-sensitive cantilever for different polymers.

	Capacitor Δf/Δc [Hz/ppm]				
	EC	PCPMS	PDMS	PECH	PEUT
n-Heptane	$1.72 \cdot 10^{-1} \pm 3.45 \cdot 10^{-2}$	$-1.95 \cdot 10^{-1} \pm 3.77 \cdot 10^{-3}$	$-1.62 \cdot 10^{-1} \pm 1.00 \cdot 10^{-2}$	$1.78 \cdot 10^{-1} \pm 6.02 \cdot 10^{-2}$	$-9.08 \cdot 10^{-2} \pm 3.64 \cdot 10^{-3}$
n-Octane	$3.64 \cdot 10^{-1} \pm 4.45 \cdot 10^{-2}$	$-4.99 \cdot 10^{-1} \pm 5.04 \cdot 10^{-2}$	$-4.18 \cdot 10^{-1} \pm 4.41 \cdot 10^{-2}$	$5.07 \cdot 10^{-1} \pm 7.73 \cdot 10^{-2}$	$-3.20 \cdot 10^{-1} \pm 1.75 \cdot 10^{-2}$
Toluene	$6.78 \cdot 10^{-1} \pm 1.02 \cdot 10^{-1}$	$-5.45 \cdot 10^{-2} \pm 3.31 \cdot 10^{-3}$	$-4.23 \cdot 10^{-2} \pm 1.58 \cdot 10^{-3}$	$2.06 \pm 9.68 \cdot 10^{-2}$	$-2.10 \cdot 10^{-1} \pm 1.40 \cdot 10^{-2}$
Methanol	$3.88 \cdot 10^{-1} \pm 2.23 \cdot 10^{-2}$	$1.56 \cdot 10^{-1} \pm 3.25 \cdot 10^{-2}$	$1.83 \cdot 10^{-2} \pm 3.20 \cdot 10^{-3}$	$2.57 \cdot 10^{-1} \pm 1.44 \cdot 10^{-2}$	$4.00 \cdot 10^{-1} \pm 6.61 \cdot 10^{-3}$
Propan-1-ol	$1.94 \pm 6.60 \cdot 10^{-2}$	$6.75 \cdot 10^{-1} \pm 2.24 \cdot 10^{-2}$	$1.39 \cdot 10^{-1} \pm 2.68 \cdot 10^{-3}$	$1.07 \pm 2.87 \cdot 10^{-2}$	$1.99 \pm 4.64 \cdot 10^{-2}$
Propan-2-ol	$7.76 \cdot 10^{-1} \pm 5.85 \cdot 10^{-2}$	$2.48 \cdot 10^{-1} \pm 5.37 \cdot 10^{-3}$	$6.70 \cdot 10^{-2} \pm 2.48 \cdot 10^{-3}$	$4.90 \cdot 10^{-1} \pm 1.41 \cdot 10^{-2}$	$7.94 \cdot 10^{-1} \pm 4.27 \cdot 10^{-3}$
Trichloromethane	$6.71 \cdot 10^{-1} \pm 5.35 \cdot 10^{-2}$	$2.30 \cdot 10^{-1} \pm 4.65 \cdot 10^{-3}$	$1.15 \cdot 10^{-1} \pm 4.59 \cdot 10^{-3}$	$6.64 \cdot 10^{-1} \pm 2.44 \cdot 10^{-2}$	$7.28 \cdot 10^{-1} \pm 6.28 \cdot 10^{-3}$
Tetrachloromethane	$9.42 \cdot 10^{-2} \pm 3.38 \cdot 10^{-2}$	$-6.74 \cdot 10^{-2} \pm 4.02 \cdot 10^{-3}$	$-2.72 \cdot 10^{-2} \pm 1.25 \cdot 10^{-3}$	$2.40 \cdot 10^{-1} \pm 1.82 \cdot 10^{-2}$	$-5.61 \cdot 10^{-2} \pm 2.43 \cdot 10^{-3}$
Trichloroethene	$8.54 \cdot 10^{-1} \pm 1.34 \cdot 10^{-1}$	$1.09 \cdot 10^{-1} \pm 4.15 \cdot 10^{-2}$	$1.11 \cdot 10^{-1} \pm 2.26 \cdot 10^{-2}$	$9.81 \cdot 10^{-1} \pm 2.89 \cdot 10^{-2}$	$4.52 \cdot 10^{-1} \pm 9.67 \cdot 10^{-2}$
Tetrachloroethene	$8.62 \cdot 10^{-1} \pm 1.09 \cdot 10^{-1}$	$-2.86 \cdot 10^{-1} \pm 1.41 \cdot 10^{-2}$	$-1.14 \cdot 10^{-1} \pm 2.54 \cdot 10^{-3}$	$1.68 \pm 1.06 \cdot 10^{-1}$	$-3.22 \cdot 10^{-1} \pm 3.10 \cdot 10^{-2}$
Water	$6.45 \cdot 10^{-1} \pm 2.10 \cdot 10^{-2}$	$1.77 \cdot 10^{-1} \pm 1.03 \cdot 10^{-2}$	$2.46 \cdot 10^{-2} \pm 2.07 \cdot 10^{-3}$	$2.80 \cdot 10^{-1} \pm 1.85 \cdot 10^{-2}$	$7.34 \cdot 10^{-1} \pm 2.96 \cdot 10^{-2}$
Ethanol	$6.26 \cdot 10^{-1} \pm 8.38 \cdot 10^{-2}$	$2.55 \cdot 10^{-1} \pm 8.11 \cdot 10^{-3}$	$4.66 \cdot 10^{-2} \pm 4.12 \cdot 10^{-3}$	$3.88 \cdot 10^{-1} \pm 3.42 \cdot 10^{-2}$	$7.38 \cdot 10^{-1} \pm 1.68 \cdot 10^{-2}$
Ethyl acetate	$8.14 \cdot 10^{-1} \pm 2.77 \cdot 10^{-2}$	$1.77 \cdot 10^{-1} \pm 1.21 \cdot 10^{-2}$	$1.89 \cdot 10^{-1} \pm 1.28 \cdot 10^{-2}$	$1.05 \pm 4.01 \cdot 10^{-2}$	$3.21 \cdot 10^{-1} \pm 1.55 \cdot 10^{-2}$

Table A-4. Analyte sensitivities and standard deviations as measured with the capacitive sensor for different polymers.

Chapter 5

	Quality	Supplier	Product code
Methyl-(S)-(-)-lactate	Purum; ≥ 98%	Sigma-Aldrich, Buchs, Switzerland	230340
Methyl-(R)-(+)-lactate	Purum; ≥ 98%	Sigma-Aldrich, Buchs, Switzerland	277762
(±)-Methyl lactate	Purum; ≥ 97%	Fluka, Buchs, Switzerland	69822
(S)-(-)-Methyl (*S*)-2-chloropropionate	Purum; ≥ 99%	Sigma-Aldrich, Buchs, Switzerland	247030
(*R*)-(+)-Methyl (*R*)-2-chloropropionate	Purum; ≥ 99%	Sigma-Aldrich, Buchs, Switzerland	277754
(±)-Methyl-2-chloropropionate	Purum; ≥ 97%	Fluka, Buchs, Switzerland	139130

Table A-5. Supplier information for the investigated enantiomers.

Titration preparations		
	Weight [mg] or volume [ml]	Substance
NMR test tube	20 mg 0.6 ml	Pure γ-cyclodextrin derivative (mw = 2979.9699 g/mol) dissolved in Toluene-d_8 In this solution the γ-cyclodextrin concentration was $c_n = 1.896 \cdot 10^{-3}$ M and n = 0.00671 mmol.
1st Titration solution	12.3 mg 2 ml	Analyte (pure enantiomer), this equals n = 0.181 mmol Toluene-d_8
2nd Titration solution	30.69 mg 0.088 ml	Analyte (pure enantiomer), this equals n = 0.295 mmol Toluene-d_8
1st Titration	0.05 ml	Volume of the sample solution for each titration step (8 steps)
2nd Titration	0.01 ml	Volume of the sample solution for each titration step (8 steps)

Table A-6. Preparation of the test tube and the titration solutions for the NMR measurements of the enantiomers of methyl lactate.

Titration preparations			
		Weight [mg] or volume [ml]	Substance
Stock solution		118 mg 2 ml	Pure γ-cyclodextrin derivative (mw = 2979.9699 g/mol) dissolved in Toluene-d_8 This means for the following solutions: 0.085 ml contain 5 mg of the γ-cyclodextrin, this equals a concentration of $c_n = 3.356 \cdot 10^{-3}$ M (n = 0.00168 mmol). This concentration is kept constant during the titration procedure.
NMR test tube		0.085 ml 0.415 ml = 0.5 ml	γ-cyclodextrin stock solution Toluene-d_8 Total volume in the test tube
Sample solution		0.085 ml 0.0176 ml 0.3974 ml = 0.5 ml	γ-cyclodextrin stock solution Analyte (pure enantiomer), this equals m = 20 mg of n = 0.163 mmol Toluene-d_8 Total volume in the sample solution
Titration step	1	0.012 ml	Volume of the sample solution for each titration step
	2	0.013 ml	
	3	0.014 ml	
	4	0.015 ml	
	5	0.016 ml	
	6	0.016 ml	
	7	0.017 ml	
	8	0.018 ml	
	9	0.019 ml	
	10	0.020 ml	
	11	0.040 ml	
	12	0.041 ml	
	13	0.042 ml	
	14	0.043 ml	
	15	0.043 ml	
	15	0.044 ml	
	17	0.045 ml	
	18	0.046 ml	

Table A-7. Preparation of the test tube and the sample solutions in order to keep the cyclodextrin concentration constant during the NMR titration measurements of the enantiomers of methyl-2-chloropropionate.

REFERENCES

[1] Osbourn, G. C., Bartholomew, J. W., Ricco, A. J. and Frye, G. C. "*Visual-empirical Region-of-influence Pattern Recognition Applied to Chemical Microsensor Array Selection and Chemical Analysis.*" Accounts of Chemical Research **31** (5), 297-305, 1998.

[2] Massart, D. L., Vandeginste, B. G. M., Deming, S. N., Michotte, Y. and Kaufman, L. *Chemometrics: A Textbook.* Elsevier, Amsterdam, 1988.

[3] Hierlemann, A., Schweizer-Berberich, M., Weimar, U., Kraus, G., Pfau, A. and Göpel, W. *Pattern Recognition and Multi-component Analysis.* Sensors Update. VCH. **2**, 119-180, 1996.

[4] Brereton, R. G. *Multivariate Pattern Recognition in Chemometrics.* Elsevier, Amsterdam, 1992.

[5] Yan, H., Guo, J. and Feng, Y. "*Metallic Oxide Semiconductor Field Effect-transistor Array-compound-type Gas Chemical Microsensor.*" Proceedings of the SPIE **4601**, 226-233, 2001.

[6] Semancik, S., Cavicchi, R. E., Wheeler, M. C., Tiffany, J. E., Poirier, G. E., Walton, R. M., Suehle, J. S., Panchapakesan, B. and DeVoe, D. L. "*Micro-hotplate Platforms for Chemical Sensor Research.*" Sensors and Actuators B **77** (1-2), 579-591, 2001.

[7] Ricco, A. J., Crooks, R. M. and Osbourn, G. C. "*Surface Acoustic Wave Chemical Sensor Arrays: New Chemically Sensitive Interfaces Combined with Novel Cluster Analysis to Detect Volatile Organic Compounds and Mixtures.*" Accounts of Chemical Research **31** (5), 289-296, 1998.

[8] Mandou, M. J. *Fundamentals of Microfabrication.* Boca Raton, Florida, USA, CRC Press, 2002.

[9] Kovacs, G. T. A. *Micromachined Transducers.* WCB McGraw-Hill, Boston, 1998.

[10] Jakoby, B., Bastemeijer, J. and Vellekoop, M. J. "*Temperature-compensated Love-wave Sensors on Quartz Substrates.*" Sensors and Actuators A **82** (1-3), 83-88, 2000.

[11] Graf, M., Barrettino, D., Taschini, S., Hagleitner, C., Hierlemann, A. and Baltes, H. "*Metal Oxide-based Monolithic Complementary Metal Oxide Semiconductor Gas Sensor Microsystem.*" Analytical Chemistry **76** (15), 4437-4445, 2004.

[12] Afridi, M., Hefner, A., Berning, D., Ellenwood, C., Varma, A., Jacob, B. and Semancik, S. "*MEMS-based Embedded Sensor Virtual Components for System-on-a-chip (SoC).*" Solid-State Electronics **48** (10-11), 1777-1781, 2004.

[13] Grate, J. W. and Wise, B. M. "*A Method for Chemometric Classification of Unknown Vapors from the Responses of an Array of Volume-transducing Sensors.*" Analytical Chemistry **73** (10), 2239-2244, 2001.

[14] Grate, J. W. "*Acoustic Wave Microsensor Arrays for Vapor Sensing.*" Chemical Reviews **100** (7), 2627-2647, 2000.

[15] Muller, G., Deimel, P. P., Hellmich, W. and Wagner, C. "*Sensor Fabrication Using Thin Film-on-silicon Approaches.*" Thin Solid Films **296** (1-2), 157-163, 1997.

[16] Zhou, R., Hierlemann, A., Weimar, U. and Göpel, W. "*Gravimetric, Dielectric and Calorimetric Methods for the Detection of Organic Solvent Vapors Using Poly(etherurethane) Coatings.*" Sensors and Actuators B **34** (1-3), 356-360, 1996.

[17] Snow, A. W., Barger, W. R., Klusty, M., Wohltjen, H. and Jarvis, N. L. "*Simultaneous Electrical-conductivity and Piezoelectric Mass Measurements on Iodine-doped Phthalocyanine Langmuir-Blodgett-films.*" Langmuir **2** (4), 513-519, 1986.

[18] Rodriguez, J. L., Hughes, R. C., Corbett, W. T. and McWhorter, P. J. "*Robust, Wide Range Hydrogen Sensor.*" Technical Digest of IEEE International Electron Devices Meeting, San Francisco, CA, USA, 1992.

[19] Gumbrecht, W., Peters, D., Schelter, W., Erhardt, W., Henke, J., Steil, J. and Sykora, U. "*Integrated PO_2, PCO_2, pH Sensor System for Online Blood Monitoring.*" Sensors and Actuators B **19** (1-3), 704-708, 1994.

[20] Li, Y., Vancura, C., Barrettino, D., Graf, M., Hagleitner, C., Kummer, A., Zimmermann, M., Kirstein, K. U. and Hierlemann, A. "*Monolithic CMOS Multi-transducer Gas Sensor Microsystem.*" Proceedings of TRANSDUCERS '05, 2005.

[21] Trojanowicz, M. and Wcislo, M. "*Electrochemical and Piezoelectric Enantioselective Sensors and Biosensors.*" Analytical Letters **38** (4), 523-547, 2005.

[22] Stinson, S. C. "*Chiral Drugs.*" Chemical & Engineering News **78** (43), 55-78, 2000.

[23] de Camp, W. H. "*The FDA Perspective on the Development of Stereoisomers.*" Chirality **1** (1), 2-6, 1989.

[24] Gübitz, G. and Schmid, M. G. "*Chiral Separation Principles in Chromatographic and Electromigration Techniques.*" Molecular Biotechnology **32** (2), 159-179, 2006.

[25] Schurig, V. "*Chiral Separations Using Gas Chromatography.*" Trac-Trends in Analytical Chemistry **21** (9-10), 647-661, 2002.

[26] Juvancz, Z. and Szejtli, J. "*The Role of Cyclodextrins in Chiral Selective Chromatography.*" Trac-Trends in Analytical Chemistry **21** (5), 379-388, 2002.

[27] Ward, T. J. and Hamburg, D. M. "*Chiral Separations.*" Analytical Chemistry **76** (16), 4635-4644, 2004.

[28] Ward, T. J. "*Utilizing the Unique Selectivity of Macrocyclic Antibiotics.*" Abstracts of Papers of the American Chemical Society **228**, U112, 2004.

[29] Shahgaldian, P., Pieles, U. and Hegner, M. "*Enantioselective Recognition of Phenylalanine by a Chiral Amphiphilic Macrocycle at the Air-water Interface: A Copper-mediated Mechanism.*" Langmuir **21** (14), 6503-6507, 2005.

[30] Rat'ko, A. A., Stefan, R. I., van Staden, J. F. and Aboul-Enein, H. Y. "*Macrocyclic Antibiotics as Chiral Selectors in the Design of Enantioselective, Potentiometric Membrane Electrodes.*" Instrumentation Science & Technology **32** (6), 601-610, 2004.

[31] Belder, D. and Ludwig, M. "*Microchip Electrophoresis for Chiral Separations.*" Electrophoresis **24** (15), 2422-2430, 2003.

[32] Harrison, D. J., Fluri, K., Seiler, K., Fan, Z. H., Effenhauser, C. S. and Manz, A. "*Micromachining a Miniaturized Capillary Electrophoresis-based Chemical-analysis System on a Chip.*" Science **261** (5123), 895-897, 1993.

[33] Harrison, D. J., Fan, Z. H., Seiler, K., Manz, A. and Widmer, H. M. "*Rapid Separation of Fluorescein Derivatives Using a Micromachined Capillary Electrophoresis System.*" Analytica Chimica Acta **283** (1), 361-366, 1993.

[34] Bonato, P. S. "*Recent Advances in the Determination of Enantiomeric Drugs and their Metabolites in Biological Fluids by Capillary Electrophoresis-mediated Microanalysis.*" Electrophoresis **24** (22-23), 4078-4094, 2003.

[35] Hofstetter, O., Hofstetter, H., Wilchek, M., Schurig, V. and Green, B. S. "*Chiral Discrimination Using an Immunosensor.*" Nature Biotechnology **17** (4), 371-374, 1999.

[36] Hofstetter, O., Hertweck, J. K. and Hofstetter, H. "*Detection of Enantiomeric Impurities in a Simple Membrane-based Optical Immunosensor.*" Journal of Biochemical and Biophysical Methods **63** (2), 91-99, 2005.

[37] Kim, H. J., Gritti, F. and Guiochon, G. "*Effect of the Temperature on the Isotherm Parameters of Phenol in Reversed-phase Liquid Chromatography.*" Journal of Chromatography A **1049** (1-2), 25-36, 2004.

[38] Hofstetter, O., Lindstrom, H. and Hofstetter, H. "*Direct Resolution of Enantiomers in High-performance Immunoaffinity Chromatography Under Isocratic Conditions.*" Analytical Chemistry **74** (9), 2119-2125, 2002.

[39] Dominguez, R., Serra, B., Reviejo, A. J. and Pingarron, J. M. "*Chiral Analysis of Amino Acids Using Electrochemical Composite Bienzyme Biosensors.*" Analytical Biochemistry **298** (2), 275-282, 2001.

[40] Macca, C. "*The Current Usage of Selectivity Coefficients for the Characterization of Ion-selective Electrodes. A Critical Survey of the 2000/2001 literature.*" Electroanalysis **15** (12), 997-1010, 2003.

[41] Rat'ko, A. A., Stefan, R. I., van Staden, J. F. and Aboul-Enein, H. Y. "*Determination of L-carnitine Using Enantioselective, Potentiometric Membrane Electrodes Based on Macrocyclic Antibiotics.*" Talanta **63** (3), 515-519, 2004.

[42] Kieser, B., Fietzek, C., Schmidt, R., Belge, G., Weimar, U., Schurig, V. and Gauglitz, G. "*Use of a Modified Cyclodextrin Host for the Enantioselective Detection of a Halogenated Diether as Chiral Guest via Optical and Electrical Transducers.*" Analytical Chemistry **74** (13), 3005-3012, 2002.

[43] Hierlemann, A., Ricco, A. J., Bodenhöfer, K. and Göpel, W. "*Effective Use of Molecular Recognition in Gas Sensing: Results from Acoustic Wave and in situ FT-IR Measurements.*" Analytical Chemistry **71** (15), 3022-3035, 1999.

[44] Bodenhöfer, K., Hierlemann, A., Seemann, J., Gauglitz, G., Koppenhoefer, B. and Göpel, W. "*Chiral Discrimination Using Piezoelectric and Optical Gas Sensors.*" Nature **387** (6633), 577-580, 1997.

[45] Shahgaldian, P. and Pieles, U. "*Cyclodextrin Derivates as Chiral Supramolecular Receptors for Enantioselective Sensing.*" Sensors **6** (6), 593-615, 2006.

[46] Yan, G., Zhu, Y., Wang, C., Zhang, R., Chen, Z., Liu, X. and Wng, Y. Y. "*Integrated Bulk-micromachined Gyroscope Using Deep Trench Isolation Technology.*" Proceedings of IEEE Micro Electro Mechanical Systems, Miami, FL, USA, 2004.

[47] http://www.austriamicrosystems.com

[48] Hagleitner, C., Hierlemann, A., Lange, D., Kummer, A., Kerness, N., Brand, O. and Baltes, H. "*Smart Single-chip Gas Sensor Microsystem.*" Nature **414** (6861), 293-6, 2001.

[49] Hierlemann, A., Ricco, A. J., Bodenhöfer, K., Dominik, A. and Göpel, W. "*Conferring Selectivity to Chemical Sensors via Polymer Side-chain Selection: Thermodynamics of Vapor Sorption by a Set of Polysiloxanes on Thickness-shear Mode Resonators.*" Analytical Chemistry **72** (16), 3696-3708, 2000.

[50] Marais, S., Metayer, M., Nguyen, Q. T., Labbe, M. and Langevin, D. "*New Methods for the Determination of the Parameters of a Concentration-dependent Diffusion Law for Molecular Penetrants from Transient Permeation or Sorption Data.*" Macromolecular Theory and Simulations **9** (4), 207-214, 2000.

[51] George, S. C. and Thomas, S. "*Transport Phenomena Through Polymeric Systems.*" Progress in Polymer Science **26** (6), 985-1017, 2001.

[52] Grate, J. W. "*Inorganic/Organic Materials for Chemical Vapor Sensors.*" Abstracts of Papers of the American Chemical Society **229**, U971, 2005.

[53] Grate, J. W. and Abraham, M. H. "*Solubility Interactions and the Design of Chemically Selective Sorbent Coatings for Chemical Sensors and Arrays.*" Sensors and Actuators B **3** (2), 85-111, 1991.

[54] Marais, S., Nguyen, Q. T., Devallencourt, C., Metayer, M., Nguyen, T. U. and Schaetzel, P. "*Permeation of Water Through Polar and Nonpolar Polymers and Copolymers: Determination of the Concentration-dependent Diffusion Coefficient.*" Journal of Polymer Science B **38** (15), 1998-2008, 2000.

[55] Grate, J. W. "*Inorganic/Organic Materials for Chemical Vapor Sensors.*" Abstracts of Papers of the American Chemical Society **229**, U971-U971, 2005.

[56] Marais, S., Nguyen, Q. T., Devallencourt, C., Metayer, M., Nguyen, T. U. and Schaetzel, P. "*Permeation of Water Through Polar and Nonpolar Polymers and Copolymers: Determination of the Concentration-dependent Diffusion Coefficient.*" Journal of Polymer Science Part B **38** (15), 1998-2008, 2000.

[57] Kunt, T. A., McAvoy, T. J., Cavicchi, R. E. and Semancik, S. "*Optimization of Temperature Programmed Sensing for Gas Identification Using Micro-hotplate Sensors.*" Sensors and Actuators B **53** (1-2), 24-43, 1998.

[58] Iordanskii, A. L., Razumovskii, L. P., Krivandin, A. V. and Lebedeva, T. L. "*Diffusion and Sorption of Water in Moderately Hydrophilic Polymers: From Segmented Polyetherurethanes to Poly-3-hydroxybutyrate.*" Desalination **104** (1-2), 27-35, 1996.

[59] Nakamura, M., Sugimoto, I. and Kuwano, H. "*Chemical Sensing System Using Plasma Polymer-films and Pattern-recognition Algorithm.*" Journal of Intelligent Material Systems and Structures **5** (3), 315-320, 1994.

[60] Martin, S. J. and Frye, G. C. "*Surface Acoustic-wave Response to Changes in Viscoelastic Film Properties.*" Applied Physics Letters **57** (18), 1867-1869, 1990.

[61] Lerchner, J., Seidel, J., Wolf, G. and Weber, E. "*Calorimetric Detection of Organic Vapors Using Inclusion Reactions with Organic Coating Materials.*" Sensors and Actuators B **32** (1), 71-75, 1996.

[62] Bataillard, P., Steffgen, E., Haemmerli, S., Manz, A. and Widmer, H. M. "*An Integrated Silicon Thermopile as Biosensor for the Thermal Monitoring of Glucose, Urea and Penicillin.*" Biosensors & Bioelectronics **8** (2), 89-98, 1993.

[63] Kerness, N., Koll, A., Schaufelbuhl, A., Hagleitner, C., Hierlemann, A., Brand, O. and Baltes, H. "*N-well Based CMOS Calorimetric Chemical Sensors.*" Proceedings of IEEE Micro Electro Mechanical Systems, Miyazaki, Japan, 2000.

[64] Koll, A., Kummer, A., Brand, O. and Baltes, H. "*Discrimination of Volatile Organic Compounds Using CMOS Capacitive Chemical Microsensors with Thickness Adjusted Polymer Coating.*" Proceedings of the SPIE **3673**, 308-317, 1999.

[65] Van Herwaarden, A. W., Sarro, P. M., Gardner, J. W. and Bataillard, P. "*Liquid and Gas Micro-calorimeters for (Bio)chemical Measurements.*" Sensors and Actuators A **A43** (1-3), 24-30, 1994.

[66] Hierlemann, A., Lange, D., Hagleitner, C., Kerness, N., Koll, A., Brand, O. and Baltes, H. "*Application-specific Sensor Systems Based on CMOS Chemical Microsensors.*" Sensors and Actuators B **70** (1-3), 2-11, 2000.

[67] Hagleitner, C., Lange, D., Hierlemann, A., Brand, O. and Baltes, H. "*CMOS Single-chip Gas Detection System Comprising Capacitive, Calorimetric and Mass-sensitive Microsensors.*" IEEE Journal of Solid-State Circuits **37** (12), 1867-1878, 2002.

[68] Lange, D., Brand, O. and Baltes, H. *CMOS Cantilever Sensor Systems: Atomic Force Microscopy and Gas Sensing Applications.* Berlin Heidelberg New York, Springer, 2002.

[69] Lange, D., Hagleitner, C., Hierlemann, A., Brand, O. and Baltes, H. "*Complementary Metal Oxide Semiconductor Cantilever Arrays on a Single Chip: Mass-sensitive Detection of Volatile Organic Compounds.*" Analytical Chemistry **74** (13), 3084-3095, 2002.

[70] Kummer, A. and Hierlemann, A. "*Configurable Electrodes for Capacitive-type Sensors and Chemical Sensors.*" IEEE Sensors Journal **6**, 3-10, 2006.

[71] Steiner, F. P., Hierlemann, A., Cornila, C., Noetzel, G., Bachtold, M., Korvink, J. G., Göpel, W. and Baltes, H. "*Polymer Coated Capacitive Microintegrated Gas Sensor.*" Proceedings of TRANSDUCERS '95, 1995.

[72] Kummer, A. *Tuning Sensitivity and Discrimination Performance of CMOS Capacitive Chemical Microsensor Systems.* Ph.D. Thesis, Physical Electronics Laboratory, ETH Zurich, Zurich, Switzerland, 2004.

[73] Kummer, A. M., Burg, T. P. and Hierlemann, A. "*Transient Signal Analysis Using Complementary Metal Oxide Semiconductor Capacitive Chemical Microsensors.*" Analytical Chemistry **78** (1), 279-290, 2006.

[74] Kummer, A., Hierlemann, A. and Baltes, H. "*Tuning Sensitivity and Selectivity of Complementary Metal Oxide Semiconductor-based Capacitive Chemical Microsensors.*" Analitical Chemistry **76** (9), 2470-2477, 2004.

[75] Hagleitner, C. *CMOS Single-chip Gas Detection System Comprising Capacitive, Calorimetric and Mass-sensitive Microsensors.* Ph.D. Thesis, Physical Electronics Laboratory, ETH Zurich, Zurich, Switzerland, 2002.

[76] Kurzawski, P., Salo, T., Baltes, H. and Hierlemann, A. "*Towards a Versatile DRIE: Silicon Pit Structures Combined with Electrochemical Etch Stop.*" Journal of Microelectromechanical Systems **15** (4), 840-848, 2006.

[77] Müller, T. *An Industrial CMOS Process Family for Integrated Silicon Sensors.* Ph.D. Thesis, Physical Electronics Laboratory, ETH Zurich, Zurich, Switzerland, 1999.

[78] Müller, T., Brandl, M., Brand, O. and Baltes, H. "*An Industrial CMOS Process Family Adapted for the Fabrication of Smart Silicon Sensors.*" Sensors and Actuators A **84**, 126-133, 2000.

[79] Kloeck, B., Collins, S. D., Derooij, N. F. and Smith, R. L. "*Study of Electrochemical Etch Stop for High-precision Thickness Control of Silicon Membranes.*" IEEE Transactions on Electron Devices **36** (4), 663-669, 1989.

[80] Wallman, L., Bengtsson, J., Danielsen, N. and Laurell, T. "*Electrochemical Etch Stop Technique for Silicon Membranes with p- and n-type Regions and its Application to Neural Sieve Electrodes.*" Journal of Micromechanics and Microengineering **12** (3), 265-270, 2002.

[81] Kloeck, B., Collins, S. D., Derooij, N. F. and Smith, R. L. "*Study of Electrochemical Etch-stop For High-precision Thickness Control of Silicon Membranes.*" IEEE Transactions on Electron Devices **36** (4), 663-669, 1989.

[82] Baltes, H., Brand, O., Fedder, G., Hierold, C., Korvink, J. and Tabata, O. *CMOS-MEMS.* Weinheim, Wiley-VCH Verlag, 2005.

[83] Kovacs, G. T. A., Maluf, N. I. and Petersen, K. E. "*Bulk Micromachining of Silicon.*" Proceedings of the IEEE **86** (8), 1536-1551, 1998.

[84] Bustillo, J. M., Howe, R. T. and Muller, R. S. "*Surface Micromachining for Microelectromechanical Systems.*" Proceedings of the IEEE **86** (8), 1552-1574, 1998.

[85] Seidel, H., Csepregi, L., Heuberger, A. and Baumgartel, H. "*Anisotropic Etching of Crystalline Silicon in Alkaline-solutions.1. Orientation Depend-*

ence and Behavior of Passivation Layers." Journal of the Electrochemical Society **137** (11), 3612-3626, 1990.

[86] Laermer, F. and Schilp, A. *Anisotropic Etching of Silicon Substrates - Using a Polymerisation Process in Between Etching Stages to Protect Lateral Edges of the Etched Shape.* Patent EP 6525285-A. 1994.

[87] Kiihamaki, J. and Franssila, S. "*Pattern Shape Effects and Artifacts in Deep Silicon Etching.*" Journal of Vacuum Science & Technology A **17** (4), 2280-2285, 1999.

[88] Gottscho, R. A., Jurgensen, C. W. and Vitkavage, D. J. "*Microscopic Uniformity in Plasma-etching.*" Journal of Vacuum Science & Technology B **10** (5), 2133-2147, 1992.

[89] Ayon, A. A., Braff, R. A., Bayt, R., Sawin, H. H. and Schmidt, M. A. "*Influence of Coil Power on the Etching Characteristics in a High Density Plasma Etcher.*" Journal of the Electrochemical Society **146** (7), 2730-2736, 1999.

[90] Ayon, A. A., Braff, R., Lin, C. C., Sawin, H. H. and Schmidt, M. A. "*Characterization of a Time Multiplexed Inductively Coupled Plasma Etcher.*" Journal of the Electrochemical Society **146** (1), 339-349, 1999.

[91] Arnold, J. C. and Sawin, H. H. "*Charging of Pattern Features During Plasma-etching.*" Journal of Applied Physics **70** (10), 5314-5317, 1991.

[92] Vancura, C., Ruegg, M., Li, Y., Hagleitner, C. and Hierlemann, A. "*Magnetically Actuated Complementary Metal Oxide Semiconductor Resonant Cantilever Gas Sensor Systems.*" Analytical Chemistry **77** (9), 2690-2699, 2005.

[93] Saadaoui, M., Muller, A., Pons, P., Neculoiu, D., Bary, L., Dubuc, D., Grenier, K., Rabbia, L., Buiculescu, C., Petrini, I. and Plana, R. "*New Technologies Based on Dry and Dry Followed by Wet Backside Etching Process for Endfire Membrane Supported Millimeter Wave Antennae Manufacturing.*" Proceedings of the Micromechanics Europe Workshop, 2003.

[94] Chu, H.-Y. and Fang, W. "*Fabrication of 3D Microstructures and Microactuators on (100) SOI Wafers Using the DAWN Process.*" Proceedings of IEEE Micro Electro Mechanical Systems, Miami, FL, USA, 2004.

[95] Dijkstra, P., Puech, M., Launay, N., Arnal, N., Rolland, L. and Gruffat, J. M. "*New Developments in Silicon and Oxide ICP Etching for MEMS.*" Proceedings of the MicroMechanics Europe Workshop, 2003.

[96] Müller, T., Feichtinger, T., Breitenbach, G., Brandl, M., Brand, O. and Baltes, H. "*Industrial Fabrication Method for Arbitrarily Shaped Silicon n-well Micromechanical Structures.*" Technical Digest of IEEE Micro Electro Mechanical Systems, 1998.

[97] http://www.ammt.com

[98] Bodenhöfer, K., Hierlemann, A., Schlunk, R. and Göpel, W. "*New Method of Vaporizing Volatile Organics for Gas Tests.*" Sensors and Actuators B **45** (3), 259-264, 1997.

[99] Riddick, J. A., Bunger, W. B. and Sakano, T. K. *Organic Solvents.* New York, NY, USA, Wiley Interscience, 1986.

[100] Kurzawski, P., Hagleitner, C. and Hierlemann, A. "*Detection and Discrimination Capabilities of a Multi-transducer Single-chip Gas Sensor System.*" Analytical Chemistry **78** (19), 6910-6920, 2006, submitted.

[101] Weissberger, A. *Organic Solvents.* Wiley, New York, 1986.

[102] Lide, D. R. *Handbook of Chemistry and Physics.* Boca Raton, FL, CRC Press, 1994.

[103] Grate, J. W., Patrash, S. J., Abraham, M. H. and Du, C. M. "*Selective Vapor Sorption by Polymers and Cavitands on Acoustic-wave Sensors: Is this Molecular Recognition?*" Analytical Chemistry **68** (5), 913-917, 1996.

[104] Hierlemann, A., Zellers, E. T. and Ricco, A. J. "*Use of Linear Salvation Energy Relationships for Modeling Responses from Polymer-coated Acoustic-wave Vapor Sensors.*" Analytical Chemistry **73** (14), 3458-3466, 2001.

[105] Aminabhavi, T. M. and Khinnavar, R. S. "*Diffusion and Sorption of Organic Liquids Through Polymer Membranes.10. Polyurethane, Nitrile-butadiene Rubber and Epichlorohydrin Versus Aliphatic-alcohols (C1-C5).*" Polymer **34** (5), 1006-1018, 1993.

[106] http://csi.chemie.tu-darmstadt.de/ak/immel/index.html

[107] Atkins, P. *Atkins' Molecules.* Cambridge University Press, 2003.

[108] Friedman, L. and Miller, J. G. "*Odor Incongruity and Chirality.*" Science **172** (3987), 1044-1046, 1971.

[109] Hillberg, A. L., Brain, K. R. and Allender, C. J. "*Molecular Imprinted Polymer Sensors: Implications for Therapeutics.*" Advanced Drug Delivery Reviews **57** (12), 1875-1889, 2005.

[110] Mahony, J. O., Nolan, K., Smyth, M. R. and Mizaikoff, B. "*Molecularly Imprinted Polymers-potential and Challenges in Analytical Chemistry.*" Analytica Chimica Acta **534** (1), 31-39, 2005.

[111] Schurig, V. "*Practice and Theory of Enantioselective Complexation Gas Chromatography.*" Journal of Chromatography A **965** (1-2), 315-356, 2002.

[112] Szejtli, J. "*Introduction and General Overview of Cyclodextrin Chemistry.*" Chemical Reviews **98** (5), 1743-1753, 1998.

[113] http://www.raell.demon.co.uk/chem/CHIbook/chiral.htm

[114] Szejtli, J. "*Past, Present, and Future of Cyclodextrin Research.*" Pure and Applied Chemistry **76** (10), 1825-1845, 2004.

[115] Altria, K. D. and Elder, D. "*Overview of the Status and Applications of Capillary Electrophoresis to the Analysis of Small Molecules.*" Journal of Chromatography A **1023** (1), 1-14, 2004.

[116] Juvancz, Z. and Petersson, P. "*Enantioselective Gas Chromatography.*" Journal of Microcolumn Separations **8** (2), 99-114, 1996.

[117] Khan, A. R., Forgo, P., Stine, K. J. and D'Souza, V. T. "*Methods for Selective Modifications of Cyclodextrins.*" Chemical Reviews **98** (5), 1977-1996, 1998.

[118] Mele, A., Raffaini, G., Ganazzoli, F., Juza, M. and Schurig, V. "*Macrocycle Conformation and Self-inclusion Phenomena in Octakis(3-O-butanoyl-2,6-di-O-pentyl)-gamma-cyclodextrin (Lipodex E) by NMR Spectroscopy and Molecular Dynamics.*" Carbohydrate Research **338** (7), 625-635, 2003.

[119] Lipkowitz, K. B., Coner, R. and Peterson, M. A. "*Locating Regions of Maximum Chiral Discrimination: A Computational Study of Enantioselection on a Popular Chiral Stationary Phase Used in Chromatography.*" Journal of the American Chemical Society **119** (46), 11269-11276, 1997.

[120] König, W. A. *Gas Chromatographic Enantiomer Separation with Modified Cyclodextrins.* Heidelberg, Hüthig Buch-Verlag, 1992.

[121] Lipkowitz, K. B. "*Atomistic Modeling of Enantioselection in Chromatography.*" Journal of Chromatography A **906** (1-2), 417-442, 2001.

[122] Lipkowitz, K. B. "*Applications of Computational Chemistry to the Study of Cyclodextrins.*" Chemical Reviews **98** (5), 1829-1873, 1998.

[123] Schurig, V. and Schmidt, R. "*Extraordinary Chiral Discrimination in Inclusion Gas Chromatography. Thermodynamics of Enantioselectivity Between a Racemic Perfluorodiether and a Modified Gamma-cyclodextrin.*" Journal of Chromatography A **1000** (1-2), 311-324, 2003.

[124] Jung, M., Schmalzing, D. and Schurig, V. "*Theoretical Approach to the Gas Chromatographic Separation of Enantiomers on Dissolved Cyclodextrin Derivatives.*" Journal of Chromatography **552** (1-2), 43-57, 1991.

[125] Bodenhöfer, K., Hierlemann, A., Juza, N., Schurig, V. and Göpel, W. "*Chiral Discrimination of Inhalation Anesthetics and Methyl Propionates by Thickness Shear Mode Resonators: New Insights into the Mechanisms of Enantioselectivity by Cyclodextrins.*" Analytical Chemistry **69** (19), 4017-4031, 1997.

[126] Spanik, I., Krupcik, J. and Schurig, V. "*Comparison of Two Methods for the Gas Chromatographic Determination of Thermodynamic Parameters of*

Enantioselectivity." Journal of Chromatography A **843** (1-2), 123-128, 1999.

[127] Terabe, S., Ishihama, Y., Nishi, H., Fukuyama, T. and Otsuka, K. "*Effect of Urea Addition in Micellar Electrokinetic Chromatography.*" Journal of Chromatography **545** (2), 359-368, 1991.

[128] Bodenhöfer, K., Hierlemann, A., Noetzel, G., Weimar, U. and Göpel, W. "*Performances of Mass-sensitive Devices for Gas Sensing: Thickness Shear Mode and Surface Acoustic Wave Transducers.*" Analytical Chemistry **68** (13), 2210-2218, 1996.

[129] Bodenhöfer, K. *Chirale Erkennung mit Schwingquarzsensoren.* Institute of Physical and Theoretical Chemistry, University of Tübingen, 1997.

[130] König, W. A., Krebber, R. and Mischnick, P. "*Cyclodextrins as Chiral Stationary Phases in Capillary Gas Chromatography. 5. Octakis(3-O-butyryl-2,6-di-O-pentyl)-gamma-cyclodextrin.*" Journal of High Resolution Chromatography **12** (11), 732-738, 1989.

[131] Krebber, R. *Neue Cyclodextrinderivate als chirale stationäre Phasen für die gaschromatographische Enantiomerentrennung.* Ph.D. Thesis, Institute of Organic Chemistry, University of Hamburg, Hamburg, 1991.

[132] Bogdanski, A., Institute of Organic Chemistry, University of Tübingen

[133] Junge, M. and König, W. A. "*Selectivity Tuning of Cyclodextrin Derivatives by Specific Substitution.*" Journal of Separation Science **26** (18), 1607-1614, 2003.

[134] http://www.sigmaaldrich.com

[135] http://www.chemexper.com

[136] http://www.sigmaaldrich.com/

[137] Köhler, J. E. H., Hohla, M., Richters, M. and König, W. A. "*Cyclodextrin Derivatives as Chiral Selectors - Investigation of the Interaction with (R,S)-methyl-2-chloropropionate by Enantioselective Gas Chromatography, NMR-spectroscopy, and Molecular-dynamics Simulation.*" Angewandte Chemie **31** (3), 319-320, 1992.

[138] König, W. A. "*Collection of Enantiomeric Separation Factors Obtained by Capillary Gas Chromatography on Chiral Stationary Phases.*" Journal of High Resolution Chromatography **16** (10), 569-586, 1993.

[139] Ide, J., Nakamoto, T. and Moriizumi, T. "*Discrimination of Aromatic Optical Isomers Using Quartz-resonator Sensors.*" Sensors and Actuators A **49** (1-2), 73-78, 1995.

[140] Bodenhöfer, K., Hierlemann, A., Seemann, J., Gauglitz, G., Christian, B., Koppenhoefer, B. and Göpel, W. "*Chiral Discrimination in the Gas Phase Using Different Transducers: Thickness Shear Mode Resonators and Re-*

flectometric Interference Spectroscopy." Analytical Chemistry **69** (15), 3058-3068, 1997.

[141] Skoog, D. A., Holler, F. J. and Nieman, T. A. *Principles of Instrumental Analysis*. Thomson Lerning Inc., 1998.

[142] Dube, H., Laboratory for Organic Chemistry, ETH Zurich

ACKNOWLEDGEMENTS

First and foremost, I would like to express my gratitude to my supervisors and mentors: Prof. Andreas Hierlemann and Prof. Henry Baltes for giving me the opportunity to conduct my Ph.D. thesis at the Physical Electronics Laboratory (PEL). You have not only created but also retained an environment that exhibits remarkable working conditions and a genial atmosphere. Over the last years, I could do no other than come to respect your achievements and your abundant knowledge.

Andreas, thank you for always having an open door and ear for my concerns; it must have been grating at times. Your patience is apparently ceaseless. I am grateful for your guidance and support throughout my thesis and particularly for your nonpareil ability of proof-reading. You managed to make the most out of my work.

Henry, thank you for your support throughout these years. You are always concerned with our spiritual well-being (mentally and liquid-wise). Moreover, you always openly shared your professional expertise as well as your personal insight with me, allowing me to benefit from both.

I am indebted to Prof. Jiři Janata. Art, I feel privileged that you immediately agreed to be my co-examiner, not knowing what you would get into. Thank you for your support and especially for your encouragement during the last steps of my thesis.

I am much obliged to Christoph Hagleitner, whose antecedent labor on the sensor system made my work possible. I appreciate your instant help, when I struggled with occurring problems. Kai-Uwe Kirstein has helped me through parts of this thesis, never growing tired after my hundred-and-some questions on circuitry and the workings of the chip. I owe you one. Nils Goedecke has proof-read parts of this thesis. I heard, cooking helps to regenerate from this tiresome work and in me you have a willing guinea pig to your culinary experiments. Thank you. Special thanks go to Stefano Taschini, Sadik Hafizovic and Urs Frey for helping me to debug the system.

I am very much in debt to Anja Bogdanski and Henry Dube. Both contributed greatly to this work in doing the synthesis of the coatings and analytes, aiding with measurements and enlightening an ignoramus in the field of chemistry in sharing their knowledge. I am grateful to Tomi Salo, with whom it was a pleasure to slave away in the cleanroom for hours in a row, while developing the "combined process".

I am much obliged to the micromachining team for their post-work on the systems: Markus Graf, Frauke Greve, Tomi Salo, Donat Schreiwiller, and Cyril Vančura.

While being a Ph.D. student the people one is closest to - and spends most time with - are one's office friends. This thank you is dedicated to Frauke Greve, Markus Graf, and Adrian Kummer, whose friendship and support eased the sometimes seemingly endless - and sometimes frustrating - hours of research. Over the years several semester and diploma students contributed to the enjoyable atmosphere in our office: Claudia Küttel, Samuel Mezger, Marko Mihailovic, Jürg Müller, Rene Pedron, Ivan Schen-

ker, and René Tölke. I would like to thank Samuel and Marko for their contribution to the new calorimetric sensor array. Guys, we will get the system running - eventually.

Fruitful work would not have been possible without those people, who keep the administrative and technical parts of the PEL-machinery running: Erna Hug and Yelena von Allmen, Christoph Kolb, Igor Levak, and Donat Schreiwiller. Your support eased many problems that otherwise would have been difficult to handle. Thank you.

I would like to express my thanks to all my other colleagues not having been mentioned so far: Diego Barretino, Oliver Brand, Wendy Franks, Flavio Heer, Nicole Kerness, Yue Li, Jan Lichtenberg, Jürg Schwitzer, Wan Ho Song, Robert Sunier, Tobias Vancura, Tormod Volden, and Martin Zimmermann. With your friendship and your technical knowledge you all contributed to my work, in one way or the other. It was a pleasure working with you.

Cyril, thank you for always being there for me.

Mom and Robin, from your love, trust, and support I always drew comfort and strength - knowing you would be there to catch me, if I stumbled.

I dedicate this work to my father.

PUBLICATION LIST

PATENTS

European patent application of ETH Zurich:

P. Kurzawski, A. Hierlemann, A. Bogdanski, and V. Schurig. "Enantioselective Capacitive Sensor", *EP application No. 06 012004.5*, 10.6.2006, unpublished

JOURNAL PAPERS

M. J. Powers, K. Domansky, M. R. Kaazempur-Mofrad, A. Kalezi, A. Capitano, A. Upadhyaya, P. Kurzawski, K. E. Wack, D. B. Stolz, R. Kamm, and L. G. Griffith. "A microfabricated array bioreactor for perfused 3D liver culture", *Biotechnology and Bioengineering* **78** (2002), 257-269

P. Kurzawski, T. Salo, H. Baltes, and A. Hierlemann. "Towards a Versatile DRIE: Silicon Pit Structures Combined with Electrochemical Etch Stop", *Journal of Microelectromechanical Systems* **15** (2006), 840-848

P. Kurzawski, C. Hagleitner, and A. Hierlemann. "Detection and Discrimination Capabilities of a Multi-Transducer Single-Chip Gas Sensor System", *Analytical Chemistry* **78**, 19 (2006), 6910-6920

CONFERENCE CONTRIBUTIONS

C. Brenan, K. Domansky, P. Kurzawski, and L. Griffith. "BioMEMS Applied to the Development of Cell Based Bioassay Systems", *Proceedings of SPIE - Progress in Biomedical Optics, Micro- and Nanotechnology for Biomedical and Environmental Applications*, San Jose, CA; USA **3912** (2000), 76-87

P. Kurzawski, I. Lazic, C. Hagleitner, A. Hierlemann, and H. Baltes. "Multi-transducer Recordings from a Single-chip Gas Sensor System Coated with Different Polymers", *Proceedings International Conference on Solid-State Sensors, Actuators and Microsystems (TRANSDUCERS)*, Boston, MA, USA **2** (2003), 1359-1362

P. Kurzawski, C. Hagleitner, V. Schurig, H. Baltes, and A. Hierlemann. "Applications and Performance of a Polymer-coated Monolithic CMOS Gas Sensor Microsystem", *Proceedings of 10th International Meeting on Chemical Sensors (IMCS)*, Tsukuba, Japan (2004), 116-117

T. Salo, P. Kurzawski, A. Hierlemann, and H. Baltes. "Novel Micromachining Sequence to Improve Performance and Yield of Calorimetric Microsensors", *Proceedings of 10th International Meeting on Chemical Sensors (IMCS)*, Tsukuba, Japan (2004), 320-321

P. Kurzawski, T. Salo, and A. Hierlemann. "Towards a Versatile DRIE: Silicon Pit Structures Combined with Electrochemical Etch Stop", *Proceedings IEEE Conference on Micro Electro Mechanical Systems (MEMS)*, Miami, FL, USA (2005), 504-507

P. Kurzawski and A. Hierlemann. "Applications and Performance of a Polymer-coated Monolithic CMOS Gas Sensor Microsystem", *Proceedings of EuroSensorsXX*, Gothenburg, Sweden (2006)

CURRICULUM VITAE

PETRA KURZAWSKI

Born October 28th, 1973

German Citizenship

EDUCATION

July 2002 – present	Doctoral thesis work in the field of polymer-based chemical sensors at the Physical Electronics Laboratory, Department of Physics, ETH Zurich
Sept. 2001 – June 2002	Research assistant at the Institute of Microsensors, -actuators and -systems (IMSAS), University of Bremen, Germany
Oct. 1996 – Sept. 2001	Graduate studies of Electrical Engineering at the University of Bremen, Germany, *Diploma degree* 2001
Feb. 1997 – June 2001	Student assistant at the Institute of Microsensors, -actuators and -systems (IMSAS), University of Bremen, Germany
April 1999 – Sept. 1999	Internship at the Department of Chemical Engineering and at the Department of Mechanical Engineering at the Massachusetts Institute of Technology (MIT), Boston, United States
April 1996 – Sept. 1996	Language course/sojourn in Ste. Maxime, France
Oct. 1993 – Sept. 1996	Studies of Electrical Engineering at the University of Bremen, Germany, *Pre-degree in Electrical Engineering* 1996
Aug. 1986 – May 1993	Grammar school at the Gymnasium an der Willmsstrasse, Delmenhorst, Germany, *Abitur* (German school leaving certificate) 1993

RESEARCH PROJECTS

Internship research project	Micromechanical methods for a liver cell chip for health care applications
Student research project	Development of a contact finishing for preventing stiction of gold contacts
Master thesis	Design, characterization and optimization of a silicon-based microchamber for rapid polymerase chain reaction